UNIVERSITÀ DI PADOVA  FACOLTÀ DI INGEGNERIA

Dipartimento di Ingegneria dell'Informazione

Scuola di Dottorato di Ricerca in Ingegneria dell'Informazione
Indirizzo: Bioingegneria

CICLO XXII

Integrating electroencephalography (EEG) and functional magnetic resonance imaging (fMRI) in epilepsy

Direttore della Scuola: Ch.mo Prof. Matteo Bertocco

Supervisore: Ch.mo Prof.ssa Gianna Maria Toffolo

Dottoranda: Ing. Emanuela Formaggio

Gennaio 2010

CONTENTS

SUMMARY

Introduction

Combined electroencephalography (EEG) and functional magnetic resonance imaging (fMRI) studies enables to non invasively investigate human brain function and to find the direct correlation of these two important measures of brain activity. The combination of these technologies provides informations and details on the spatio-temporal aspects of human brain processing.

fMRI has an excellent spatial resolution and allows the localization of brain regions in which there is a change in the level of neuronal activity during an experimental condition compared to a control condition. In contrast, EEG measures neuronal currents directly from the subject's scalp with a high temporal resolution in the range of milliseconds. Combined recording wants to overcome the spatial limitations of EEG and the temporal limitations of fMRI, using their complementary features.

For instance, combined EEG-fMRI technique can be used to identify the neural correlates of clinically or behaviourally important spontaneous EEG activity, such as interictal spikes, the alpha rhythm and sleep waves.

The presurgical evaluation of patients with epilepsy is one of the areas where combining EEG and fMRI has considerable clinical relevance for localizing the brain regions generating interictal epileptiform activity.

fMRI is mostly used in the study of sensory, motor and cognitive functions, where there is a difference between experimental condition and control condition. In the context of epilepsy, one can consider the control condition to occur when the EEG is at baseline and experimental condition to correspond to the presence of an epileptic discharge.

The conventional analysis of EEG-fMRI data is based on the visual identification of the interictal epileptiform discharges (IEDs) on scalp EEG which are used in conjunction with a General Linear Model (GLM) approach to analyze fMRI data. A model is obtained by the convolution of the EEG events, which are

represented as stick functions of unitary amplitude, with a model of the event-related fMRI response, represents by the haemodynamic response function (HRF); maps showing regions of significant IED-related change are obtained through voxel-wise fitting of the model and application of appropriate statistical thresholds.

In this thesis we present an easy to use approach for combined EEG-fMRI analysis developed to improve the identification of the IEDs. The novel automatic method is based on Independent Component Analysis (ICA) and allows to detect IED activity in order to use it as a parametric modulator in fMRI analysis.

The Novel Method

Data quality is a crucial issue in multimodal functional imaging and data integration. Both fMRI and EEG data acquisition processes can severely affect the other's performance through electromagnetic interactions, therefore the pre-processing is necessary for both EEG and fMRI data. While for fMRI data the pre-processing is generally standard, apart from the choice of spatial smoothing; the EEG pre-processing requires a complex and not one-way procedure to remove the artifacts. In literature different methods have been developed to remove gradient and pulse artifacts, considering both hardware and software solutions. The gradient EEG artifact removal method implemented in our EEG system acquisition did not give completely satisfactory results; so we decided to developed a novel method. Since the project regarding the gradient filter started together with the novel EEG-fMRI integration method and the analysis on patients with partial epilepsy are still in progress to avoid the introduction of a further variable in the validation of the method we decided to use the algorithms implemented in the SystemPlus software.

After a pre-processing applied on EEG data and composed by a re-reference and filtering, a method based on ICA decomposition was applied. In the field of biomedical signal processing, Blind Source Separation (BSS) methods are generally used to separate multi-channel recordings into their constituent components; ICA is a subset of such techniques used to separate statistically independent components from a mixture of data. ICA decomposition of the data was performed using FastICA algorithm implemented in EEGLAB.

The novel method consists in four fundamental steps:

- Selection of components
- Reconstruction of EEG signal
- Selection of channel and FFT analysis
- Construction of EEG regressor

The crucial point is the selection of components. To select the components related to IED activity, we used a time-frequency representation obtained by using wavelet-based analysis. We computed the wavelet power for all the components in the epochs of interest and then, for each component, we selected from the frequency bins the one with the maximal power over total recording session. Finally power was averaged along time, obtaining one value for each component. Components that exceeded mean value ± standard deviation were chosen for further analysis. After the components of interest have been selected, they were back projected to obtain a new EEG signal (reconstructed EEG). A Fast Fourier Transform (FFT) analysis was applied on the time series of the selected channel (where the IED activity is clearly visible) for epochs acquired during each fMRI volume. Then the power time course created for all volumes was used to form the EEG regressor used in GLM analysis.

Discussion

The aim of the research project here described is the development of an innovative procedure for integrating neurophysiological and functional neuroimaging data.

In fMRI processing the selection of the experimental paradigm as difference between task and rest conditions is of great importance, in fact the information related to the experimental events and to the rest condition are to be used as input in GLM analysis. Regressors of interest are typically obtained by convolving impulses or boxcar functions, which are representations of the events or conditions of interest, with a model of the BOLD response (HRF). In the study of spontaneous EEG activity without a task condition we can use the EEG signal to derive the input for GLM.

In literature several methods for the analysis of simultaneous acquired EEG-fMRI data are proposed. The aim is to find regions of BOLD change linked to the

discharges. In the conventional approach each event is marked by visual inspection of the EEG data recorded in the scanner, then a series of identical impulses functions (delta functions) are created and convolved with a canonical HRF, obtaining the regressor for a GLM.

The methods presented in Formaggio et al., 2008 and Manganotti et al., 2008 are two attempts of EEG and fMRI integration. However in the first study signals were recorded simultaneous but their correlation analysis was as whether they were recorded in separate sessions, while in the second one we used a conventional approach based on the creation of the regressor as a set of stick functions representing the timing of IED activity. Hence the necessity to developed a new method of integration.

The new method aimed to improve upon existing methods since the epileptiform activity, recorded from a scalp EEG, is used to modulate changes in BOLD signal. ICA decomposition is used to identify signals representing activity of interest but one of the major difficulties is their identification. We proposed an automatic selection based on wavelet analysis, because typically IEDs activity is higher in amplitude than background activity and its power increases. The reconstructed EEG signal is obtained with the only contribution of the selected components, method used in many studies to remove artifact from EEG traces. Like in the resting state studies, where alpha rhythm or its spectrum is used as a regressor in GLM analysis, the power time series of EEG signal is used as GLM input. Using conventional approach each event is treated as equal, although epileptic spikes may vary in amplitude, duration and also in appearance. They ignore the fact that IED activity is continuous and contains also fluctuating subthreshold epileptic activity, not clearly seen on surface EEG recordings. In contrast, such meaningful information is contained in the ICA factors employed in our method.

Analysis of in silico data validates the method, since demonstrates the reliability of reconstructed IED regressor. All five patients with partial epilepsy we enrolled in this study had frequent interictal focal slow wave activity on routine EEG. In all continuous EEG-fMRI recording sessions, after fMRI artifact removal, we obtained a good quality EEG that allowed us to detect spontaneous IEDs and analyze the related BOLD activation. In their focal distribution, these BOLD activations resembled the focal IEDs seen on routine scalp EEG and EEG recorded during EEG-fMRI sessions; and they are in agreement with the clinical history of the patients.

We plan to increase the number of patients and also test this method on EEG with various patterns other than the epileptiform discharges, for example in resting state analysis where, like in the context of epilepsy, the activation task used to drive GLM analysis is missing. For this reason EEG signal is necessary to evaluate hemodynamic changes in fMRI and its analysis is fundamental to derive informations on the electrical activity.

Even if it is believed that the HRF to epileptic spikes does not vary significantly from that to external stimuli, HRF could shows different peak times or even non canonical shape in the epileptogenic zone. This observation may be advanced as a working hypothesis for further investigating the choice of HRF in patients with epilepsy; future developments possibly involve a study of BOLD signal in this category of patients, and its relation with the electrical activity. In this way the sensitivity of EEG-fMRI studies in epilepsy could be improved with the use of different HRFs.

Moreover, in the future, we will test the integration method to data filtered with the new algorithm in order to conclude this project.

SOMMARIO

Introduzione

La registrazione simultanea fra l'elettroencefalogramma (EEG) e la risonanza magnetica funzionale (fMRI) è un importante strumento nel campo del neuroimaging funzionale che unisce l'alta risoluzione spaziale delle immagini fMRI (1-2 mm) con l'alta risoluzione temporale dell'EEG (ms). Registrare il segnale EEG durante l'acquisizione di immagini fMRI permette di identificare l'attività cerebrale e di ottenere informazioni localizzatorie sui generatori di tale attività. Nonostante i numerosi problemi legati alla presenza di artefatti sul segnale e sulle immagini, dovuti all'interazione fra le due apparecchiature, tale metodica si sta affermando e rafforzando all'interno delle neuroscienze.

I campi di applicazioni sono diversi e in particolare la coregistrazione EEG-fMRI può essere utilizzata per studiare e descrivere l'attività elettrica spontanea durante una condizione di riposo (resting state), durante il sonno o causata da forme di epilessia. Molti pazienti con una forma di epilessia farmaco-resistente non possono sottoporsi ad un intervento chirurgico, in quanto la semplice risonanza magnetica non permette l'individuazione della sorgente epilettogena. In questo senso la registrazione simultanea dell'EEG e della fMRI permetterebbe l'identificazione di una possibile sorgente, legata direttamente all'attività elettrica del paziente. Il cambiamento dell'attività neuronale, infatti, è associato ad un cambiamento del rapporto di concentrazione nel sangue fra l'emoglobina ossigenata e quella deossigenata e tale cambiamento può essere misurato attraverso l'effetto BOLD (Blood Oxygen Level Dependent). Le attivazioni cerebrali, infatti, sono date da alterazioni coordinate dell'attività elettrica regionale e del flusso sanguigno cerebrale. La tecnica di coregistrazione EEG-fMRI permette di evidenziare, nel momento in cui si verifica un evento elettrico, un'area di alterato contenuto di desossiemoglobina dovuta ad un aumentato afflusso ematico nella zona cerebrale che genera tale segnale EEG.

In genere l'fMRI è usata in studi in cui è presente una condizione sperimentale che differisce da una condizione di riposo, entrambe controllate da un operatore. Il principio base dell'analisi fMRI è il confronto tra un'attività basale cerebrale ed un'attività dovuta ad un evento da studiare (spontaneo o evocato), al fine di ottenere una variazione relativa di flusso ematico. Nello studio dell'epilessia si può considerare l'EEG a riposo come condizione di controllo mentre come condizione sperimentale può essere usato il segnale EEG caratterizzato dalla presenza di eventi parossistici (crisi o attività intercritica). L'analisi convenzionale applicata ai dati EEG-fMRI consiste nell'individuazione visiva da parte del neurologo degli intervalli temporali di interesse, che caratterizzano l'attività intercritica del paziente. Dalla convoluzione degli eventi, rappresentati matematicamente da impulsi, con un modello di risposta emodinamica (haemodynamic response function: HRF), si ottiene il regressore utilizzato nell'analisi General Linear Model (GLM). Si producono così mappe di elevata risoluzione spaziale delle aree cerebrali che generano l'evento patologico osservato. Inoltre l'EEG-fMRI associata ad altre metodiche come video-EEG, risonanza magnetica nucleare (RMN) convenzionale, tomografia computerizzata ad emissione di fotoni singoli (SPECT), tomografia ad emissione di positroni (PET), spettroscopia ecc. contribuisce allo studio di pazienti epilettici candidati alla terapia chirurgica.

Lo scopo della presente tesi è quello di sviluppare un metodo automatico, basato sull'analisi delle componenti indipendenti (ICA), per individuare l'attività intercritica in esame, al fine di utilizzare il segnale EEG in toto per la generazione di mappe di attivazione fMRI.

Il Nuovo Metodo

La qualità dei dati è molto importante nel processo di integrazione; pertanto è necessario applicare un pre-processing ad entrambe le tipologie di dati. Mentre tale elaborazione è standard per i dati fMRI, non lo è per i dati EEG. In letteratura sono stati sviluppati diversi metodi per rimuovere l'artefatto da gradiente di campo magnetico e quello da pulsazione cardiaca. Il metodo per la rimozione dell'artefatto da gradiente implementato nel nostro sistema di acquisizione EEG non ha dato dei risultati completamente soddisfacenti in alcune situazioni. Pertanto è stato necessario

implementare un nuovo metodo. Tuttavia l'implementazione di questo nuovo filtro è iniziata contemporaneamente all'implementazione del nuovo metodo di integrazione EEG-fMRI e la sua applicazione su segnali di pazienti epilettici è ancora in atto. Per questi motivi e per non introdurre ulteriori variabili nella validazione del metodo di integrazione, è stato deciso di utilizzare l'algoritmo implementato nel software di acquisizione EEG.

In seguito ad un pre-processamento dei dati, caratterizzato da un cambio di referenza e da opportuni filtraggi, è stato applicato il metodo delle componenti indipendenti. L'ICA è una tecnica statistica che permette di individuare le componenti che stanno alla base di una serie multidimensionale di dati, assumendo che le sorgenti siano statisticamente indipendenti e la loro distribuzione non sia gaussiana. Tale analisi è stata effettuata utilizzando l'algoritmo FastICA implementato in EEGLAB ed ha prodotto un numero di componenti per ciascun tracciato pari al numero dei canali EEG.

Il nuovo metodo può essere suddiviso in 4 passaggi:

- Selezione delle componenti
- Ricostruzione del segnale EEG
- Selezione del canale ed analisi FFT
- Costruzione del regressore EEG

Il punto cruciale è la scelta delle componenti che descrivono l'attività intercritica in esame. Per ogni componente si è calcolata la trasformata wavelet continua negli intervalli di interesse che fornisce i valori di potenza nel tempo in funzione della frequenza. Selezionando la frequenza massima si è ottenuto un segnale dipendente esclusivamente dal tempo. Successivamente è stato calcolato il valore medio nell'intervallo temporale e sono state scelte le componenti con più elevata potenza. In seguito si è ricostruito il segnale EEG utilizzando solo il contributo delle componenti scelte. E' stata applicata un'analisi in frequenza utilizzando la Fast Fourier Transform (FFT) ad epoche di durata pari al tempo di acquisizione di un volume di fMRI; la potenza ottenuta è stata convoluta con la risposta emodinamica scelta ottenendo un modello chiamato 'regressore' usato successivamente nella stima GLM dell'analisi fMRI.

Questo metodo è stato validato utilizzando dati simulati, ed in seguito applicato a due datasets: il primo composto da due soggetti sani a cui è stata fatta la

coregistrazione EEG-fMRI durante apertura e chiusura degli occhi, il secondo composto da 5 pazienti con epilessia parziale a cui è stata fatta la registrazione simultanea in condizione di riposo.
L'applicazione del metodo ai dati simulati ha portato alla sua validazione. In tutte e tre le simulazioni si sono ottenute delle forme d'onda, rappresentanti i regressori, molto simili ai regressori assunti come "veri". Nei due soggetti sani, che hanno svolto un task di apertura e chiusura degli occhi, l'analisi ha prodotto un'attivazione degli occhi ed una deattivazione occipitale, in accordo con i networks ormai noti dalla letteratura. Per quanto riguarda i pazienti, l'integrazione dei due segnali ha portato ad attivazioni concordi con l'attività elettrica e con il loro quadro clinico in 4 pazienti su 5. Le componenti scelte in base al metodo rispecchiano visivamente l'attività parossistica visibile nel tracciato EEG registrato durante acquisizione fMRI e confrontato con l'EEG standard acquisito di routine.

Discussione

In questo lavoro è stato presentato un nuovo metodo di integrazione fra un segnale neurofisiologico (EEG) e dati di neuroimaging funzionale (fMRI), basato sull'analisi delle componenti indipendenti.
Il paradigma sperimentale (protocollo) è un dato molto importante per l'analisi fMRI, infatti le informazioni legate al task e alla condizione di riposo sono utilizzate come ingresso nell'analisi GLM. In assenza di un task, come nello studio dell'epilessia, è necessario utilizzare il segnale EEG per pilotare l'analisi GLM.

In letteratura sono stati proposti diversi metodi di integrazione. Nell'approccio convenzionale il protocollo, formato dagli intervalli temporali degli eventi di interesse individuati in seguito ad ispezione visiva, viene convoluto con un modello di risposta emodinamica, ottenendo il regressore per l'analisi GLM.
I metodi presentati in Formaggio et al., 2008 e in Manganotti et al., 2008 rappresentano due primi tentativi di integrazione. Tuttavia nel primo studio i segnali vengono analizzati come se fossero stati acquisiti in due sessioni separate, mentre nel secondo studio viene utilizzato l'approccio convenzionale. Da qui la necessità di sviluppare un nuovo metodo di integrazione.

Il nuovo metodo ha lo scopo di migliorare quelli già esistenti sfruttando l'informazione derivante da tutto il segnale EEG e non tenendo conto dei soli intervalli temporali di interesse. Il punto cruciale è l'identificazione del segnale legato all'attività di interesse. E' stato proposto un metodo automatico per facilitare tale scelta, basato sulle trasformate wavelet e valorizzando il contenuto energetico del segnale. Il segnale EEG ricostruito è ottenuto con il solo contributo delle componenti scelte ed in fine la sua potenza spettrale viene utilizzata come ingresso nell'analisi GLM.

Uno degli scopi futuri sarà quello di aumentare il numero dei pazienti e di testare il metodo anche su altre tipologie di EEG, come ad esempio quello legato alla condizione di resting state. Anche in questo caso, infatti, manca la presenza di un task che possa pilotare l'analisi GLM, e l'EEG risulta l'unico strumento di informazione per poter arrivare a delle mappe di attivazione.

Un ulteriore progetto futuro è legato alla scelta della risposta emodinamica HRF. Tale risposta potrebbe non essere identica a quella ottenuta in seguito ad un task o ad uno stimolo esterno; il suo picco e la sua forma potrebbero infatti essere diversi nella zona epilettogena. In questo senso la sensibilità degli studi EEG-fMRI nell'epilessia potrebbe migliorare utilizzando diverse HRF.

In fine verrà applicato il nuovo metodo di integrazione a dati EEG filtrati con il nuovo algoritmo sviluppato.

INTRODUCTION

Electroencephalography (EEG) has been a key tool in the study of the brain for decades (Caton, 1875; Berger, 1929). However, despite its multiple clinical and research uses, such as in epilepsy, sleep staging and psychophysiology, little is yet known about underlying generators of EEG activity in humans. Functional magnetic resonance imaging (fMRI) recorded simultaneous with EEG may provide a method for localizing and identifying these sources. By using the EEG signal as a reference for fMRI maps generation, EEG-fMRI coregistration studies enables to non invasively investigate human brain function and to find the direct correlation of these two important measures of brain activity. Neither of these technologies alone can provide informations on the spatio-temporal aspects of human brain processing.

In fact, fMRI has an excellent spatial resolution and allows the localization of brain regions in which there is a change in the level of neuronal activity during an experimental condition compared to a control condition. This change is accompanied by a change in the ratio of concentration of oxy- and deoxy- hemoglobin in the blood. This change can be measured through the Blood Oxygen Level Dependent (BOLD) effect (Bandettini et al., 1992; Kwong et al., 1992; Ogawa et al., 1992). However fMRI has a poor temporal resolution (on the order of seconds).

In contrast, EEG measures neuronal currents directly from the subject's scalp with a high temporal resolution in the range of milliseconds; however it is difficult to determine the exact location of the current sources (poor spatial resolution) because of lack of precise information regarding individual geometry and conductivity as well as the limited number of EEG channels. In recent years, many progresses have been made to enhance the spatial resolution of the conventional EEG by means of high resolution EEG approaches, which largely overcome the head volume conductor effect. However few attempts have been made to recording simultaneous high density EEG and fMRI.

Combined recordings aim to overcome the spatial limitations of EEG and the temporal limitations of fMRI, using their complementary features. By using the EEG

signal as a reference for fMRI maps, concurrent EEG-fMRI opens a new avenue for investigating specific brain function.

The first report describing an EEG recording in a magnetic resonance imaging (MRI) scanner in humans (Ives et al. 1993) revealed the potential for combining simultaneous neurophysiologic and imaging recordings. Subsequent studies have shown that EEG can be safely measured in a clinical MRI scanner using specially developed EEG equipment (Lemieux et al. 1997; Allen et al. 1998, 2000).

However high frequency gradient and radio-frequency pulsies induce large artifacts that obscure the EEG. To overcome this difficulty, especially in epilepsy studies, the EEG was monitored while the patient is in the magnet but in the absence of scanning and then functional scanning was triggered manually after identification of inter-ictal spikes in the EEG record (Ives, 1995; Warach et al., 1996; Seeck et al., 1998; Krakow et al., 1999; Patel et al., 1999; Symms et al., 1999). With this method we loose the temporal match between relevant changes in the EEG, such as subsequent spike activity, and they can not be seen during functional scanning.
Under the assumption that the response of the brain to a set of stimuli or conditions is the same when acquired at different times, several groups (Singh et al., 1998; Babiloni et al., 2001; Baillet et al., 2001) have analysed EEG and fMRI data acquired separately. More recently, methods have been described for the concurrent collection of EEG and fMRI data (Goldman et al., 2000; Eichele et al., 2009; Marques et al., 2009), thus allowing continuous monitoring of the EEG during functional scanning and a direct relationship between the two signals.

Another available functional neuroimaging techniques based on hemodynamic principles is near-infrared spectroscopy (NIRS). Over the last few decades, NIRS has been attracting interest from the psychology and medical imaging communities for its ability to non-invasively measure the cerebral hemodynamic changes associated with functional brain activity (Jobsis, 1977; Delpy et al., 1987; Cope et al., 1988; Villringer and Chance, 1997). NIRS is an optical spectroscopy technique which uses time-resolved, multi-wavelength measurements to infer changes in the optical absorption of tissue and thereby to report changes in oxy- and deoxy-hemoglobin, the two primary absorbing chromophores in biological tissue that vary dynamically with a functional task. Similar to fMRI, NIRS-based brain studies can be used to record changes in cerebral blood oxygenation during the performance of a specific activation task.

By taking advantage of the feasibility of simultaneous recording of EEG during the NIRS data acquisition, Horovitz and Gore (2004) measured event related potential (ERP) and near-infrared optical topography, and demonstrated correlation of two measurements in the language-related area. However, spatial resolution of diffuse optical measurements is less than fMRI and these technique are often used together.

The possibility to record the EEG within the MR scanner has recently opened the way to the study of spontaneous brain activity with fMRI. Combined EEG-fMRI techniques have been used to identify the neural correlates of clinically or behaviorally important spontaneous EEG activity, such as interictal spikes, the alpha rhythm in resting state, and sleep waves. The area where the greatest progress has been made is epileptic seizure localization, and the common method of integrating EEG and fMRI data is to transform EEG data into a physiologically meaningful input to be used in a voxel-based General Linear Model (GLM) (Salek Haddadi et al., 2003). Another strategy for EEG-fMRI integration is to use the results of fMRI analysis as a priori knowledge for imaging the continuous distribution of EEG source over the entire cortical surface, namely fMRI-constrained cortical current density estimation (Liu et al., 1998; Babiloni et al., 2003). In this application the use of fMRI solutions (statistically significant voxels) as a priori information improved the spatial resolution of linear inverse EEG source estimation.

EEG-fMRI research in the field of epilepsy have been summarized in (Salek-Haddadi et al., 2003; Hamandi et al., 2004; Lemieux, 2004; Yu et al., 2005; Gotman et al., 2006; Stern, 2006). In the clinical context, the obvious potential use of EEG-fMRI is a noninvasive tool to localize epileptic activity as part of presurgical evaluation of patient with focal epilepsy. It is important, therefore, to assess the sensitivity and specificity of EEG-fMRI data, in order to evaluate the reliability of the results, but only a few reports exist in which the reliability has been determined against intracranial EEG recordings (Al-Asmi et al., 2003; De Tiege et al., 2007).

The present work, in collaboration with the Department of Neurological and Vision Sciences at the University of Verona, presents an innovative approach for combining electric and hemodynamic responses of the brain, that were simultaneous recorded. We describe a novel automatic method, based on Independent Component Analysis (ICA), to detect interictal epileptic activity in order to obtain an EEG information for fMRI analysis. One major goal is to provide an alternative method to

integrate these signals compared to our previous works (Formaggio et al., 2008; Manganotti et al., 2008) and to published methods.

In **chapter 1**, simultaneous EEG-fMRI technique and its applications, source localization and the study of spontaneous EEG activity, are described.

In **chapter 2** technical issues related to EEG quality, such as gradient and pulse artifacts, are described and methods to solve them are discussed.

In **chapter 3** two conventional methods used for the EEG and fMRI integration are presented and evaluated.

In **chapter 4** the steps of the novel method based on ICA decomposition are described, namely selection of components, reconstruction of EEG signal, selection of channel and FFT analysis and construction of EEG regressor.

In **chapter 5** dataset, experimental paradigm and analysis, based on the application of the novel method, are described.

In **chapter 6** the results obtained in silico and on real data are reported.

Chapter 1

EEG-fMRI COREGISTRATION IN EPILEPSY

The possibility to record the EEG within the MR scanner has opened the way to the study of spontaneous brain activity with fMRI. EEG-fMRI technique is used to investigate the hemodynamic changes associated with spontaneous brain activity in epileptic networks, but also to study endogenous brain rhythms of wakefulness and sleep. A more general method for combining EEG and fMRI data is also to use spatial information based on structural and fMRI data to constrain the location of EEG sources.

1.1 EEG

An EEG signal is a measurement of currents that flow during synaptic excitations of the dendrites of many pyramidal neurons in the cerebral cortex. When neurons are activated, the synaptic currents are produced within the dendrites. The current generates a magnetic field measurable by magnetoencephalography (MEG) and a secondary electrical field over the scalp measurable by EEG systems. The scalp EEG is an average of activities of many small zones of the cortical surface beneath the electrode. The International Federation of Societies for Electroencephalography and Clinical Neurophysiology has recommended the conventional electrode setting (also called 10-20) which is illustrated in Figure 1.1. The name 10-20 indicates the fact that the electrodes along the midline are placed at 10, 20, 20, 20, 20, and 10 % of the total nasion – inion distance; the other series of electrodes are also placed at similar fractional distances of the corresponding reference distances. The odd electrodes are on the left and the even ones on the right.

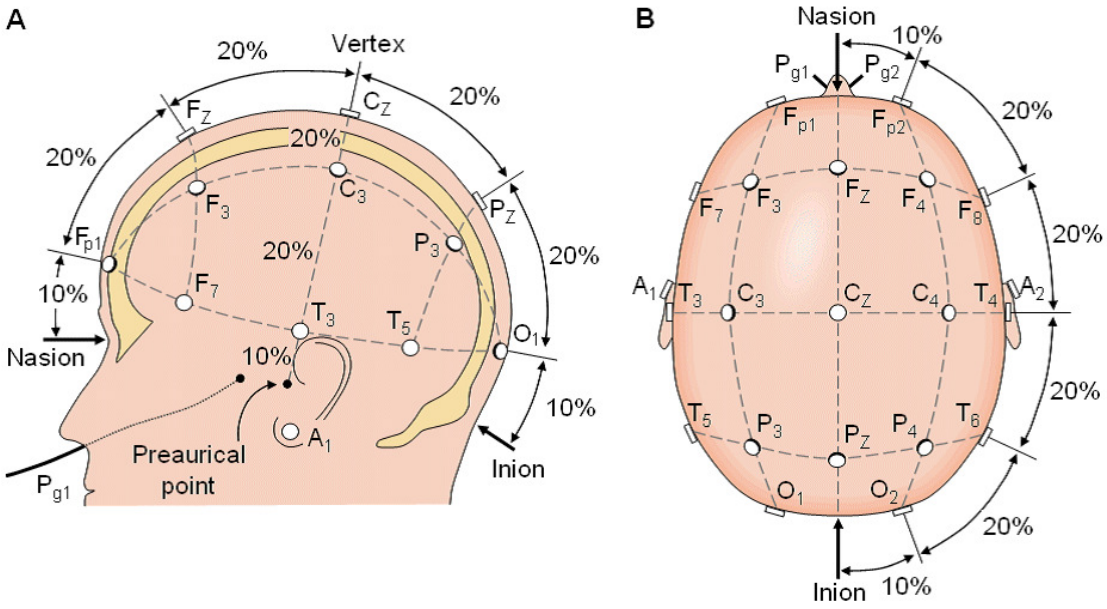

Figure 1.1. The international 10/20 system. A. Nasion, inion and ocular lobes are the anatomical landmarks used for the essential positioning of the EEG electrodes. B. T-temporal, C-central, Fp-prefrontal, F-frontal, P-parietal, O-occipital. Even numbers indicate right side, odd numbers left sides.

EEG signals exhibit several patterns of rhythmic or periodic activity (Fig. 1.2). The commonly used terms for EEG frequency (f) bands are:

- Delta (δ): $0.5 \leq f < 4$ Hz
- Theta (θ): $4 \leq f < 8$ Hz
- Alpha (α): $8 \leq f < 13$ Hz
- Beta (β): $13 \leq f < 30$ Hz
- Gamma (γ): $f \geq 30$ Hz

Delta waves are primarily associated with deep sleep and may be present in the waking state.

The term theta might be chosen to allude to its presumed thalamic origin. Theta rhythm appear as consciousness slips towards drowsiness. Larger contingents of theta wave activity in the waking adult are abnormal and are caused by various pathological problems.

The alpha rhythm is the principle resting rhythm of the brain and is common in wakeful, resting state, especially in the occipital area with bilateral synchrony. Auditory and mental arithmetic tasks with the eyes closed lead to strong alpha waves, which are suppressed when the eyes are opened.

A beta wave is the usual waking rhythm of the brain associated with active thinking, active attention, focus on the outside world, or solving concrete problems, and is found in normal adults. It is encountered over the frontal and central regions.

The frequencies above 30 Hz correspond to the gamma range. Gamma rhythms appear to be involved in higher mental activity, including perception and consciousness.

Waves in frequencies much higher than the normal activity range of EEG, mostly in the range of 200-300 Hz, have been found in cerebellar structures of animals, but they have not played any role in clinical neurophysiology.

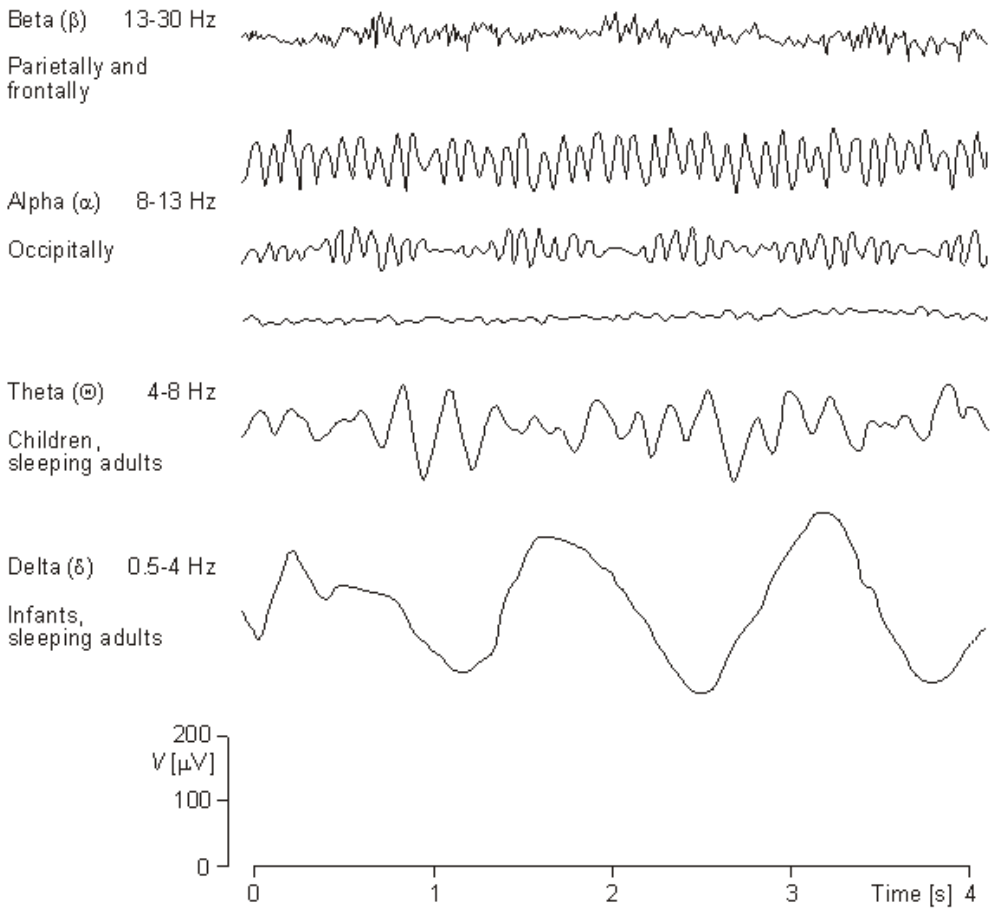

Figure 1.2. Four typical dominant brain normal rhythm, from high to low frequencies.

1.1.1 EEG and epilepsy

An EEG is said normal if it lacks abnormal patterns known to be associated with clinical disorders. One of the most common known neurological disorders is epilepsy. Epilepsy is a symptom of excessive, disorderly, neuronal discharge, clinically characterized by discrete attacks (seizures). It is known that seizures are the results of sudden, usually brief, excessive electrical discharges in a group of brain cells (neurons) and that different parts of the brain can be the site of such discharges. The clinical manifestation of seizures vary and depend on where in the brain the disturbance first starts and how far it spreads. Transient symptoms can occur, such a loss of awareness or consciousness and disturbances of movement, sensation, mood or mental function. Epilepsies are classified in five ways:

1. By their first cause (or etiology).
2. By the observable manifestations of the seizures, known as semiology.
3. By the location in the brain where the seizures originate.
4. As a part of discrete, identifiable medical syndromes.
5. By the event that triggers the seizures, as in primary reading epilepsy or musicogenic epilepsy.

Seizure types are organized firstly according to whether the source of the seizure within the brain is localized (partial or focal onset seizures) or distributed (generalized seizures). Partial seizures are further divided on the extent to which consciousness is affected. If it is unaffected, then it is a simple partial seizure; otherwise it is a complex partial (psychomotor) seizure. A partial seizure may spread within the brain - a process known as secondary generalization. Generalized seizures are divided according to the effect on the body but all involve loss of consciousness. These include absence (petit mal), myoclonic, clonic, tonic, tonic-clonic (grand mal) and atonic seizures.

While various clinical symptoms, such as loss of consciousness and uncontrolled motor activity, occur during seizures, EEG changes in the period between seizures, interictally, are not accompanied by clinical symptoms. These interictal epileptiform discharges can occur in various forms, such as spikes, poly-spikes and sharp waves and are believed to be the result of summated membrane events from abnormally hypersynchronous neurons within epileptic tissue.

So far no automatic classification of these seizures based on the EEG waveforms has been reported. This is due to the wide variety of shapes of these transient signals and their similarities to waves which are part of the background activity and to impulsive artifacts. The difficulties encountered lie in the time-varying characteristics of both relevant signals (not perfectly known signal) and noises (superposition of transient artifacts and locally stationary activities), and in the unknown firing rate of the interictal events. The clinical interpretation of EEG attempts to link pathological features (clinical symptomatology) with visual inspection and pattern recognition of EEG. Although this traditional analysis is quite useful, visual inspection of the EEG is subjective and hardly allows any systematization. Seizure detection and classification using signal processing methods has been an important issue of research for the last two decades. Researchers have tried to highlight different signal characteristics within various domains and classify the signal segments based on the measured features.

1.2 fMRI

fMRI is a type of MRI scan. It measures the hemodynamic response (change in blood flow) related to neural activity in the brain or spinal cord of humans or other animals. It is one of the most recently developed technique for neuroimaging. Since the early 1990s, fMRI has come to dominate the brain mapping field due to its low invasiveness, absence of radiation exposure, and relatively wide availability.

During the resting state condition local oxygenation concentrations are relative low, so blood contains a high concentration of the deoxyhaemoglobin, which is paramagnetic (it locally increases the static magnetic field), whereas the oxyhaemoglobin is diamagnetic. After neuronal activation, more oxygen is transported to the site of activation via an increased Cerebral Blood Flow (CBF), leading to a washout of the deoxyhaemoglobin and an increased concentration of the oxyhaemoglobin. These changes lead to an increase in BOLD signal, that indirectly reflects neuronal activation. BOLD signal is widely used to detect and delineate brain regions in which activation levels change in response to specific stimuli and tasks.

Fig. 1.3 shows a typical signal time course following neuronal activation associated with an external stimulus or spontaneous brain activity, the so-called haemodynamic

response (HDR). Initially there is a signal decrease (initial dip) of 1 to 2 s duration that has been attributed to a transient increase in the amount of deoxyhaemoglobin. Subsequently there is a positive BOLD response that persists for about 5-10 s, growing to a maximum value at about 5 s for a short duration stimulus. This maximum is known the peak of the haemodynamic response. Then, up to 30 s after the onset of the stimulus, there is a signal undershoot.

HDR is mathematically represented by a model called haemodynamic response function (HRF). The literature presents a variety of HRF models, such as standard models (Poisson, Gaussian, spline-like functions), or models using a basis sets (Fourier sines and cosines, finite impulse response, canonical HRF plus temporal and dispersion derivatives).

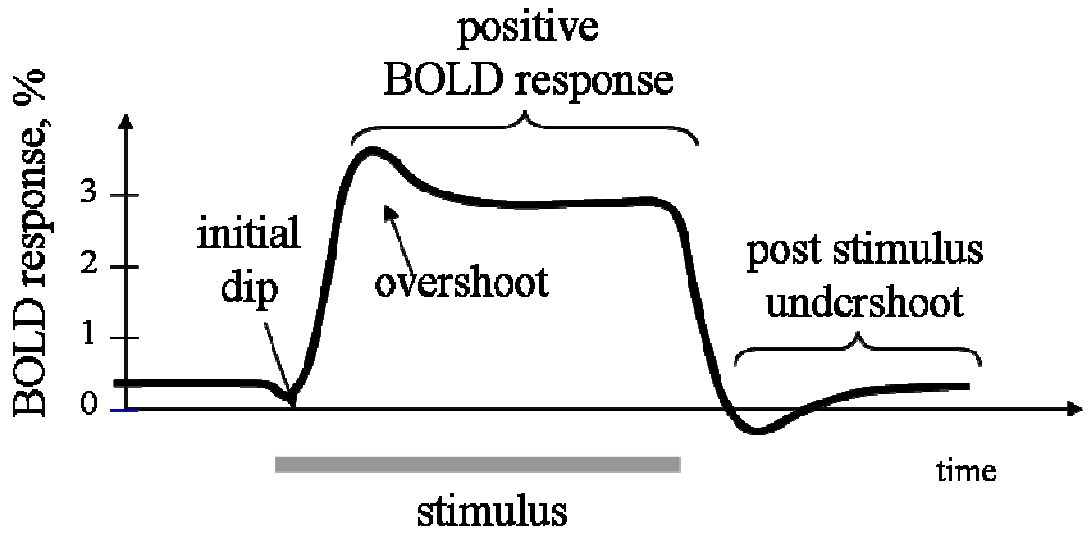

Figure 1.3. A typical HDR following a stimulus.

1.3 EEG-fMRI coregistration in epilepsy

The presurgical evaluation of patients with epilepsy is one of the areas where combining EEG and fMRI has considerable clinical relevance. EEG-fMRI has been used extensively in patients with epilepsy in recent years (Krakow et al., 2001; Jäger et al., 2002; Al Asmi et al., 2003; Archer et al., 2003).

Many patients with drug-resistant focal seizures cannot undergo epilepsy surgery because standard MRI scans fail to visualize a clear epileptic source.

Localizing the epileptogenic zone is difficult for several reasons. First, the spatial relationship between the epileptic source and irritative and ictal onset zones may be hard to establish, even if they are closely spatially related (Ebersole et al., 1991; Benbadis et al., 1996). Second, seizures are difficult to assess inside the scanner. And third, epileptic discharges may be too weak to elicit MRI changes that will localize the epileptic zone, hence the interest in highly sensitive diagnostic techniques that can record interictal epileptiform discharges (IEDs) and concurrently visualize on neuroimaging the corresponding irritative area thus reliably identifying brain areas where seizures arise and those to which they spread. A non-invasive diagnostic technique that provides valuable information for localizing the brain regions generating interictal epileptiform activity is simultaneous EEG and fMRI recording. EEG would provide high temporal resolution for precise timing of epileptiform activity and fMRI would provide high spatial resolution for precise spatial localization of epileptifotm activity. This approach has been frequently employed for the exploration of interictal as well as ictal epileptic activity with the objective of localizing epileptic foci and characterizing the relationship between epileptic activity and the hemodynamic response. Indeed hemodynamic and metabolic changes are associated with epileptiform activity. In 1934, Gibbs et al. used intracarotid temperature measurements to demonstrate an increase in cerebral blood flow during seizures compared to baseline in humans. EEG correlated fMRI is a rapidly developing non-invasive imaging technique that can map regional changes in the BOLD signal that are time-locked to IEDs identified on the simultaneously recorded EEG. In its current form, EEG-fMRI can reveal maps showing regions of BOLD change correlated to IEDs.

The first EEG–fMRI studies using EEG-triggered scanning (Krakow et al., 1999; 2001) confirmed that EEG-fMRI can noninvasively identify brain activation associated with subclinical IEDs at a high spatial resolution but achieved low diagnostic sensitivity (60%). Later studies (Lazeyras et al., 2001; Lemieux et al., 2001; Benar et al., 2002, 2006; Al-Asmi et al., 2003) showed that continuous EEG-fMRI acquisition is better than EEG-triggered recording because it allows offline analysis after artifact subtraction and provides better sensitivity (80%). Others used EEG-fMRI to analyse the various epileptiform syndromes (Boor et al., 2003; Salek-Haddadi et al., 2003, 2006; Aghakhani et al., 2004, 2005; Bagshaw et al., 2004, 2006; Gotman et al., 2004, 2005; Kobayashi et al., 2005, 2006 a, b, c, d; Laufs et al.,

2006). Additional studies using stereotaxic EEG (sEEG) and electrocortical mapping (Krakow et al., 1999; Benar et al., 2006; Kobayashi et al., 2006d) confirmed the co-localization between IEDs and fMRI activation.

fMRI is mostly used in the study of sensory, motor and cognitive functions, where there is a difference between experimental condition and control condition. In the context of epilepsy, one can consider the control condition to occur when the EEG is at baseline and experimental condition to correspond to the presence of an epileptic discharge. When EEG and fMRI are correlated, one has to account for the fact that there might be a delay of several seconds between the appearance of an EEG event, which is an instantaneous reflection of superimposed local neural activities, and the BOLD signal, which reflects the hemodynamic response of the local electrical activity. Another important issue include the fact that, despite the many technical advances in the EEG-fMRI field, the quality of EEG recorded during scanning in most centers is good, but not identical to that recorded outside the scanner. As a result, smaller epileptiform discharges may be missed, thereby reducing the statistical power of the study. Besides scalp EEG is particularly sensitive to dipole movement vectors produced at right angles to the scalp close to the cortical surface and the amplitude of a discharge on EEG is primarily influenced by the orientation/geometry of the current source, the area of source, as well as synchrony of elements within the volume. As a result, epileptiform activity may not appear on scalp EEG until it has involved sufficient tissue area developed enough synchrony. It has been shown that scalp EEG recordings can represent sites of seizure propagation instead of seizure initiation. Thus, the complex relationship of scalp EEG to intracranial source generators precludes fMRI from completely colocalizing with it, but there still remains significant overlap. fMRI is sensitive to metabolic changes in a given brain volume, so BOLD responses to epileptiform discharges may involve areas of discharge generation and/or propagation.

EEG-fMRI maps have shown significant BOLD increases and decreases both near to and distant from the presumed irritative zone (regions involved in IED generation). Some authors have focused their attention only on positive BOLD response; the neurophysiological mechanism of negative BOLD changes particularly when correlated to IEDs remains unclear and may reflect decreases in neuronal activity and blood flow.

The conventional analysis of EEG-fMRI data is based on the identification of the timing of IEDs on scalp EEG which are used in GLM analysis to create regressors representing the effects of interest. The model is obtained by the convolution of the EEG events, which are represented as stick functions of unitary amplitude, with a model of the event-related fMRI response, represents by HRF; maps showing regions of significant IED-related change are obtained through voxel-wise fitting of the model and application of appropriate statistical thresholds (Lemieux et al., 2001; Benar et al., 2002; Salek-Haddadi et al., 2003; Hamandi et al., 2004; Gotman et al., 2006).

Besides being a promising clinical tool for an accurate anatomical localization of the generator of the interictal spikes, this technique may provide information on the patho-physiological process underlying the interictal activity, since the metabolic change measured by fMRI is a consequence of the abnormal neuronal activity generating the spikes.

1.4 Equipment and setup

The fMRI technique employs rapidly changing gradient fields and changing radio-frequency electromagnetic fields. In the simultaneous EEG-fMRI acquisition setup changing electrodes magnetic fields induce significant current flow within the electrodes and wires. The EEG equipment in turn may significantly interfere with the quality of the MR images. There are some rules for the reduction of artifacts and possible patient harm in simultaneous EEG-fMRI recordings. The most important are minimizing the area comprised by loops of wires, avoiding motion and avoiding ferromagnetic substances. The use of MR compatible electrodes, paste, safety resistors and fiber optic isolation (Fig. 1.4) provides good patient safety and together with appropriately shielded electronics, impact on image quality is also minimised. Plastic electrode rings with thin layers of silver chloride exhibit low electrode impedance guarantying high sensitivity. Leads are equipped with current limiting resistors to avoid heating and to reduce EEG artifacts. The amplifier is battery powered to avoid radio frequency (RF) induced imaging artifacts and to increase patient safety. It has a dynamic range sufficiently large to prevent saturation. The optic cable ensures the absence of an electrically conductive bridge between the

outside and the inside of the scanner room, which would break the magnetic shielding of the scanner room and deteriorate the quality of MR images. A schematic of our EEG-fMRI set-up is provided in Fig. 1.5. The MR compatible EEG amplifier (SD MRI 32, Micromed, Treviso, Italy) is placed at the end of the magnet bore, while the recording computer is placed outside the magnet room via optical fiber cable.

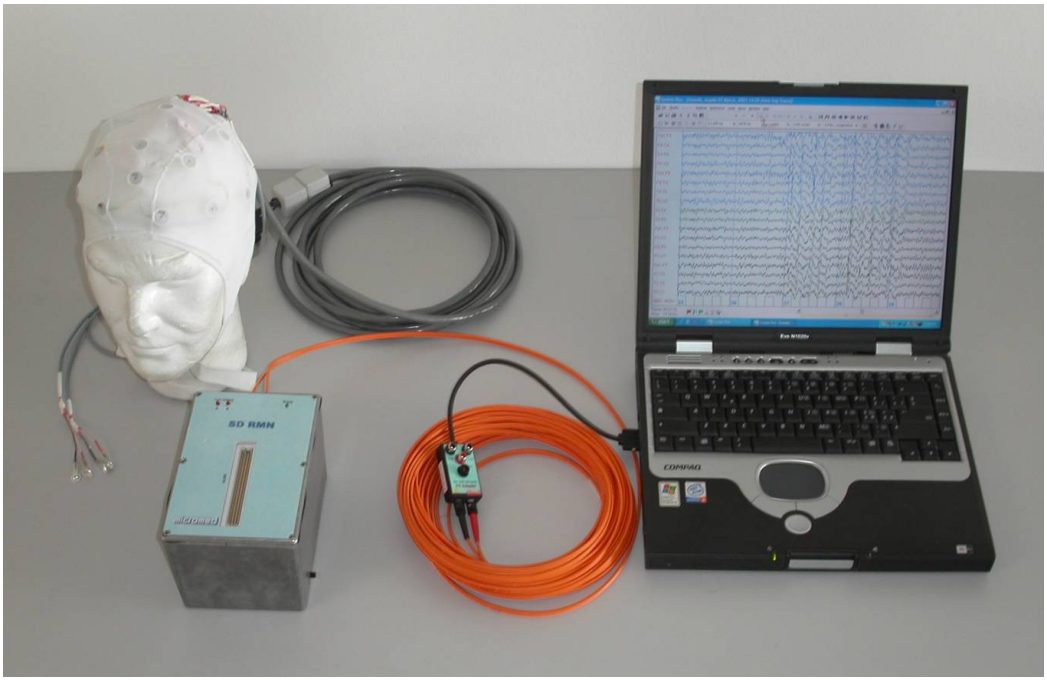

Figure 1.4. EEG-fMRI co-registration equipment.

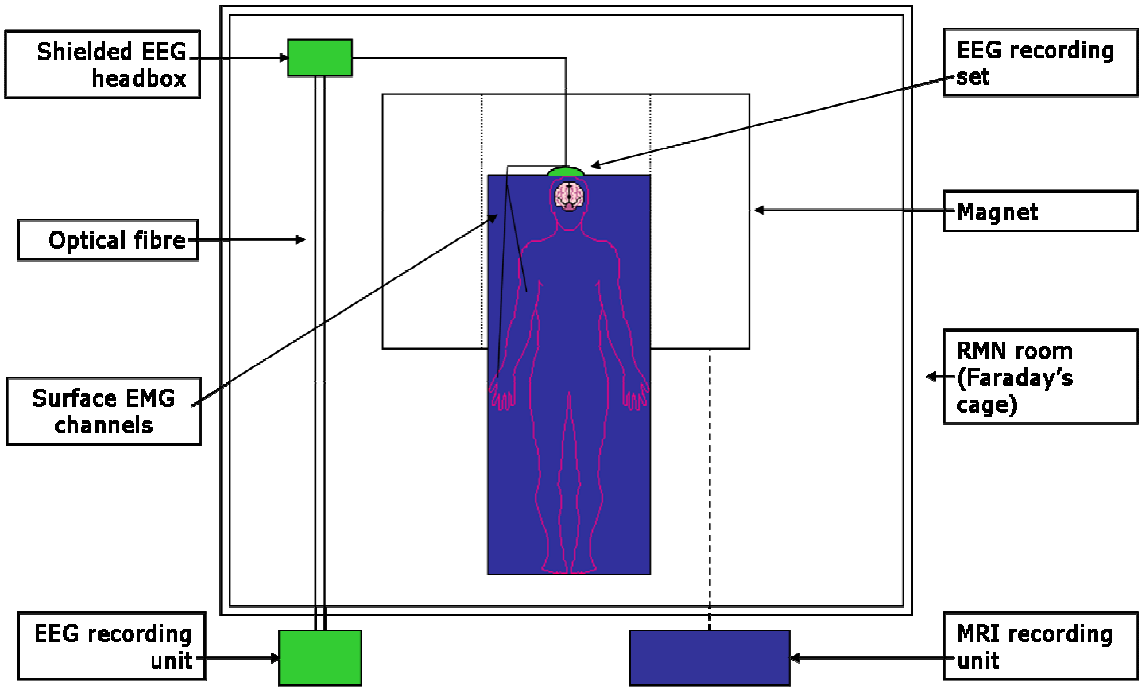

Figure 1.5. Block diagram of the cable and instrumentation layout for obtaining an EEG from a subject during an MRI scan.

1.5 Applications

1.5.1 Spontaneous EEG activity

Combined EEG-fMRI techniques can be used to identify the neural correlates of clinically or behaviourally important spontaneous EEG activity, such as interictal spikes, the alpha rhythm and sleep waves. The common method of integrating EEG and fMRI data is to transform EEG data into a physiologically meaningful input to be used in a voxel-based GLM (Salek-Haddadi et al., 2003).

The alpha rhythm (8-12 Hz) dominates the EEG of an awake subject with closed eyes. It was one of the first phenomena observed in the human EEG by Berger (1929) and has been studied exhaustively; however the functional significance of the alpha rhythm in humans is not known definitively. New insight into brain regions involved has been obtained in recent EEG-fMRI studies (Goldman et al., 2002; Laufs et al., 2003a,b, 2006; Moosmann et al., 2003; Gonçalves et al., 2006; De Munck et al., 2007), where EEG-fMRI measurement is attractive for the investigation of hemodynamic correlates of spontaneous oscillatory EEG signatures. All these studies

were based on a relation between BOLD signal changes, during a resting state condition, and EEG signal. This relation was described by the convolution between the alpha band power and a canonical HRF.
Using EEG-fMRI co-registration during sleep condition a study (Lovblad et al., 1999) reported occipital activation and frontal deactivation during Rapid Eye Movement (REM) sleep. A silent MR sequence was used in order to prevent disruption of sleep. Other groups have used EEG-fMRI to successfully stage sleep, but not to address the fMRI changes associated with various specific sleep EEG phenomena. The combination of silent fMRI and EEG seems to offer a promising technical approach for future sleep studies, which might be useful specifically for sleep disorder research.

1.5.2 Source localization

An application of EEG-fMRI coregistration is in the determination of the location of the cortical sources. Localization of brain signal sources only from EEG has been an active area of research during the last two decades. Such source localization is necessary to study brain physiological, mental, pathological, functional abnormalities, and problems related to various body disabilities, and to specify the sources of abnormalities such as tumours and epilepsy. One common approach uses dipoles to model the neural activity. Dipoles are a good model of electric field generated by specific neural sources that are active above the background EEG. However, the different electrical conductivity of brain, skull, and scalp markedly blurs the EEG potential distributions and makes the localization of the underlying cortical generators problematic. In last decade, techniques known as high-resolution EEG had allowed to estimate precisely the cortical activity from non-invasive EEG measurements (Gevins, 1989, 1991, 1999; Nunez, 1995; Babiloni et al., 1997; Michel et al., 1999; He and Lian, 2002; He et al., 2002). This body of EEG techniques includes the use of a large number of scalp electrodes and realistic models of the head derived from structural MRI.

Source localization based on scalp potentials require a solution to an ill-posed inverse problem with many possible solutions. Selection of a particular solution often requires a priori knowledge acquired from the overall physiology of the brain. Neural

sources of EEG can be localized by making a priori hypothesis on their number and extension. The solution space can be reduced by using information deriving from hemodynamic measures (fMRI-BOLD phenomenon). The rationale of a multimodal approach is that neural activity, modulating neuronal firing and generating EEG potentials, increases glucose and oxygen demands (Liu et al., 1998; Magistretti et al., 1999; Dale et al., 2000). This results in an increase in the local hemodynamic response that can be measured by fMRI (Grinvald et al., 1986; Puce et al., 1997). Hence, fMRI responses and cortical sources of EEG data can be spatially related (Logothetis et al., 2001). The contribution of each cortical source to the scalp recorded signals can then be computed, and best-fitting dipole orientations and strengths can be estimated from a linear inverse solution (Scherg and Von Cramon, 1985; Liu et al., 1998; Babiloni et al., 2003). fMRI is used as a priori knowledge in the resolution of the linear inverse problem used for the estimation of the cortical activity.

Chapter 2

ARTIFACTS REMOVAL METHODS

2.1 EEG quality

A major problem in recording EEG during fMRI scanning is due to the presence of artifacts that arise from interactions between the patient, EEG electrode leads, and the magnetic fields in the scanner. Several factors are involved in this reduction, such as small movements of the electrode wires caused by subtle head movements or vibrations of the scanner. Movement of the leads themselves within the static field of the magnet (not during MRI acquisition) induces an electromotive force (EMF) in a wire loop according to Faraday's law:

$$\oint \vec{E} \bullet d\vec{s} = -\frac{d\Phi_B}{dt}, \tag{2.1}$$

where the line integral of $\vec{E}$ around the closed loop *s* is the induced EMF around the loop and the right hand side refers to the rate of change of the magnetic flux $\vec{B}$ through the area bounded by the closed loop.

This movement is also related to heart pulse that produces a *ballistocardiographic artifact* (BCG) clearly visible on EEG recorded inside the MR scanner even in the absence of scanning, and with amplitudes and frequencies that are close to the range of the usual EEG signal (Ives et al., 1993; Muri et al., 1998; Goldman et al., 2000) (Fig. 2.1). During scanning the situation is different. The switching magnetic fields applied during fMRI acquisition may induce an EMF in the electrode leads and in a wire loop. While these currents may be sufficiently small to be safe for the patient, they result in artifacts on the EEG that is normally very large and completely obscures the EEG (Allen et al., 1998, 2000); this is called *gradient artifact* (Fig. 2.2). This is a periodic artifact with multiple spectral lines in

the Fourier spectrum, and the fundamental frequency is governed by scan parameters like repetition time (TR) and number of slices (ns) according to:

$$f = \left(\frac{TR}{ns} \right)^{-1} \tag{2.2}$$

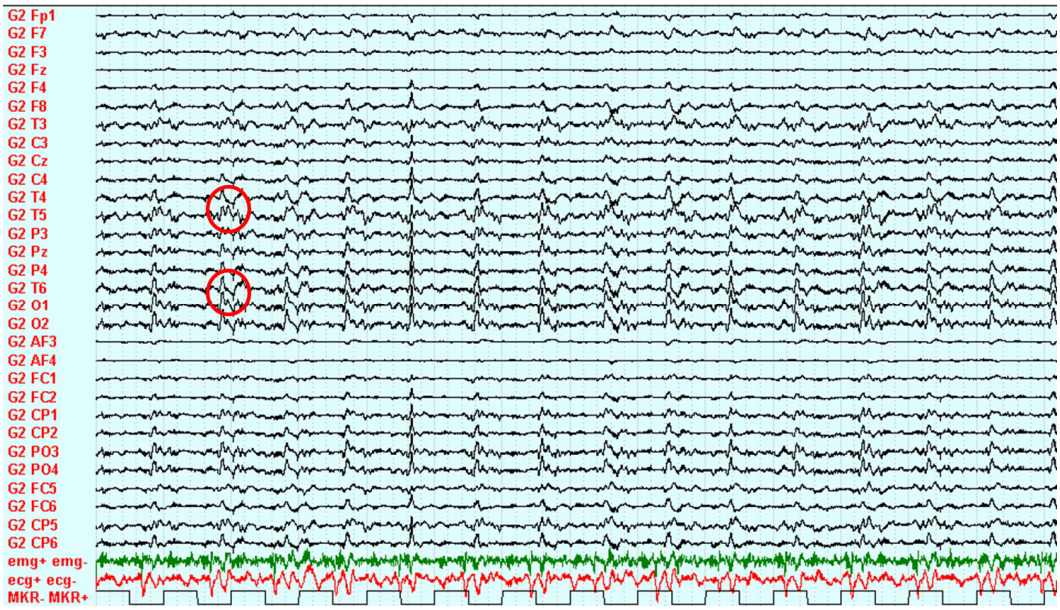

Figure 2.1. Example of BCG artifact.

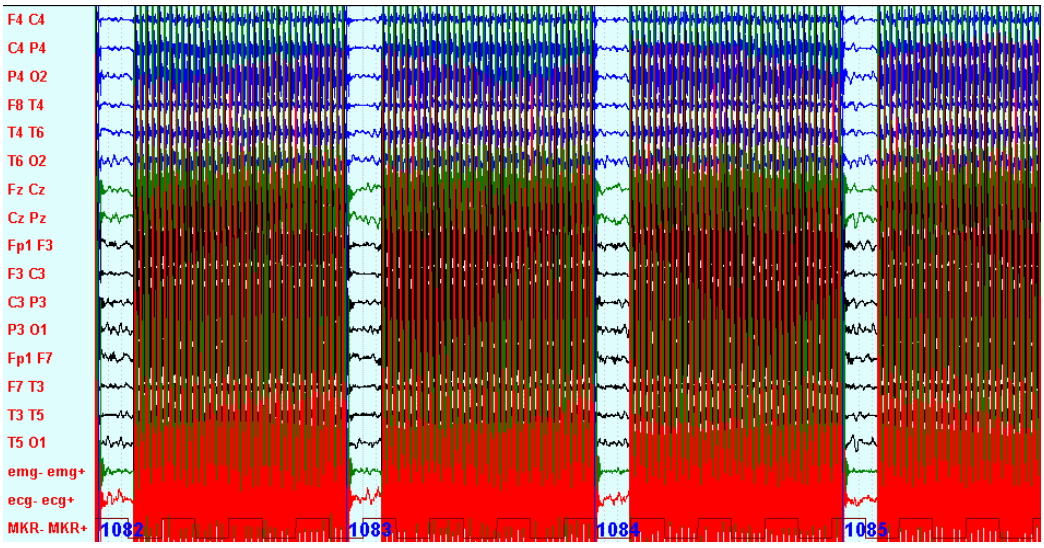

Figure 2.2. Example of gradient artifact.

2.2 Gradient and Pulse artifact removal

In literature different methods have been developed to remove these problems, considering both hardware and software solutions.

The BCG artifact is a distortion in the EEG data caused by cardiac-related activities. Its magnitude increases with the intensity of the static magnetic field, and is 3 to more times that of the EEG, varying considerably in any signal EEG channel.
Most methods for eliminating BCG artifacts have focused on averaged artifact subtraction (AAS), adaptive filtering technique and ICA technique.
Using the first method, AAS, an artifact template is first created from all the occurrences of the BCG artifact by means of averaging and, afterwards, subtracted from each occurrence to obtain a clean EEG (Allen et al., 1998). Adaptive filtering technique makes use of correlation between a reference electrocardiography (ECG) channel and EEG channels to estimate the contribution of the BCG artifact in the EEG signals, which is then subtracted to yield clean signals. ICA method allows to separate brain signals from artifacts; the occurrence of a large correlation value between the component and a reference signal (ECG) indicates that the source signal has to be considered as an artifact (Mantini et al., 2007).

Gradient artifact is characterized by very high amplitude, which can be of the order of 50 times the background EEG, and its range of frequency overlaps that of the EEG. Its shape and amplitude vary from one EEG channel to another, due to the different localization of electrodes, but inside the channel it is very similar for each slice repetition.
Two categories of methods have been proposed to remove this artifact: frequency domain filtering (Hoffmann et al., 2000) and average subtraction in the temporal domain (Niazy et al., 2005). Frequency domain filtering consists in determining the spectrum of the artifact template and subsequently correcting the signal power spectrum by setting artifact frequencies to zero. However, this approach can affect EEG, since its band may overlap.
In the average-subtraction method, a gradient artifact template, computed by averaging N gradient artifact occurrences, is subtracted from each individual artifact, followed by adaptive noise cancellation in order to remove residual artifact components, (Hoffmann et al., 2000). In recent work, principal component analysis

(PCA) is introduced to support this algorithm in order to capture temporal variations in the artifact. In (Allen et al., 2000), PCA is applied to generate an optimal set of basis functions that best describes the temporal variations of the artifacts. These basis functions are then fitted and subtracted from the EEG to reduce the artifacts. More recently, an interesting method based only on average subtraction was developed (Gonçalves et al., 2007). The algorithm preliminarily estimates the MR sequence timing parameters in order to correct misalignments between EEG and fMRI data, and then removes gradient artifact by subtracting an artifact template calculated both on slice and on volume acquisitions.

2.3 A novel gradient artifact removal method

In our laboratory we used the software package SystemPlus (Micromed, Treviso, Italy) and EEGLAB Toolbox plug-in FASTR (FMRI Artifact Slice Template Removal) (Allen et al., 2000; Gonçalves et al., 2007) for gradient artifact removal. Both of them are based on the average subtraction method, and the second one uses PCA to remove residual artifact. Their application to our data did not give completely satisfactory results, since FASTR was too slow to go through PCA and adaptive noise cancellation, and SystemPlus manual triggered signal was not completely filtered. Therefore we developed a novel method, based on the average-subtraction approach, to remove gradient artifact, able to preserve EEG integrity and adapt to any dataset avoiding MRI trigger, using complexity-free mathematical procedures. After a realignment process of EEG data depending on slice repetition time, the algorithm performs an iterative subtraction of the estimated slice artifact, according to the following steps: artifact waveform analysis, computation of signal average waveform affected by gradient artifact, artifact estimate by weighted least squares minimization, subtraction of estimated artifact.

Segmentation: The operations to remove the artifact need to be executed within every channel, one volume at a time. The channel segmentation is performed according to the EEG time only, without any trigger signal sourced from the MR scanner, to avoid inevitable misalignments. Channel division in *nv* volumes is performed by inserting automatic triggers in recorded EEG data for every scan interval, after a preliminary visual inspection in which first scan beginning is

identified. Subsequently, volume subdivision in *ns* slices is obtained by segmenting it in the same way. Before the segmentation an interpolation of a factor 5 is needed to guarantee a good quality alignment.

Algorithm: The algorithm is based on the hypothesis that the recorded EEG signal $y(t)$ is the sum of a true underlying EEG signal $eeg(t)$ and a signal $u(t)$ containing artifact components:

$$y(t) = eeg(t) + u(t) \tag{2.3}$$

and consists in three fundamental steps that are repeated iteratively:

1. *Signal affected by gradient artifact average.*

A template for artifact waveform, $f(t)$, is computed by averaging all volume's slices:

$$f(t) = \frac{1}{ns}\sum_{i=1}^{ns} y_i(t) \tag{2.4}$$

where *ns* is the number of slice per volume.

2. *Artifact estimate by weighted least squares minimization.*

Since artifact does not repeat identically at every slice, it was described by the following parametric expression:

$$\hat{u}_i(t) = \frac{a_i f(t - t_{0i})}{k_i}, \quad i = 1,....,ns \tag{2.5}$$

where a_i is the amplitude variation, t_{0i} is the time shift, k_i is the warping coefficient. Observing the data, the slice variation is related especially to the amplitude term, hence Eq. (2.5) gets to be simpler:

$$\hat{u}_i(t) = a_i f(t) \ . \tag{2.6}$$

Since the model depends linearly on the unknown parameter a_i, it is possible to estimate it from the data using the weighted least squares approach:

$$a_i = \left(f^T \Sigma_v^{-1} f\right)^{-1} f^T \Sigma_v^{-1} z \tag{2.7}$$

where f is the average artifact vector, z the data one and Σ_v the covariance matrix. Σ_v is a diagonal matrix computing considering the variance of the slice samples for each volume:

$$\Sigma_v = \begin{bmatrix} \sigma_1^2 & 0 & 0 & 0 \\ 0 & \sigma_2^2 & 0 & 0 \\ 0 & 0 & ... & 0 \\ 0 & 0 & 0 & \sigma_n^2 \end{bmatrix} \tag{2.8}$$

where σ_n^2 is the variance of the *nth* slice sample.

3. *Subtraction of estimated artifact*.

The estimated artifact is subtracted from the raw data, one slice at a time.

After the first subtraction the obtained signal shows a sinusoidal modulation, described as follow:

$$s_i(t) = y_i(t) - \hat{u}_i(t) = eeg_i(t) + u(t) - \hat{u}_i(t) = r(t)\sum_{j=1}^{N} \sin(w_j t), \tag{2.9}$$

where N is the number of sinusoidal components, making null the template for the average artifact waveform. To avoid this inconvenient, before the average artifact calculation a device has been created to straighten all the slices as follows:

$$s_i(t) = r(t)\left|\sum_{j=1}^{N} \sin(w_j t)\right|. \tag{2.10}$$

The algorithm terminates when the spectrum of the estimated artifact $\hat{u}_i(t)$ is similar to that of an artifact-free EEG, thus indicating that gradient artifact has been successfully removed. Finally, the output is smoothed by a Butterworth low pass filter (LPF) with a cut-off frequency of 70 Hz applied in forward and reverse directions to give zero phase distortion in order to isolate EEG components in the range of interest.

In order to test the effectiveness of the algorithm, the spectra of EEG signals recorded inside the scanner during fMRI scanning were calculated after any subtraction using Fast Fourier Transform (FFT) spectral analysis, after down sampling to 256 Hz. Average spectra were computed from 2s non overlapped epochs of EEG and the activity in four frequency bands (δ 1-4 Hz, θ 4-8 Hz, α 8-13 Hz and β 13-30 Hz) were calculated for each EEG channel.

Validation: In order to test the method effectiveness, a comparison between the original subjects data and the filtered simulated ones was done in frequency and time

domain. An index R was computed, according to Eq. (2.11), to quantitatively evaluate the performance of the artifact reduction method:

$$R = \frac{\sqrt{\sum_{i=1}^{n}\left(Y_i - \hat{Y}_i\right)^2}}{\sqrt{\sum_{i=1}^{n} Y_i^2}} \tag{2.11}$$

where Y_i is the free-artifact EEG spectrum $\hat{Y}_i$ is the estimated EEG signal spectrum after artifact correction, n is the number of signal samples.

As regard the time domain, a visual comparison was done between the original subjects EEG and the recovered signal to clinically evaluate the artifact removal.

The method was validated on simulated data; a signal inside the scanner was generated in silico by adding the artifact acquired from a water phantom to an EEG recorded outside the scanner in an healthy subject (original EEG). The EEG was acquired using the same EEG system described in chapter 1 (SD MRI 32, Micromed, Treviso, Italy). The average spectrum, computed for phantom data only recorded during fMRI session, shows that artifact contaminates the volume acquisition frequency as well its harmonics by producing large power peaks at the frequencies of Eq. (2.2) where TR=3.7s and ns=36. Thanks to the phantom-based gradient artifact these simulated signals adequately represent the temporal variations in artifact morphology, except the physiological artifacts, such as the BCG. The raw EEG signal with gradient artifact during fMRI scanning is shown in Fig. 2.3, whereas Fig. 2.4 shows the ability of our method to remove artifact gradient.

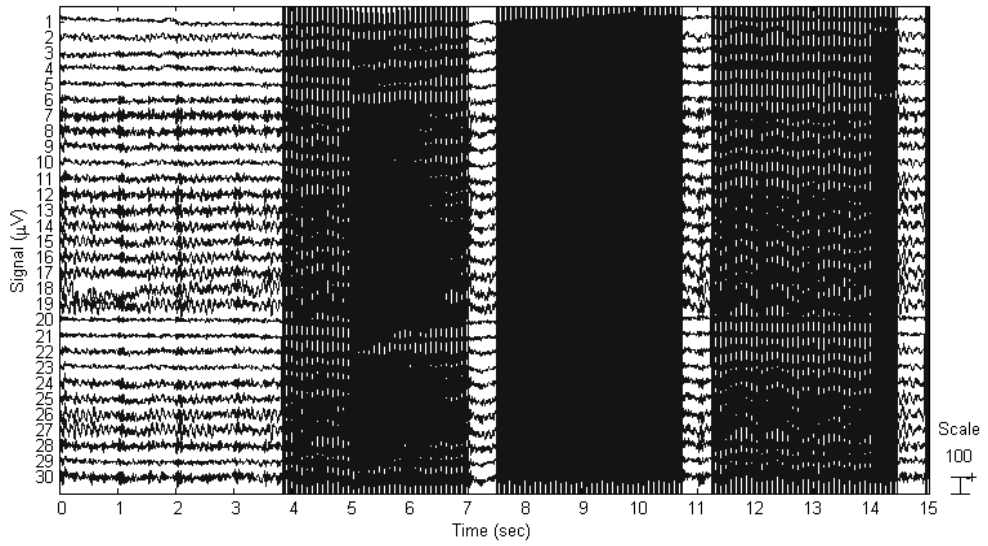

Figure 2.3. Raw EEG signal during fMRI scanning (original EEG plus gradient artifact).

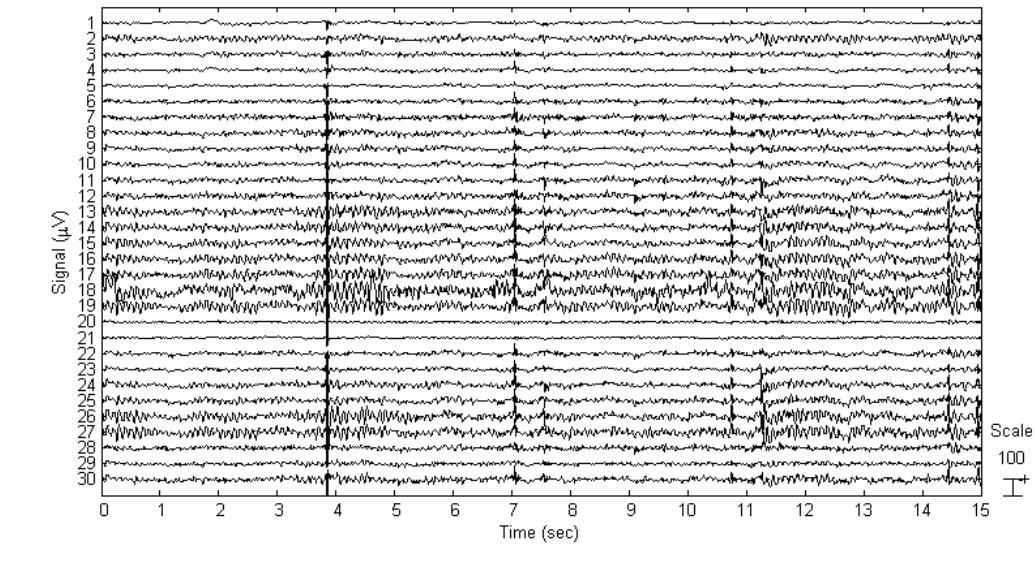

Figure 1.4. EEG signal corrected for gradient artifact after LPF (70 Hz).

Results obtained both in silico and real data (normal subjects) indicate that the method is successful in removing the gradient artifact. In silico data the best end subtraction must be evaluated by comparison of spectral components, by visual inspection of frequency-domain spectra and by computing the index R, after each iteration. The first one seems to be sufficient to remove gradient artifact in [1-30 Hz] range, but in comparison with its frequency-domain spectrum, as shown in Fig. 2.5, it demonstrates that some residual artifact still remains, producing a nasty time-

domain data. From further subtractions, it results that the third and the fourth ones remove signal components in delta range, therefore in this case the second iteration is the best end condition for the algorithm in order to preserve the signal integrity. The component at 50 Hz is due to an amplification of power line interference in the scanner, while the BGC artifact is low because the real EEG used to create the simulated signal was recorded outside the scanner.

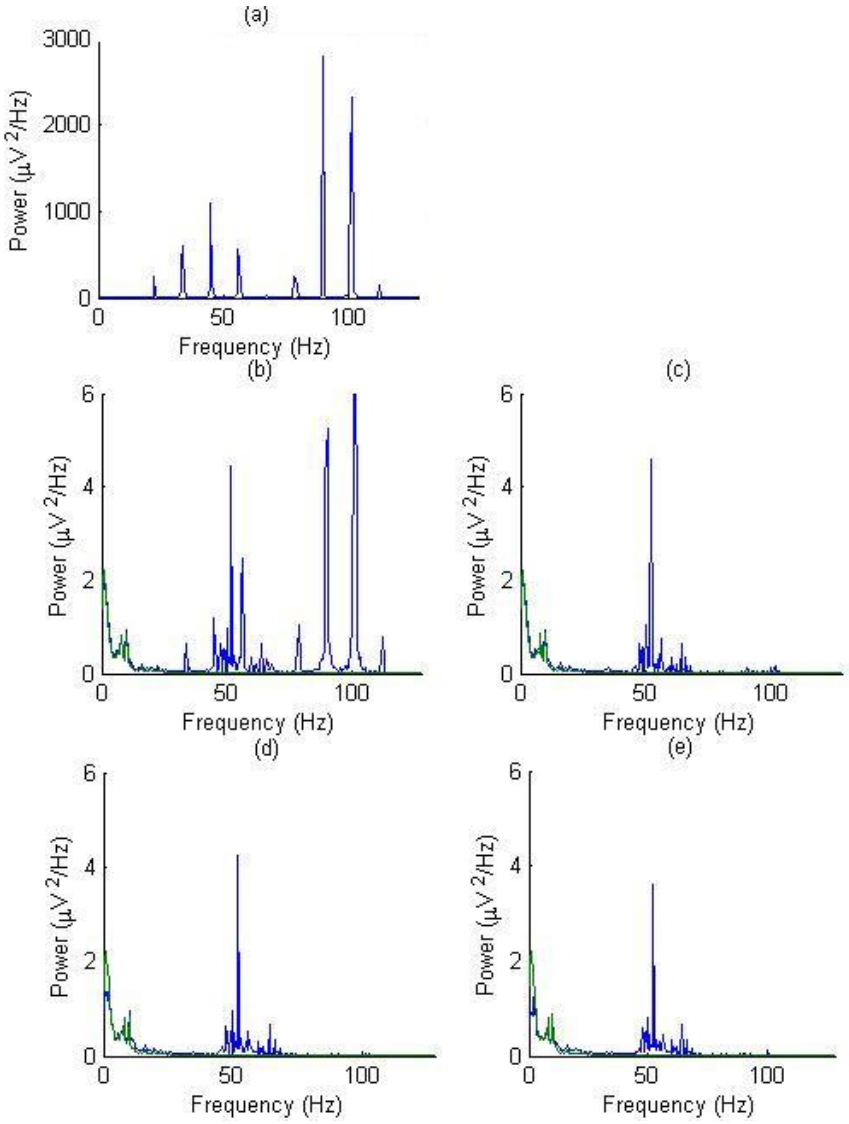

Figure 2.5. In silico experiment: (Fp1 channel) EEG spectra before (a) and after (b,c,d,e) the iterative steps of the novel method. Green line indicates the original EEG, blue line the filtered EEG.

As regards the estimated parameter, the sinusoidal modulation is evident in Fig. 2.6, especially for the second and the third iteration, while the first one indicates that the original artifact maintains the same amplitude level throughout the signal. As for the fourth iteration, the random trend of the *a* amplitude is justified by the estimates accuracy analysis. The *a* CVs increase with the number of iterations

because it is getting harder to fit the artifact waveform in the signal, meaning that it is already successfully removed in the previous iterations.

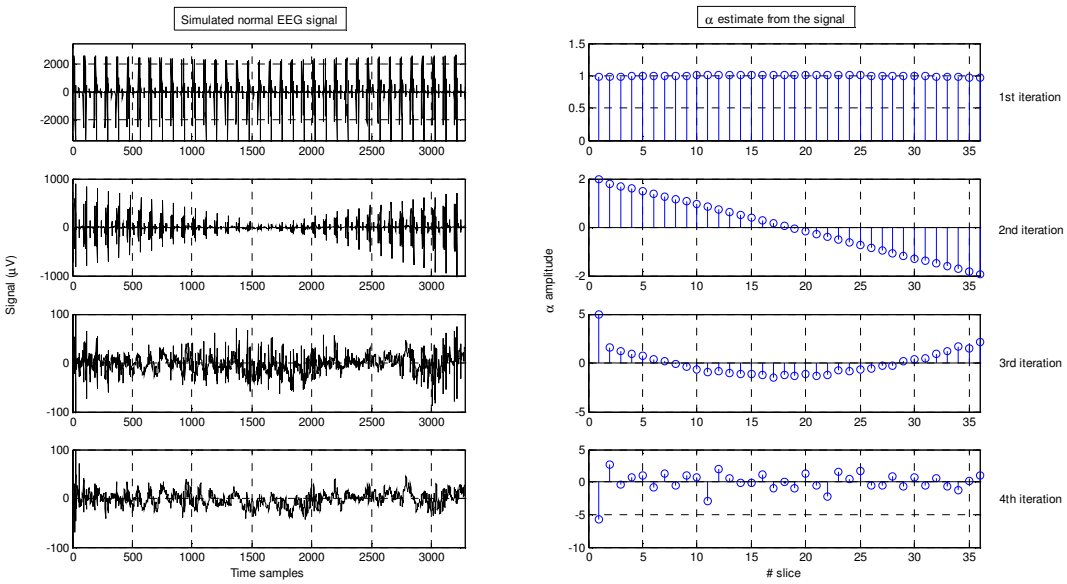

Fig. 2.6. Simulated normal EEG signal and estimated parameters *a* at each iteration for the channel C3, volume 10.

As shown in Table 2.1 the R value decreases with the number of iterations, meaning that the filtered EEG signal well matches the original EEG signal recorded outside the scanner. These values are very different from the first to the second subtraction, while they don't change too much from the second to the third.

Table 2.1. R values at each iteration for channels F3, C3, T4, Pz.

Channels	R (1st)	R (2nd)	R (3rd)	R (4th)
F3	13,15	3,20	2,62	2,03
C3	18,13	3,47	2,09	1,78
T4	9,53	3,02	2,71	2,87
Pz	15,32	3,86	3,37	2,87

In real data spectral analysis is executed for each artifact subtracted considering the range [1-30 Hz]. As shown for a representative channel in Fig. 2.7, we can see that the first subtraction removes most part of gradient artifact in particular for alpha and beta bands, while the others adjust frequency contents in delta and theta ranges. Since after the second iteration there are not evident variations

in alpha and beta bands, in this case only two iterations are needed in order to best preserve the integrity of the signal.

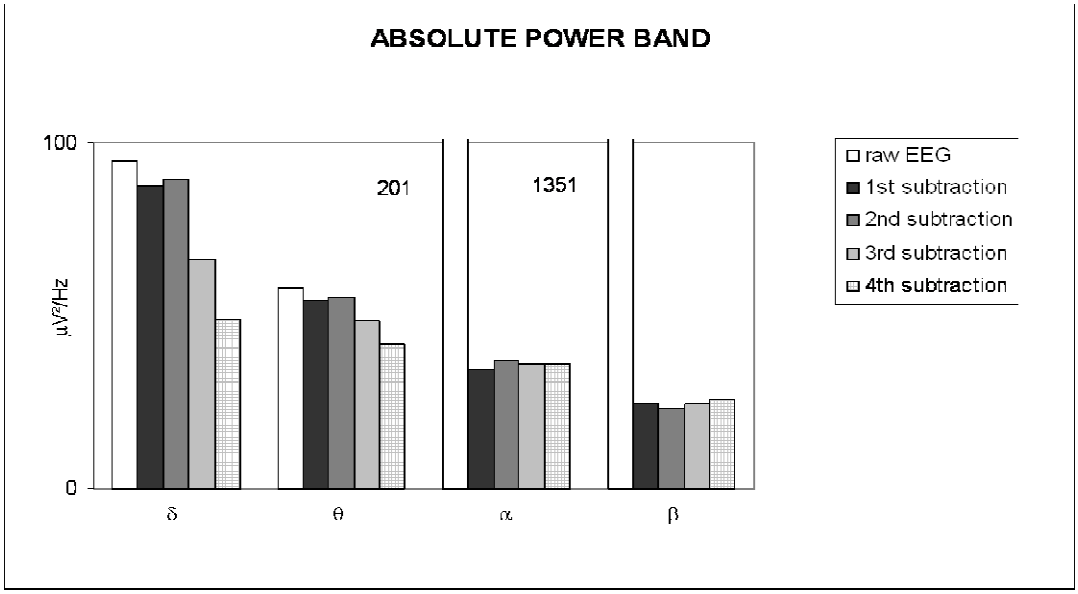

Figure 2.7. Real experiment: (Fp1 channel) absolute power in δ, θ, α and β bands after all subtractions compared to those of the raw EEG.

This software can provide a powerful tool for automatic EEG spectrum interpretation, saving time, but analysis on patients with partial epilepsy, to check the ability of the method to preserve the characteristic waveform of epileptic EEG activity during coregistration, are still in progress.

The project regarding the gradient filter started together with the novel EEG-fMRI integration method, for this reason and to avoid the introduction of a further variable that can influence the validation of the integration method, we decided to use for the routine analysis the algorithms implemented in the SystemPlus software. The first one for BCG artifact removal based on the average subtraction method, and the second one for gradient artifact removal based on an adaptive filtering technique (Fig. 2.8).

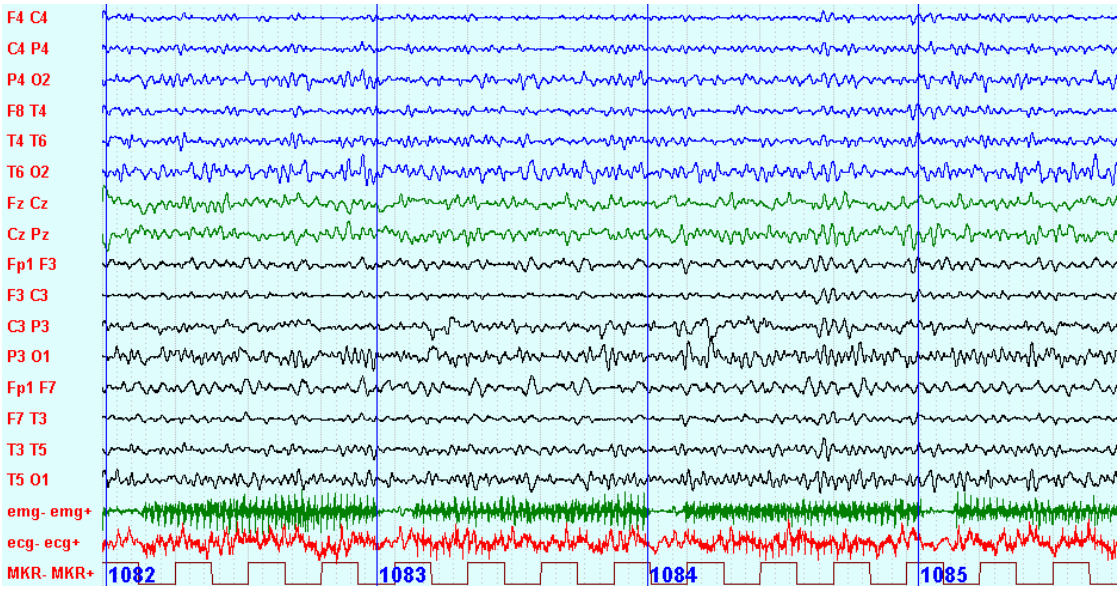

Figure 2.8. EEG of Fig. 2.2 after gradient artifact and BCG subtraction.

Chapter 3

CONVENTIONAL METHODS IN EEG-fMRI INTEGRATION: theory and application

3.1 Introduction

Here we present two conventional approaches to integration, which were presented in Formaggio et al., 2008 and Manganotti et al., 2008. In the first study (Formaggio et al., 2008) we used combined EEG-fMRI to determine the possible correlation between topographical movement-related EEG changes in brain oscillatory activity recorded from EEG electrodes over the scalp and BOLD cortical responses in motor areas during finger movement. Movement-related brain oscillatory activity during co-registered EEG-fMRI was investigated in a few studies: in (Parkers et al., 2006) a beta band synchronization was observed during movement while the EMG activity during the coregistration EMG-fMRI was analyzed in (van Duinen et al., 2005).

In the second study we applied, like other studies (Al Asmi et al., 2003; Aghakhani et al., 2004; Salek-Haddadi et al., 2006), the conventional EEG-fMRI analysis in epilepsy based on the identification of the time of IEDs on scalp EEG which are used to build a regressor in GLM analysis. A model was obtained by convolution of the EEG events, which were represented as blocks, with a HRF; maps showing regions of significant IED-related change were obtained through voxel-wise fitting of the model and application of appropriate statistical thresholds (Manganotti et al., 2008).

3.2 EEG-fMRI coregistration to investigate the cortical oscillatory activity during finger movement.

Subjects and Experimental paradigm

Data were recorded in 9 right-handed healthy subjects in G.B. Rossi Hospital, Verona. While lying inside the MRI chamber the subjects did a right-hand thumb abduction. During the task they were instructed to keep their eyes open, avoid blinking, and to look at a stationary fixed point positioned at 20 cm. Attention was reinforced before each recording. During fMRI acquisition, 100 volumes of 3700 ms were acquired, alternating 5 activations and 5 control cycles (rest), resulting in 6 minutes of echo planar imaging (EPI) recording. The movements of the thumb of the right hand were metronome paced at 1 Hz.

Data acquisition

The EEG was acquired using the same EEG system described in chapter 1 (SD MRI 32, Micromed, Treviso, Italy).

Functional images were acquired on a 1.5 T MR scanner (Symphony, Siemens, Erlangen, Germany) equipped with EPI capability and a standard transient/receive (TR) head coil. fMRI data were acquired with a T2* weighted EPI sequence (36 slices, TR= 3700 ms, TE= 50 ms, 64×64 matrix, FOV = 256×256, slice thickness 3 mm; voxel size= 3×3×3 mm, axial slice orientation).

A T1-weighted anatomical scan (192 slices, TR = 1990 ms, TE = 3 ms; scanning matrix 512×512, FOV = 256×256; slice thickness 1 mm; sagittal slice orientation) was also acquired for each subject.

Data analysis

The gradient and BCG artifacts were digitally removed off-line using SystemPlus software. Before segmentation into non-overlapping epochs of 2s, a notch filter (50 Hz) was also applied to all channels. Data for electrode leads were analyzed. EEG epochs with ocular, muscular and other types of artifact were preliminarily identified and then rejected. To evaluate power spectra, a FFT was applied to non-overlapping epochs, each containing 2048 data points, for all electrodes and for the two experimental conditions (rest and activation), with

maximum resolution (0.5 Hz) and then averaged across epochs under the same conditions. Recordings were Hamming-windowed to control spectral leakage (window length=10%). Based on power spectra (μV^2), power in upper alpha (10-12 Hz) and beta (13-30 Hz) frequency range were evaluated.

To reduce the effects of inter-subject and inter-electrode variation in absolute spectral power values and to quantify the event-related relative changes of EEG power in alpha and beta bands, at an electrode *x*, an accepted event related desynchronization/synchronization (ERD/ERS) procedure was used (Pfurtscheller and Aranibar, 1979; Pfurtscheller and Neuper, 1994), according to equation (3.1).

$$ERD_x = \frac{\left(P_{xactivation} - P_{xrest}\right)}{P_{xrest}} \cdot 100 \qquad (3.1)$$

The ERD/ERS transformation was defined as the percentage decrease/increase of instant power density at the 'event' compared with a 'pre-event' baseline value. Event-related power decreases ('cortical activation state') that implied a decrease in synchrony of the underlying neuronal populations, were therefore expressed as negative values, whereas event-related power increases ('cortical idling state') were expressed as positive values. We computed a topographic map showing changes in ERD/ERS for each subject for the alpha and beta ranges using Matlab 7 (The MathWorks Inc., Natick, MA), and a grand mean map for the 9 subjects. Wilcoxon's rank sum test comparing values between contralateral and ipsilateral ERD on the 5% significance level was run for alpha and beta frequency bands. For the alpha range the electrodes providing informative data over the region of activation in the contralateral motor area were Cp5, P3, PO3, T3, T5 and Cp1; whereas in the ipsilateral area were P4, PO4, T4, T6 and Cp2. For the beta range the contralateral electrodes were C3, T3, Cp5, Cp1, P3, PO3, O1 and T5; and the ipsilateral electrodes were C4, T4, Cp2, P4, PO4, O2 and T6.

A paired sample two-tailed t-test was computed to compare the differences between ERD/ERS values, in alpha and beta ranges, and a reference condition to verify where desynchronization and synchronization values are significant. Two-dimensional grand mean t-maps of ERD were then computed from the t-values to check the topographical distribution of the significance. ERD/ERS t-maps were thresholded at $p<0.05$ ($|t|>2.306$).

The functional data were analyzed using BrainVoyager (QX 1.2, Brain Innovation, Maastricht, The Netherlands) running in windows XP environment.

Preprocessing of functional MRI included three-dimensional motion correction, slice scan time correction (sinc interpolation), linear trend removal by temporal high pass filtering (3 cycles in time course) and transformation into Talairach coordinate space. Neither spatial nor temporal smoothing was used.

In each subject, activated voxels were identified with a single-subject GLM approach for time series data (see Appendix). To account for the hemodynamic delay, the boxcar waveform representing the rest and task conditions (p) (Fig. 3.1) was convolved with a single gamma HRF (Boynton et al., 1996) according to:

$$x(t) = p(t) \otimes HRF(t) = \int_0^{\infty} HRF(\tau)p(t-\tau)d\tau \qquad (3.2)$$

The results were displayed on parametric statistical maps in which the pixel Z value is expressed on a colorimetric scale. Statistical maps were thresholded at $p<0.045$ (corrected for multiple comparisons: Bonferroni).

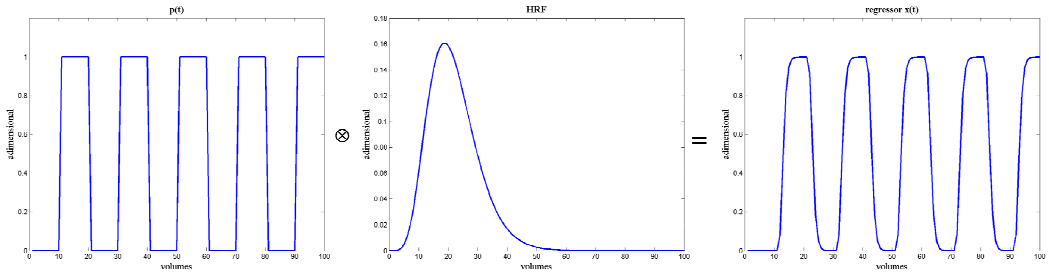

Figure 3.1. Regressor construction. The convolution between the boxcar waveform (p) and the Boynton HRF.

EEG-fMRI Integration For all subjects a linear correlation (Pearson's product moment correlation coefficient R) between the positive-negative ratio of BOLD peaks (pnr) and ERD value was estimated for all recording channels. The BOLD peak in the contralateral and ipsilateral motor area was selected manually. We selected the max and min value on the ROI defined, and then we computed the pnr. The linear correlation and the correlation maps between pnr and the ERD alpha value were estimated in the electrodes providing informative data over the region of activation in the contralateral motor area (C3, T3, Cp5, P3 and PO3) and only for subjects in whom fMRI showed ipsilateral activation (C4, Cp2 and T4). Two-dimensional maps of the correlation between ERD and pnr were computed from the R-values to check the topographical distribution.

Results

The mean alpha map showed a significant ERD decrease ($p<0.03$) prominent over central parietal and central temporal areas contralateral to the movement; whereas the mean beta map showed an ERD decrease over the central area (Cz, Cp2) and over temporal and posterior parietal areas. T-maps showed significant changes for both desynchronization and synchronization oscillatory activity; there are significant changes in t-maps over the electrodes of interest, on which we noted the presence of ERD especially in alpha band (C3, T3, Cp5, P3 and PO3); while in beta band there are significant changes in central and posterior areas (Cz, Cp2, PO4, PO3). These maps reflect the changes obtained with mean maps (Fig. 3.2).

In the group analysis (Fig. 3.2), fMRI showed significant BOLD activation ($p<0.005$) in the supplementary motor area (SMA), and contralateral and ipsilateral sensorimotor area (SM1) and also in ipsilateral cerebellum. These activations were statistically consistent ($p<0.045$) across all the subjects for the contralateral SM1 and SMA. Additional activation was observed in the ipsilateral gyrus postcentralis (GPOC) (Broadmann's area 40) in four subjects and in the ipsilateral GPOC (Broadmann's area 43) in one subject.

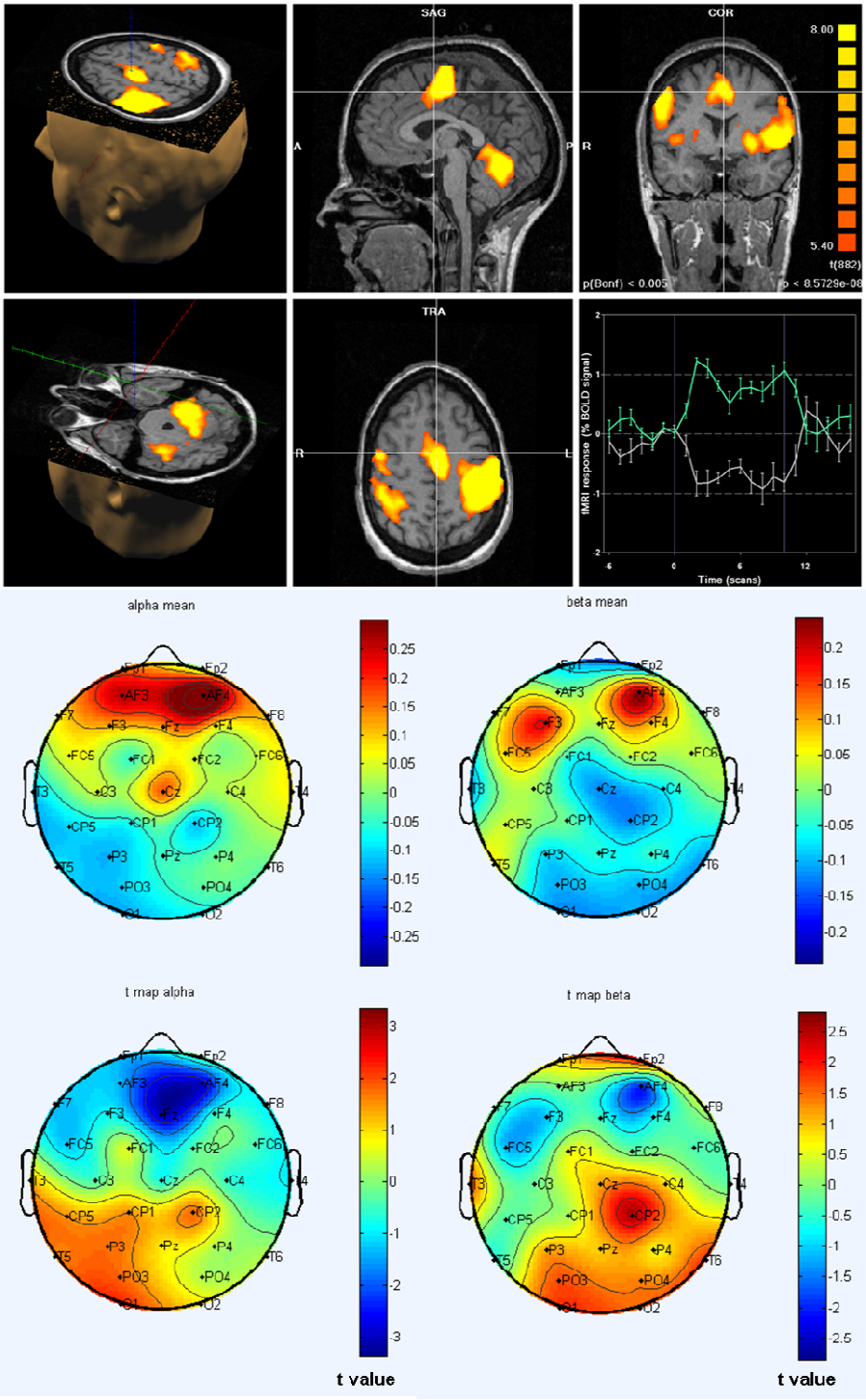

Figure 3.2. (Top): Mean fMRI activation map during right finger movement with the functional image overlaid onto the 3-D anatomical image in Talairach space in a group analysis. Color bar on the right indicates the z score of the statistical comparisons. The BOLD signal in GPRC (Brodmann's area 4) (bottom right) during active (green) and during rest condition (gray). The BOLD signal curve averaged across all conditions in all subject. The error bars show the standard error across all measurements. (Centre): Topographic maps of ERD/ERS in alpha band (left) and beta band (right), averaged of nine subjects. Blue color coding indicates maximal ERD desynchronization. (Bottom): T- maps of ERD/ERS mean values in alpha band (left) and beta band (right) thresholded at p<0.05 (|t|>2.306).

In brain regions contralateral to movement, individual alpha EEG power changes in all subjects correlated directly and closely with BOLD activity (R = -0.7, p<0.05). In the five subjects for whom fMRI showed ipsilateral activation a significant correlation was found between BOLD activation and changes in oscillatory activity over these regions (R = 0.95, p<0.05) (Fig.3.3). The correlation maps showed significant changes over the electrodes of interest: there is a negative correlation in contralateral side, whereas there is a positive correlation in ipsilateral side. The correlation maps showed significant changes for both contralateral (P3, PO3, CP1; p<0.05) and ipsilateral areas (CP2, P4; p<0.05) (Fig. 3.3).

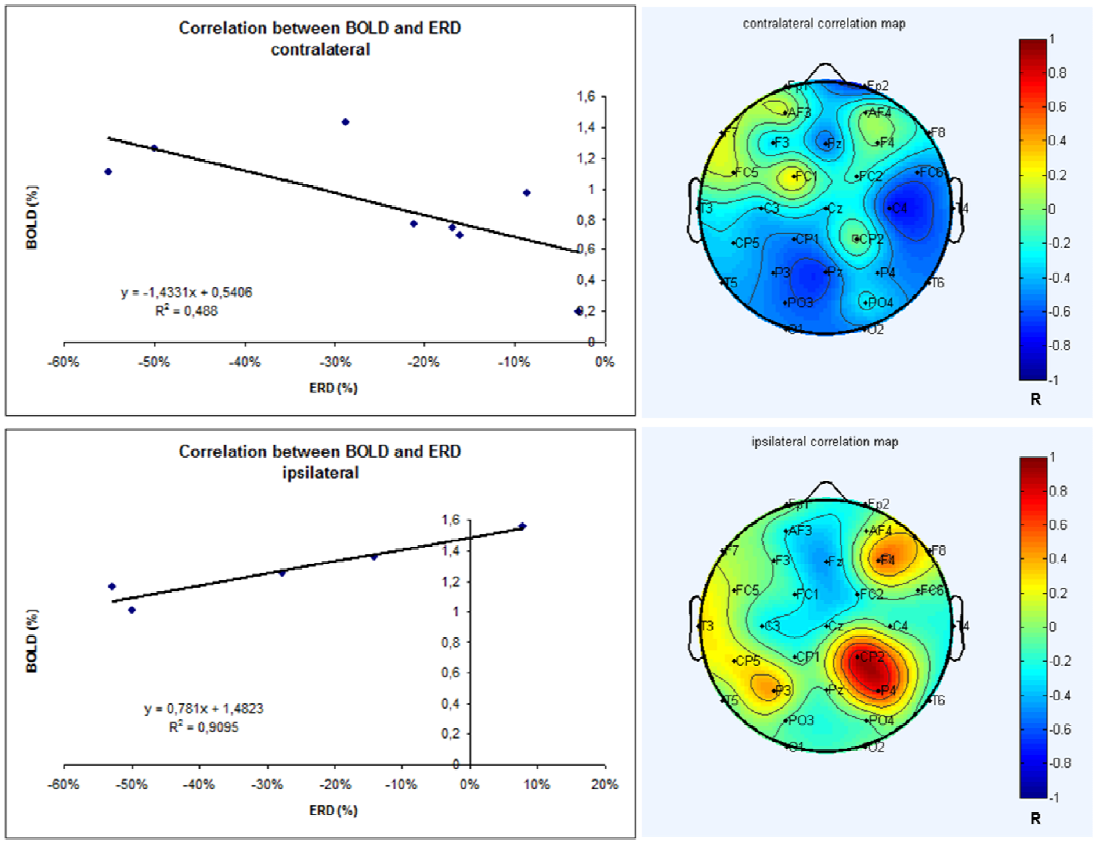

Figure 3.3 (Top): Graphic correlation and correlation map between positive-negative ratio of BOLD's peaks and ERD values (alpha) in contralateral primary motor area. (Bottom): Graphic correlation and correlation map between positive-negative ratio of BOLD's peaks and ERD values (alpha) in ipsilateral primary motor area.

Discussion

In this study, using combined EEG-fMRI we obtained useful new information on the description of the changes in oscillatory activity in alpha and beta bands during voluntary movement and on the investigation of the sites of BOLD activity as possible sources in generating these rhythms. When healthy subjects did the movement task inside the scanner, EEG recording showed a movement-related alpha and beta rhythm desynchronization over the bilateral sensorimotor area predominantly on the side contralateral to the movement. Therefore, despite of technical problems related to filtering and MRI artifacts we were able to detect oscillatory changes during thumb movements and map this activity.

One limitation of our study is that we didn't investigate alpha and beta ERD as regressor to emphasize the relative BOLD correlates within individual data sets because we didn't investigate the time course of ERD. However, we observed after the MRI artifact subtraction the persistence of oscillatory activity during rest and movement condition. In addition in our study under steady state condition we noted a desynchronization during movements, particularly over the bilateral sensorimotor regions. This is an important attempt to systematically relate individual EEG attenuations during motor blocks (ERD) to simultaneous fMRI effects and on an individual level. To our knowledge this represents an attempt to reproduce ERD maps in coregistration EEG/FMRI investigations.

In conclusion this study shows the possibility to investigate the map of oscillatory activity of the brain using fMRI, even under steady state motor conditions. The improvement of digital analysis in EEG signal and the possibility to use it as regressor for fMRI analysis allow examination of possible sources of activation and review sheds light on BOLD activation.

3.3 Continuous EEG-fMRI in patients with partial epilepsy and focal interictal slow-wave discharges on EEG.

Patients To obtain a homogeneous study sample we selected eight patients with partial epilepsy whose routine EEG recordings showed 5-6 Hz focal activity (slow waves, slow spike waves, high amplitude slow waves) over a few lateralized electrodes. Of the eight patients selected for study, three had a structural lesion on

MRI: two had hippocampal atrophies secondary to mesial temporal sclerosis (MTS) and one had a cavernous angiomas. One patient had cryptogenic epilepsy. Finally, four patients had non lesional (idiopathic) epilepsy. In one patient with MTS (patient # 4), the patient with cryptogenic epilepsy (patient # 2) and the one with idiopathic epilepsy (patient # 7), routine EEG showed slow-wave activity; in the patient with a cavernoma (patient # 3) and the two patients with idiopathic epilepsy (patients # 5 and # 8) they showed slow spike waves; and in the other patients with idiopathic epilepsy (patient # 6) and the second patient with MTS (patient # 1), they showed high amplitude slow-waves (>130 μV).

Data acquisition

EEG and fMRI signals were acquired using the same equipments and a single electroencephalographer visually reviewed the filtered EEGs and marked the time of onset and duration of each IED. Automatic IED identification was thus avoided.

Data analysis

EEG and fMRI signals were pre-processed as described in the previous paragraph. In each subject, activated voxels were identified with a single-subject GLM approach for time series data (Worsely and Friston, 1995; Worsely et al., 2002). From Eq.(3.2) a model is obtained by the convolution of the EEG events (the timing of IEDs), which are represented as stick functions of unitary amplitude p(t), with a model of the event-related fMRI response, represents by a canonical HRF (two gamma) (Fig. 3.4); maps showing regions of significant IED-related change are obtained through voxel-wise fitting of the model and application of appropriate statistical thresholds.

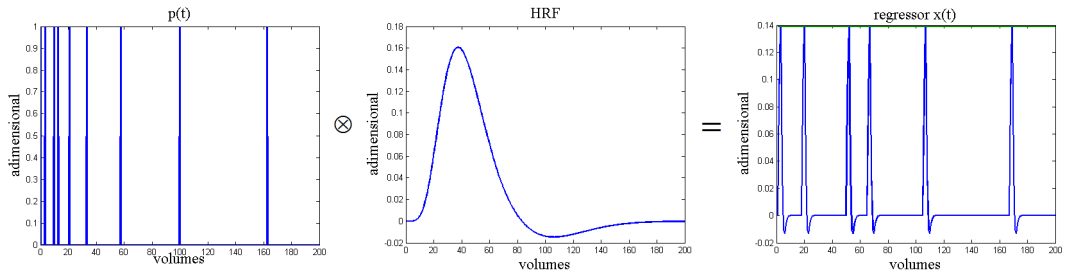

Figure 3.4. Regressor construction. The convolution between the stick functions (p) and the HRF.

Results

In all patients, EEG showed unilateral focal activity during the EEG-fMRI session. IEDs recorded inside the scanner had a localization, amplitude and morphology similar to those in previous routine EEG recordings. In two patients (patient #1 and 6), EEG recordings showed focal high-amplitude slow waves and in the other two patients (patients # 2 and 4) slow-wave discharges over the temporal electrodes. In another patient (patient # 7), we detected slow-wave activity in the extratemporal (F7) region. In the patient with a cavernoma (patient #3 - Fig. 3.5), focal EEG activity was characterized by focal slow-spiked wave activity, reaching maximal amplitude over the left temporal electrodes (T5). In the other two patients (patients # 5 and 8) we detected slow-spiked waves; in patient # 5 in the extratemporal (F3) region and in patient # 8 in the temporal region (T4, T6). In patient # 8, EEG tracings also showed high-amplitude spiked slow wave activity. In all patients, fMRI analysis showed a significant focal BOLD activation in a single activated area related to the EEG irritative focus.

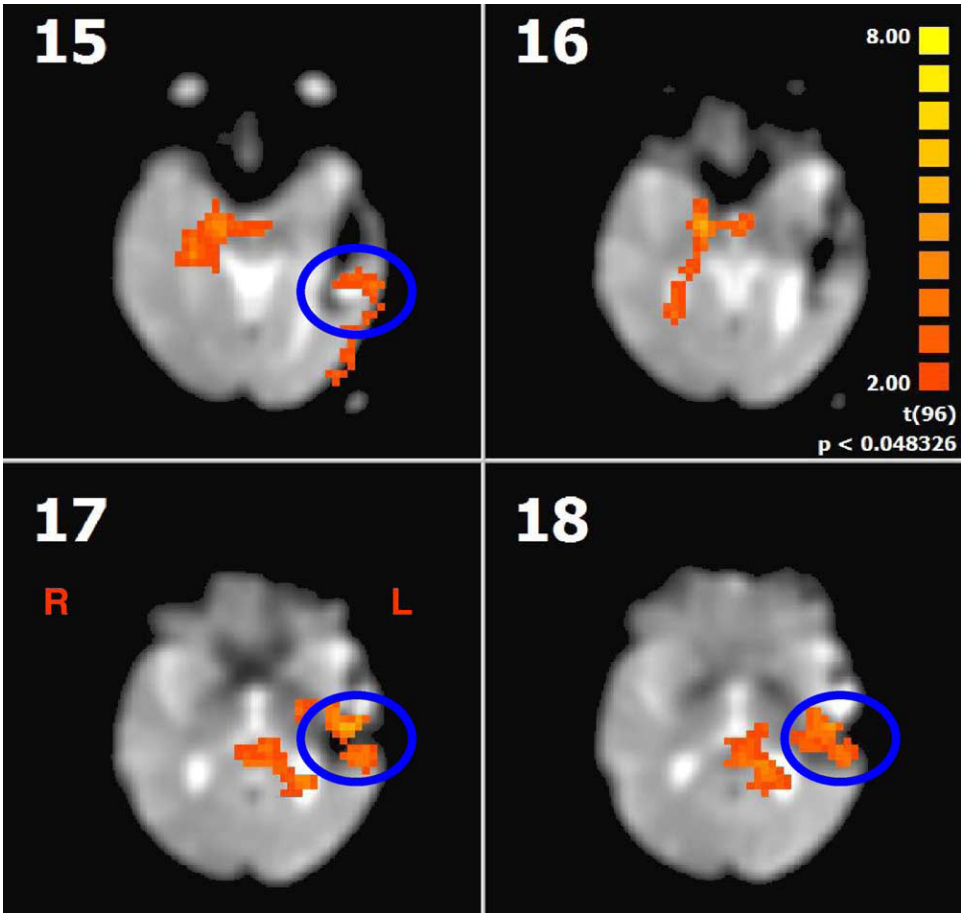

Figure 3.5. Patient # 3. fMRI activation maps in the left temporal cortex around the poro-encephalic cavity (site of previous surgical treatment of the cavernoma).

Discussion

The main finding in this EEG-fMRI study of patients with partial epilepsy is that focal interictal slow-wave activity was invariably associated with increased focal fMRI activation responses in a spatially related brain area. Our study therefore extends current knowledge on epileptic foci localization and confirms previous reports suggesting that EEG-fMRI activation associated with modelled slow activity might have a role in localizing the epileptogenic region even in the absence of clear interictal spikes.

The conventional method used for EEG-fMRI integration was based on visual inspection of EEG events. The time ranges selected were represented as blocks and they were used as input for GLM analysis. In this way some EEG information may be lost.

Chapter 4

A NOVEL EEG-fMRI INTEGRATION METHOD

4.1 Introduction

Here we describe a novel automatic method to detect IED activity in order to use it as a parametric modulator in fMRI analysis. The novelty is that ICA decomposition is used to extract IED activity from an EEG signal, since to be used as a regressor in GLM. The rationale is that epileptic discharges correspond to highly synchronizes and high-frequency activity of neurons, and the original component of epilepsy spikes is different from that of normal brain activities and other noise background.

4.2 Independent Component Analysis (ICA)

In the field of biomedical signal processing, Blind Source Separation (BSS) methods are generally used to separate multi-channel recordings into their constituent components; ICA is a subset of such techniques used to separate statistically independent components from a mixture of data (Fig. 4.1).

In electroencephalography it has been used to remove artifacts and to differentiate components of the epileptiform activity (Jung et al., 2000; Iriarte et al., 2003). This method successfully separate ocular artifacts from brain activity (Jung et al., 2000) and has been demonstrated to extract neurophysiologically meaningful sources reflecting epileptiform brain activity associated with seizures (Kobayashi et al., 1999; Hesse et al., 2004) and spikes (Ossadtchi et al., 2004). ICA decomposes mixed input data into a set of independent outputs, without any information about the distribution of sources. ICA does not require either data averaging or any assumption regarding generator model in the head. The central limit theorem ensures that a linear

mixture of any source signals tends to be Gaussian; source signals tend to be statistically independent from each other. These considerations suggest that, if a signal mixture can be decomposed into a set of statistically independent, non-Gaussian signals, these signals are likely to be the source signals of that signal mixture.

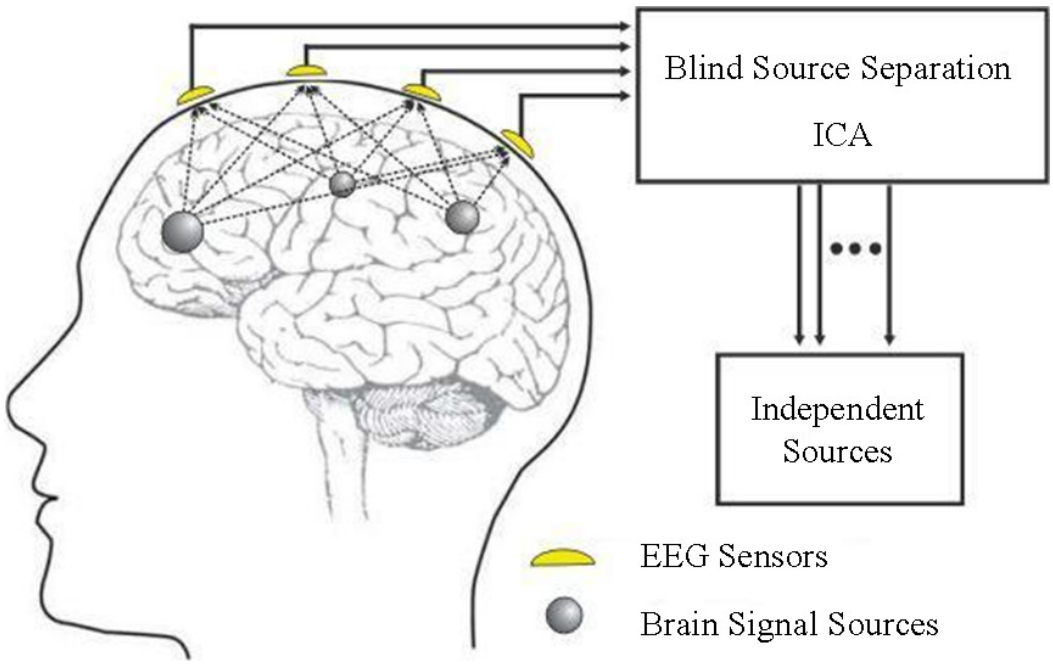

Figure 4.1. ICA concept; mixing and blind separation of EEG signal.

Algorithms for ICA include Information-maximization (Infomax) described by Bell and Sejnowski in 1995; FastICA, invented by Aapo Hyvärinen at Helsinki University of Technology, and JADE introduced by Cardoso and Souloumiac, but there are many others also. In this study FastICA algorithm was used and ICA was evaluated as a potential method to characterize the electric activity of spikes, burst of spikes and slow waves with different amplitudes and durations.

4.3 The novel method

The scalp EEG is a linear summation, or mixture, of electrical activity from sources at various brain regions (Nunez and Katznelson, 1981). We assume here that the electric process of epileptic activity is an additional component independent from the background activity and artifacts. Epileptic discharges correspond to highly

synchronizes and high-frequency activity of neurons, so it is rationally considered that the original component of epilepsy spikes is different from that of normal brain activities and other noise background.

This novel method consists in four fundamental steps:

1. Selection of components
2. Reconstruction of EEG signal
3. Selection of channel and FFT analysis
4. Construction of EEG regressor

A schematic representation of the different steps in EEG-fMRI analysis is shown in Fig.4.2.

1. Selection of components. The relationship between data and sources can be written as:

$$x = As \tag{4.1}$$

where **x** is the data, **s** the original sources (the components) and **A** the mixing matrix.

ICA decomposition of data was performed using FastICA algorithm implemented in EEGLAB (Appendix) and the independent components **y** were obtained by:

$$y = Wx \tag{4.2}$$

where $W = A^{-1}$. Each component can be described on the basis of a spatial pattern (map), representing its spatial distribution (W^{-1}), and a time course, representing its temporal evolution. Topographic maps were constructed with the EEGLAB toolbox.

To select components related to IED activity, we used a time-frequency representation obtained by using wavelet-based analysis (Continuous Morlet wavelet Transform CMT) (Appendix). We computed the wavelet power for all the epochs of interest (chosen by an experienced neurophysiologist) and for all the components using Matlab. For each component we selected from the frequency bins the one with the maximal power over total recording session. Finally power was averaged along time, obtaining one value for each component. These values are represented in an histogram. Components that exceeded mean value ± standard deviation were chosen for further analysis. IED components were selected based on their power because typically IEDs activity is higher in amplitude than background activity and its power increases, and we used wavelet analysis because of the non stationarity of the signal.

2. Reconstruction of EEG signal. After the components of interest have been selected, they were back projected to obtain a reconstructed EEG signal according to:

$$x_p = x - W^{-1}Zy \tag{4.3}$$

where x_p is the new vector representing the reconstructed EEG signal and Z is a diagonal matrix where each element z_{ii} was set equal to 1 if the i-th component is to delete, while it was set equal to 0 otherwise (Mantini et al., 2007).
In this way, the unwanted components not selected were subtracted from the EEG recordings, and the reconstruction of the EEG signal was completed, maintaining its correct spatial distribution.

3. Selection of channel and FFT analysis. To automate the selection of the EEG channel that it will be used for the construction of EEG regressor we compared the reconstructed EEG with the filtered EEG (called original) by computing the cross correlation between signals; the channel related to interictal activity with a high correlation coefficient (r) was chosen for the analysis. A frequency power analysis was applied on the time series of the selected channel (IED activity) by computing FFT of epochs acquired during each fMRI volume (the duration of which was equal to the repetition time: TR). This technique has mostly been applied to the study of alpha rhythm (Moosmann et al., 2003; Feige et al., 2005; Gonçalves et al., 2006; De Munck et al., 2007), it can also be used to examine oscillations at higher or lower frequency. The power spectrum of the selected channel, created for all functional volumes, was used to form the EEG regressor.

4. EEG regressor. The power time series $p(t)$ was convolved with the canonical two gamma HRF(t) provided by Brain Voyager and were down-sampled to the temporal resolution of the fMRI data (TR). This signal (the EEG regressor) was used as a predictor for the BOLD signal in GLM analysis:

$$x(t) = p(t) \otimes HRF(t) = \int_0^{\infty} HRF(\tau)\, p(t-\tau) d\tau \tag{4.4}$$

where $\otimes$ denotes the convolution operation (Fig. 4.3).

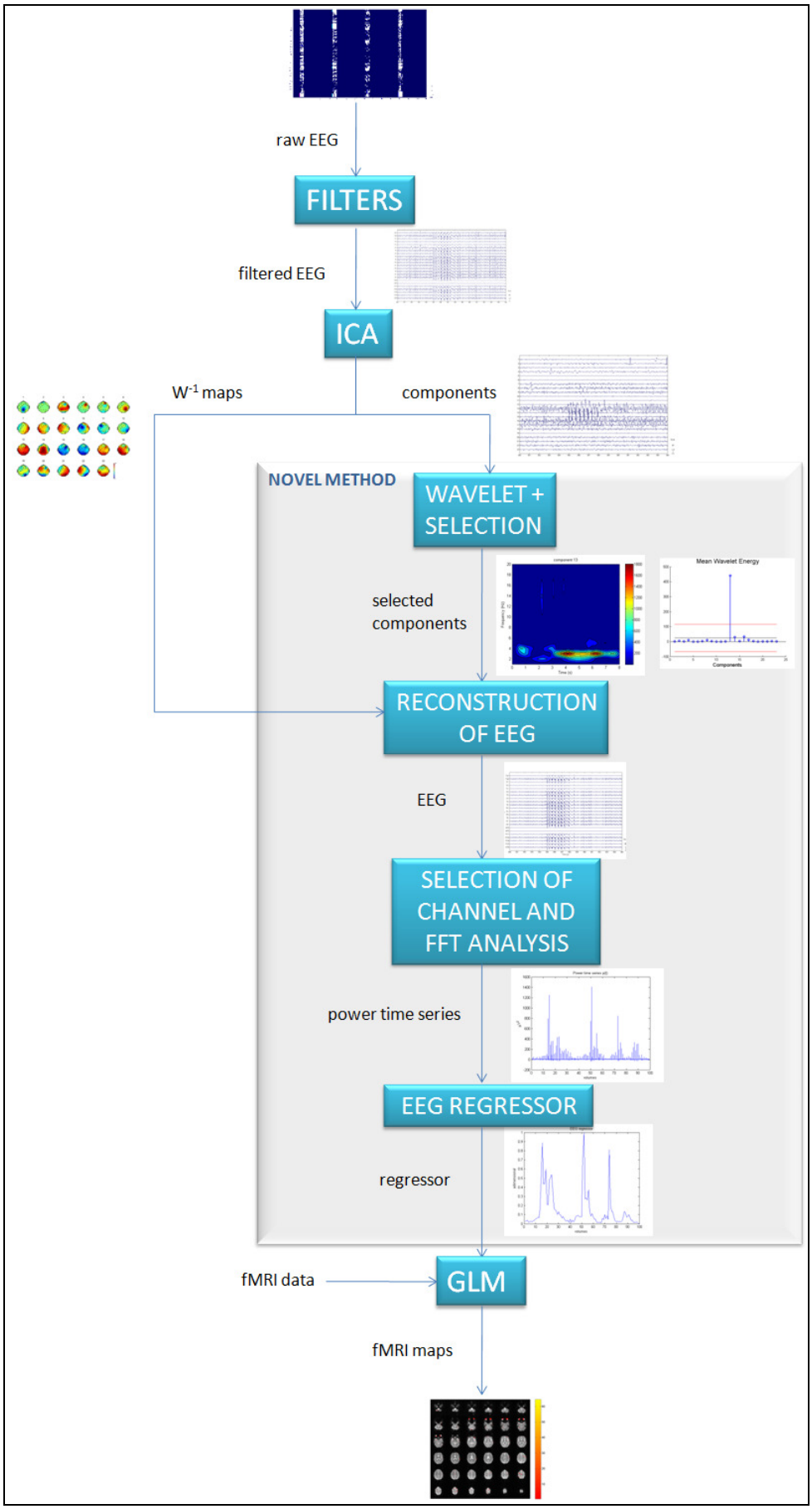

Figure 4.2. A schematic representation of the different steps in EEG-fMRI analysis

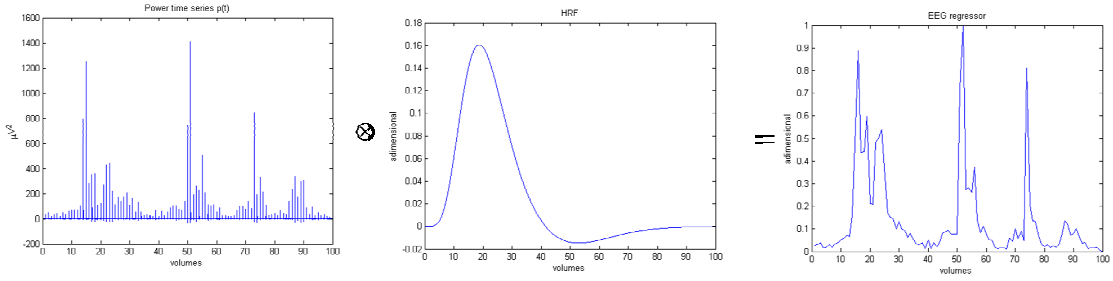

Figure 4.3. EEG regressor construction. The convolution between the power time course (p) and the two gamma HRF.

For HRF(t) several different models have been proposed such as the gamma function (Cohen, 1997; Lange and Zeger, 1997), combination of gamma functions (Friston et al., 1998), the Gaussian function (Rajapakse et al., 1998; Kruggel and von Cramon, 1999a,b), the spline-like function (Gossl et al., 2001a,b), Fourier sines and cosines (Lange and Zeger, 1997; Ardekani et al., 1999), the finite impulse response (Goutte et al., 2000), and a voxel specific function obtained by deconvolution (Lu et al., 2007). However, in clinical applications HRF(t) is usually described by using the so-called "canonical HRF" model (Friston et al., 1998) according to the equation:

$$h(t) = \left(\frac{t}{d_1}\right)^{a_1} \exp\left(\frac{-(t-d_1)}{b_1}\right) - c\left(\frac{t}{d_2}\right)^{a_2} \exp\left(\frac{-(t-d_2)}{b_2}\right) \qquad (4.5)$$

where $d_j = a_j b_j$ is the time to the peak, and $a_1 = 6$, $a_2 = 12$, $b_1 = b_2 = 0.9\,\mathrm{s}$ and $c = 0.35$ (Glover, 1999).

For this reason in our analysis we used the "canonical" model (two gamma function) (Fig. 4.3).

Chapter 5

IN SILICO AND REAL DATA FOR THE ASSESSMENT OF THE NOVEL METHOD

The method was validated on simulated data and then applied on real data set: consisting of 2 normal subjects and 5 patients with partial epilepsy. Regarding the two normal subjects, the EEG-fMRI protocol was performed under two condition: opened and closed eyes, because the activated networks are known from the literature (Feige et al., 2005; Henning et al., 2006) and this is a further validation of the method.

5.1 In silico data

A schematic representation of the different steps of the simulation is shown in Fig. 5.1.

To simulate EEG components of spontaneous interictal activity, we selected them from two different patients (components #7 and 14 in Fig. 5.2), because of their variability in amplitude and shape. Then we derived the components (# 1-6, 8-13, 15-20) related to awake background activity by applying ICA on EEG data of a normal subject. The duration of the sample window was 75 s. These components were stored in matrix $\mathbf{s}$. In silico data ($\mathbf{z_1}$) (Fig. 5.3) were computed according to:

$$z_1 = As \tag{5.1}$$

where the mixing matrix A was generated randomly with zero mean and variance equal to one. In order to derived the "true" regressor, only due to the contribution of the components # 7 and 14, the two components were back projected to obtain a new EEG signal (reconstructed EEG) $z_2 = z_1 - W^{-1}Zs$, where $W = A^{-1}$ and Z is constructed as described in Appendix A.1. In order to define the "true" regressor, we compared z_2 with the original EEG z_1 by computing the cross correlation between signals; the channel with a high correlation coefficient was chosen for the analysis

and its spectrum p was convolved with the two gamma HRF, defining the "true" regressor x:

$$x(t) = p(t) \otimes HRF(t) \tag{5.2}$$

After that the new method was applied to the signal z_1 the EEG regressor $\hat{x}$ was estimated:

$$\hat{x}(t) = \hat{p}(t) \otimes HRF(t) \tag{5.3}$$

Finally, in order to compare the two waveforms, the "true" and estimated EEG regressors were compared using an index H defined as: $H = \frac{\sqrt{\sum_{i=1}^{n}(x_i - \hat{x}_i)^2}}{\sum_{i=1}^{n} x_i}$ where n is the number of samples. This index is computed as difference between the areas under the two waveforms compared to the area under the true waveform. We decided to not use a relative index like Root Mean Square Error (RMSE) because the regressor's waveform has many zero values which increase the index value.

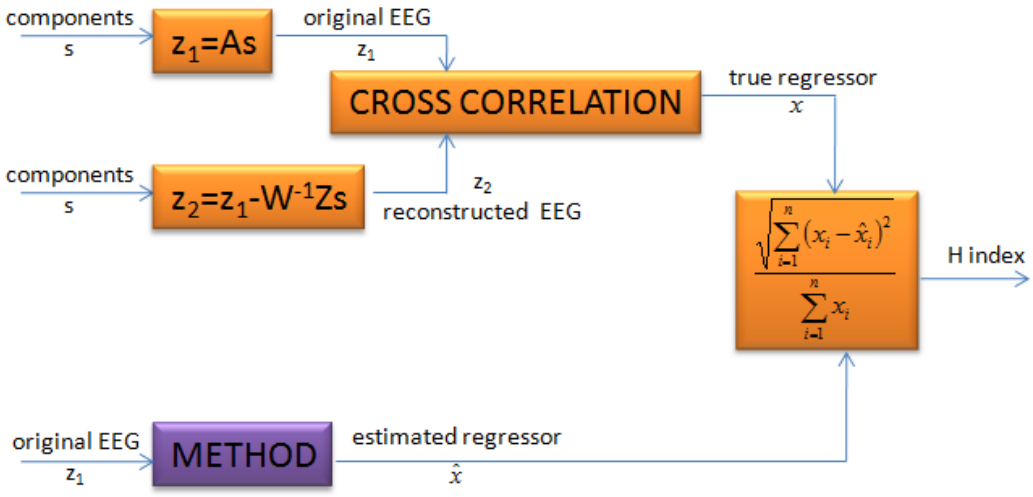

Figure 5.1. A schematic representation of the different steps of the simulation.

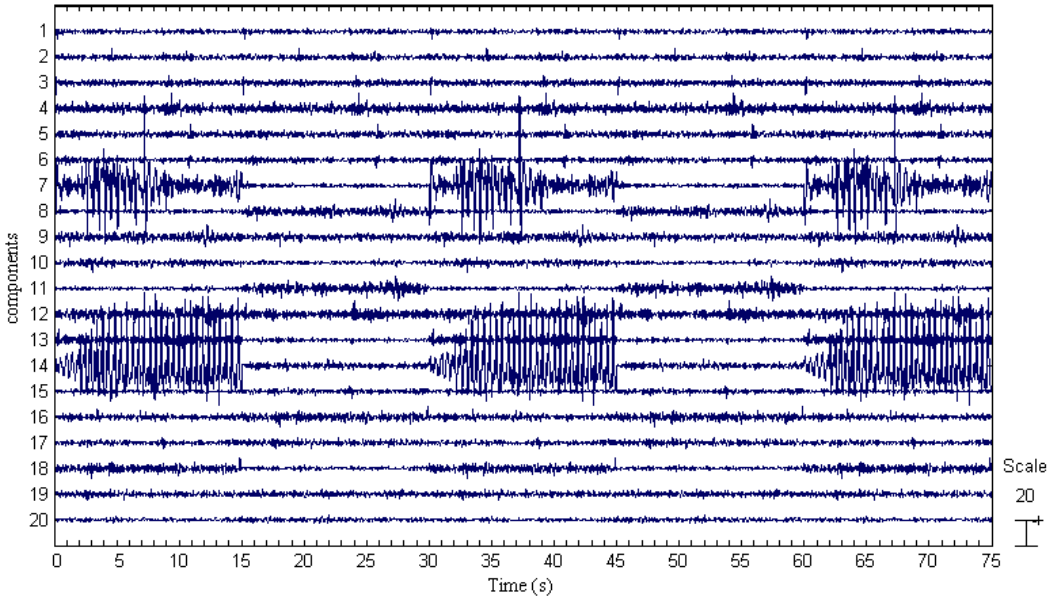

Figure 5.2. Twenty EEG components including awake background activity from a normal subject and two superimposed epileptiform IED activites (components # 7 and 14 represent epileptiform activities from two different patients).

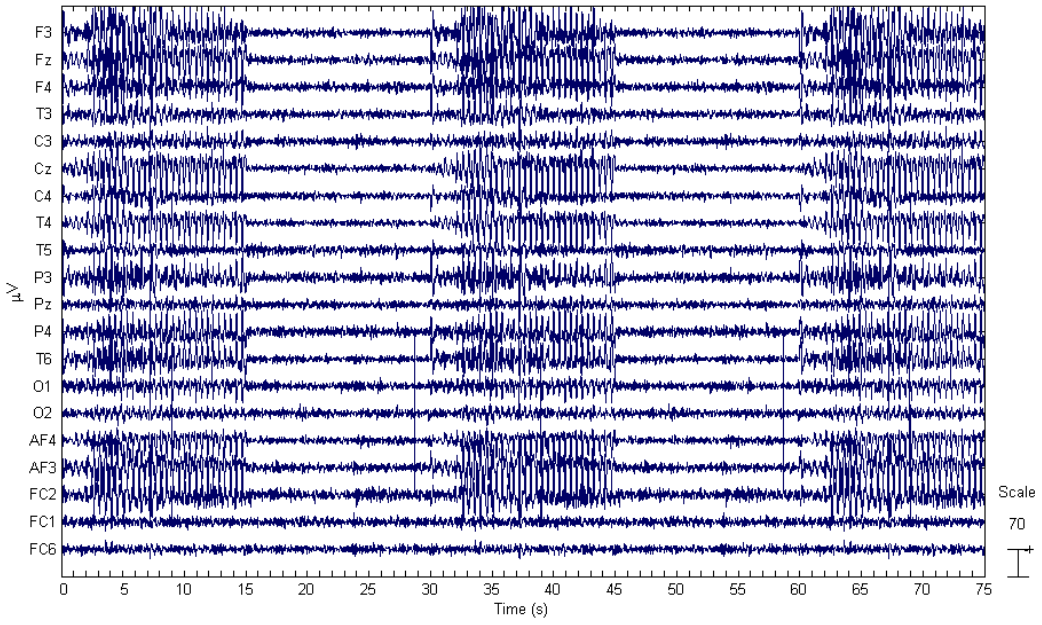

Figure 5.3. Example of silico data z_1.

5.2 Real data

In this study we used two different sets of data. The first set consists of EEG data from 2 subjects which make a task. The second set consists of EEG data form 5 patients with partial epilepsy.

Subjects Data were recorded in 2 healthy subjects (1 man and 1 woman). All subjects gave written informed consent for the study in accordance with the Declaration of Helsinki. The experiment was approved by the Local Ethics Committee of the University Department and Hospital.

Patients To obtain a homogeneous study sample we selected five patients with partial epilepsy whose routine EEG recordings showed 5-6 Hz focal EEG activity (slow waves, slow spike waves, high amplitude slow waves) over a few lateralized electrodes.

Patient #1 is affected by cerebral palsy with extensive ischemic lesion over the right hemisphere involving the frontal, the central, the parietal and temporal regions. The clinical neurological examination shows a severe left hemiparesis with mild hand movement and hypertonia on the left leg. The walking is possible only with an help of a care giver. Mild cognitive impairment is present, but the patient is collaborative and responsive.

Patient #2 is affected by focal seizure in infantile age with speech arrest without loss of consciousness. With the adult age and the introduction of therapy the seizures evolved with focal seizure, clonic movement to the right arm and leg and following generalization with loss of consciousness. Actually the seizure showed focal clonic movements followed by loss of consciousness.

Patient #3. Seizures with clonic movements and head and eyes version. EEG right central temporal isolated spikes and waves. In the following years she is treated with antiepileptic drugs. The seizures are still present in random way and some of these seizures generalized. Spikes and waves over the right central-temporal regions. More evident during drowsiness and sleep. Theta activity over the right frontal temporal regions was also present.

Patient #4 has a head trauma with hemorrhagic lesion over the left frontal region. The patients showed focal seizures with temporal semeiology as starting clinical symptoms following by head version and tonic posturing of the arms without loss of consciousness.

Patient #5 had a head trauma at 16 years with bleeding in the left temporal regions. After two years from the head trauma he had the first seizure during the night described as grand mal seizures with tonic clonic movements in upper and lower limbs. Cyclic clinical tonic clonic seizures with a frequency at 2-3 episodes at week. With additional therapy no more seizures. Small head trauma in left temporal regions with small seizures characterized by lost of consciousness. Other seizures are described with motor seizures, the comprehension is still present but he has a speech arrest.

Experimental paradigm Inside the bore of the scanner subjects and patients were laid supine on a bed with their elbows flexed at 120° and hands pronated in a relaxed position. Their head was stabilized with adjustable padded restraints on both sides. During fMRI acquisition subjects were instructed via headphones when to open an close their eyes. 100 volumes of 3700 ms were acquired, alternating 5 activations (eyes open) and 5 control cycles (eyes closed), resulting in 6 minutes of echo planar imaging (EPI) recording (Fig. 5.4). The run started with eyes closed condition. Each subject was trained for several minutes before the experiment to perform the task correctly.

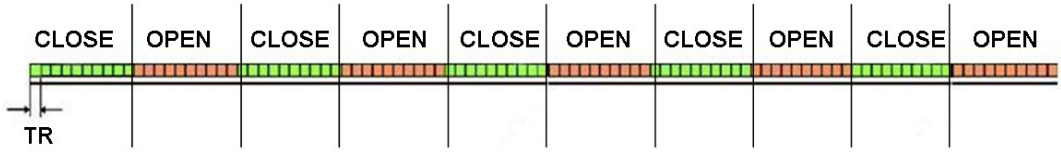

Figure 5.4. Recording paradigm: alternation of eyes closed and open during fMRI acquisition.

During fMRI acquisition patients were instructed to remain as still as possible throughout the experiment with eyes closed. 140 volumes were acquired for patient #1, 100 volumes for patients # 2 and 3, 200 volumes for patients # 4 and 5, the duration of volumes was 3700 ms.

5.3 EEG data acquisition

The EEG was acquired using a MR compatible EEG amplifier (SD MRI 32, Micromed, Treviso, Italy) and a cap providing 32 Ag/AgCl electrodes positioned according to a 10/20 system (impedance was kept below 10 kΩ). To remove pulse and movement artifacts during scanning two of these electrodes were used to record the electrocardiogram (ECG) and electromyogram (EMG). The EMG electrode was placed on the right abductor pollicis brevis muscle.

The reference was placed anterior to Fz, and the ground posterior to Fz as in other studies (Gonçalves et al. 2006; Formaggio et al. 2008; Manganotti et al. 2008) using the same system. To ensure subjects' safety, the wires were carefully arranged to avoid loops and physical contact with the subject. To minimize the variability in the EEG artifacts due to the MR sequence and avoid wire movement caused by mechanical vibration the wires rested on foam pads.

EEG data were acquired at the rate of 1024 Hz (and in two dataset at 2048 Hz) using the software package SystemPlus (Micromed, Treviso, Italy). To avoid saturation, the EEG amplifier had a resolution of 16 bits with a range of ±25,6 mV. An anti-aliasing hardware band-pass filter was applied with a bandwidth between 0.15-269.5 Hz.

5.4 fMRI data acquisition

Functional images were acquired on a 1.5 T MR scanner (Symphony, Siemens, Erlangen, Germany) equipped with EPI capability and a standard transient/receive (TR) head coil. fMRI data were acquired with a T2* weighted EPI sequence (36 slices, TR= 3700 ms, TE= 50 ms, 64×64 matrix, FOV= 256×256, slice thickness 3 mm; voxel size= 3×3×3 mm, axial slice orientation).

A T1-weighted anatomical scan (192 slices, TR = 1990 ms, TE = 3 ms; scanning matrix 512×512, FOV = 256×256; slice thickness 1 mm; sagittal slice orientation) was also acquired for each subject and patient.

5.5 EEG processing and analysis

Pre-Processing. Processing of the data was performed using Matlab 7 and EEGLAB 4.51 (Delorme and Makeig, 2004), a freely available open source software toolbox (EEGLAB toolbox for single trial data analysis, Swartz Center for Computational Neurosciences, La Jolla, CA; http://www.sccn.ucsd.edu/eeglab).
The EEG artifact induced by the magnetic field gradient was digitally removed off-line using an adaptive filter (Micromed). The EEG artifact associated with pulsatile blood flow, BCG, was also digitally removed offline using a simple averaging procedure (Allen et al. 1998) implemented in the software SystemPlus. Reference-free recordings were then obtained by calculating the local average reference using EEGLAB. A notch filter (50 Hz) was also applied to all channels. EEG recordings were band-pass filtered from 1-20 Hz using a Finite Impulse Response (FIR) filter. The signal was then baseline corrected and detrended. The two dataset acquired at 2048 Hz were down-sampled to 1024 Hz. A scalp EEG is a non-stationary time series that usually presents artifacts due to electrooculogram (EOG), EMG and ECG, among others. Sometimes artifacts are presented during a few seconds and can be obviated because they obscure only a small portion of the EEG. They make the mathematical analysis of scalp EEG signal difficult. For this reason, epochs with artifacts were visually identified and excluded from further analysis. The filtered signal was reviewed by an experienced neurophysiologist to mark the time of onset of epileptic activity.

Analysis. After ICA decomposition the components were selected using a wavelet representation as described in the *Selection of components* step in paragraph 4.3. A family of Morlet wavelets was first constructed at 1 Hz frequency intervals ranging from 1 to 20 Hz to study all the frequency ranges of interest. Our wavelet family was computed using a ratio of 8 oscillations for patients and 20 oscillations for subjects (Appendix). Using these values we could best investigate power changes as the optimal compromise in time-frequency. For each component we selected from the frequency bins, centered around 1 and 20 Hz for patients and around 8 and 12 Hz for subjects, the one with the maximal power over the total recording session. For subjects we chose 8-12 Hz range to study alpha rhythm during eyes open and closed

condition. After the components of interest have been selected, they were back projected to obtain a reconstructed EEG signal and finally, as described in paragraph 4.3, the EEG regressor was constructed.

5.6 Images processing and analysis

Pre-processing. The functional data were pre-processed using BVQX software version 1.9 (Brain Innovation, Maastricht, The Netherlands) running in Windows Vista environment. The MR images were realigned to reduce the effect of head motion (three-dimensional motion correction with trilinear interpolation). To correct for the different acquisition times, a slice scan time correction was used with ascending, interleaved scanning order with linear interpolation in time. Data were then pre-processed with linear trend removal, to remove all the drifts, and with a temporal high-pass filter (3 cycles in time course) to reduce the influence of breathing and physiological noises. The anatomical and functional data were kept in the subject's native space. The optional temporal smoothing filter was not used during BVQX analysis while spatial Gaussian smoothing was used with Gaussian kernel 6-mm full width at half maximum (FWHM).

GLM analysis. Pre-processed fMRI data were analyzed by using a in-house software implemented in Maltab 7 (MathWorks, Natick, MA) environment based on the GLM approach (Friston et al., 1995) (Appendix). To account for the hemodynamic delay, the EEG power time series was convolved with the canonical HRF (two gamma) (Friston et al. 1998) as described in paragraph 4.3. Brain activation was detected by comparing the signal intensity of task performance images (ON) with that of resting images (OFF) based on the changes in local BOLD signals. Images acquired during the ON condition were compared with images acquired from the same location during the OFF condition. Based on estimate β parameters, activation maps were calculated by using the voxel-wise student's *t*-test and Bonferroni correction to identify activated voxels corrected p-value$\leq$0.05. For Bonferroni correction the number of voxels related to the brain volume was considered. One can control the family-wise error rate (FWE), the probability of at least one false positive on any voxel in the image, using Bonferroni correction or other methods like false discovery

rate (FDR) or random field theory (RFT). Bonferroni correction has the advantage that there is less multiplicity adjustment because of reduced number of voxels. Indeed a mask is applied to the image, so that only voxels inside the brain are considered in the multiplicity adjustment. This improves the power to detect activated voxels inside the brain and uncovered by the mask (Logan and Rowe, 2003). After Bonferroni correction, t-maps representing brain activation were generated. The results were displayed on parametric statistical maps in which the pixel t value is expressed on a colorimetric scale.

Chapter 6

PERFORMANCE OF THE NOVEL METHOD

The method was validated in silico on 3 simulations, corresponding to 3 different choices for the mixing matrix **A** and then applied to two real datasets.

6.1 In silico data

In all 3 simulations, the set of spatio-temporal components decomposed by ICA included two components which appear to correspond to the epileptiform activity (in Fig. 6.1 components # 2 and 8). The remaining components showed the background activity or artifacts and not any feature of epileptiform activity. Application of wavelet transform indicates that components that exceeded mean value ± standard deviation were # 2 and 8, representing the simulated waveforms (Fig. 6.2). After the construction of the "true" and the estimated EEG regressor (Eq. 5.2 and 5.3) we compared them (Fig. 6.3) using the index H. In all the 3 simulations the EEG regressor estimated by the method well matches the true one since index H is below 5% (simulation1: H=0.0307; simulation2: H=0.0402; simulation3: H=0.0306).

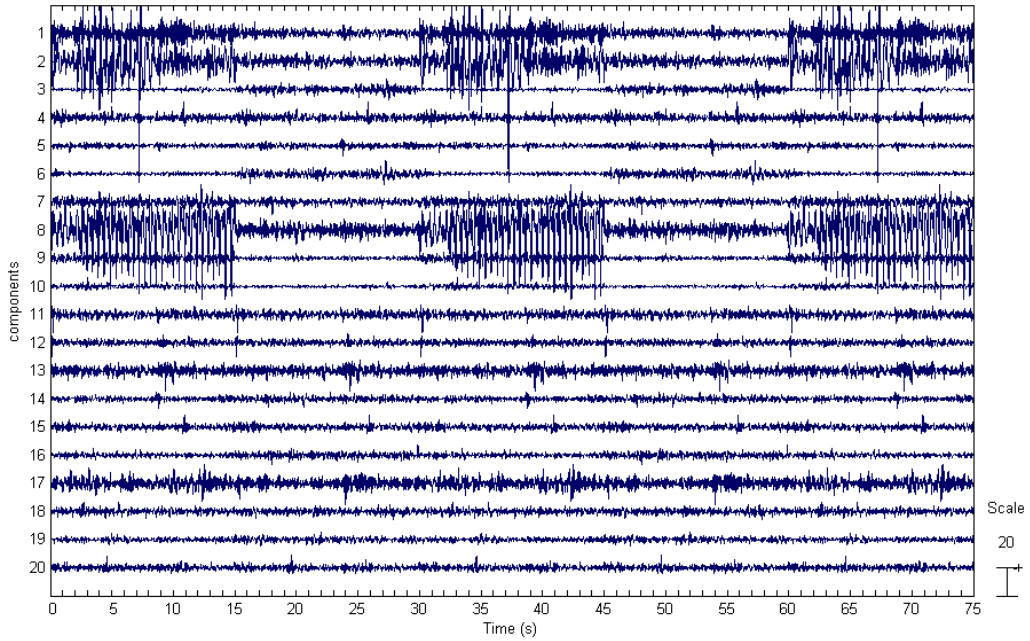

Figure 6.1. Components obtained by ICA decomposition of EEG signal shown in Fig. 5.3. Components # 2 and 8 have 'spike-wave' waveform similar to components # 7 and 14 of Fig. 5.2, respectively.

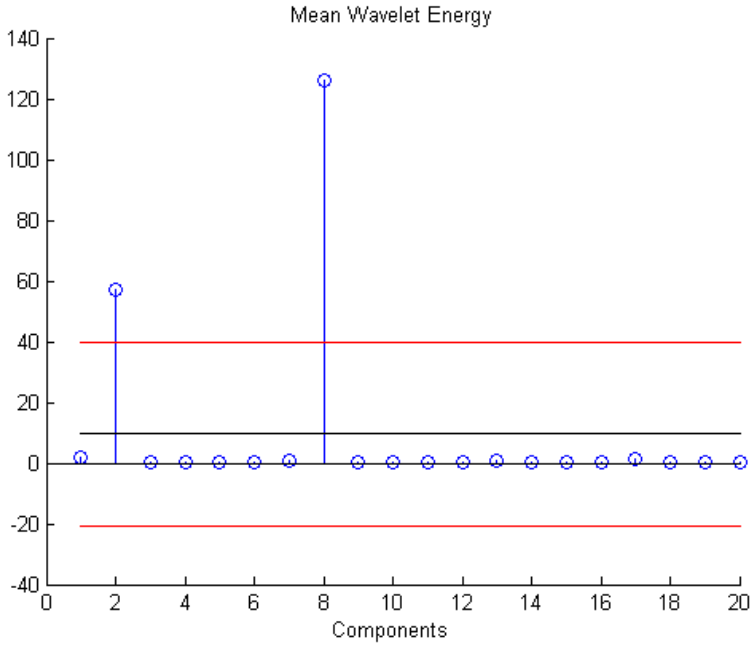

Figure 6.2. Wavelet energy of EEG components selected. Components are # 2 and 8.

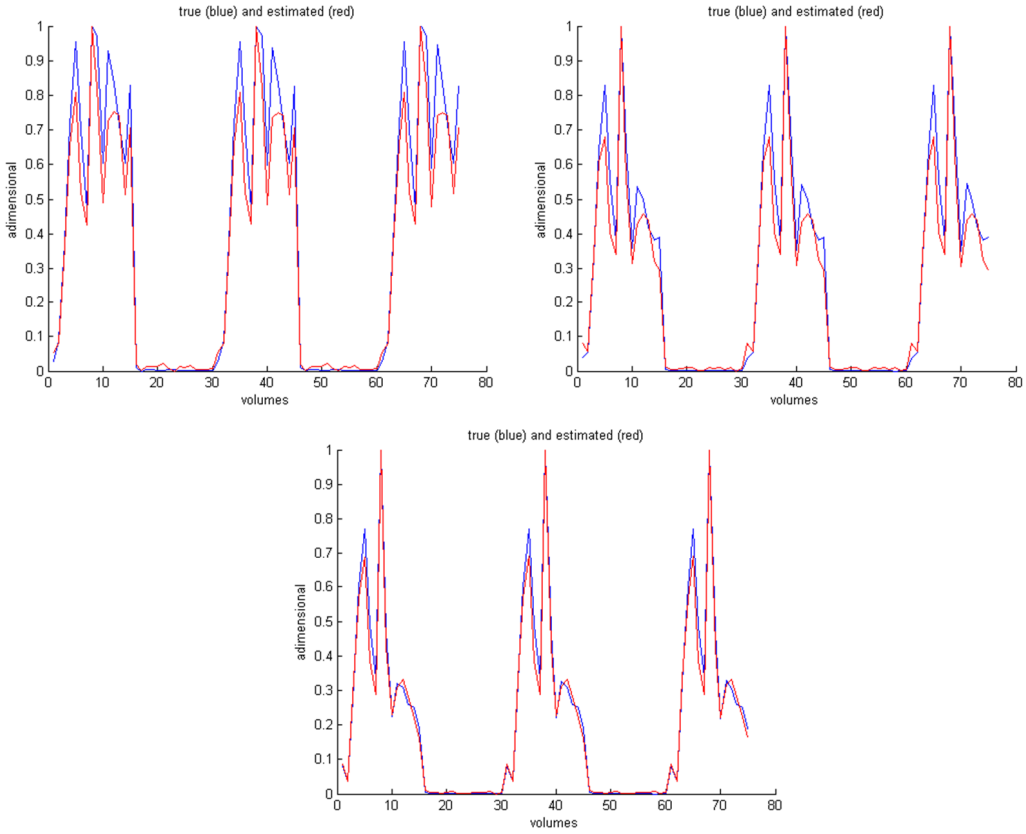

Figure 6.3. Results of the convolution between EEG regressor and HRF model in the three simulations. Comparison between the true (blue) and the estimated (red) results.

6.2 Real Data

Normal Subjects

During fMRI acquisition two subjects were instructed to open an close their eyes according to an experimental design (Fig. 5.4).

Subject #1: After EEG pre-processing ICA decomposition was applied according to Eq. 2 (Appendix) (Fig. 6.4).

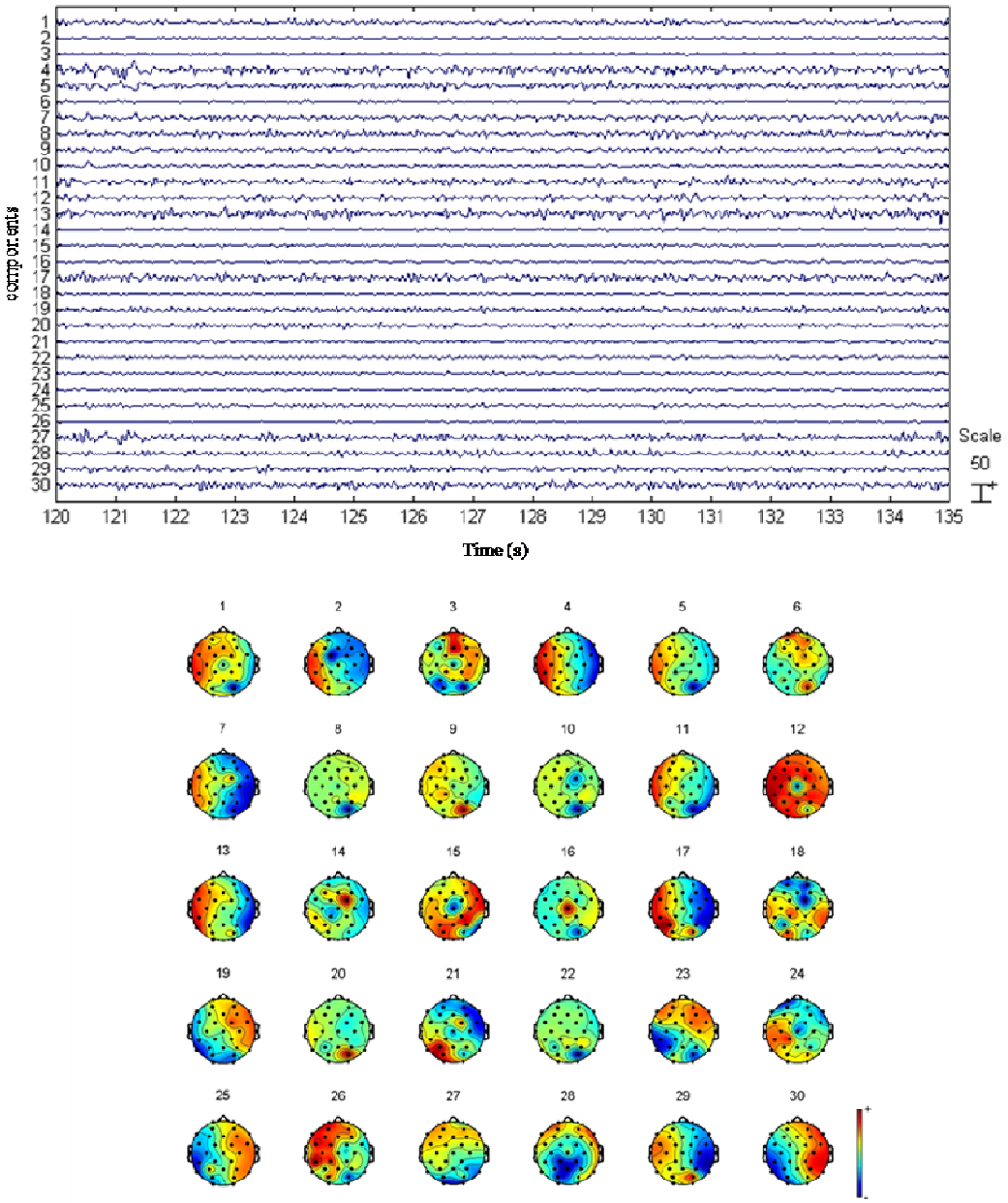

Figure 6.4 Subject #1: EEG components after ICA decomposition (top). EEG component scalp maps (W^{-1}) obtained from ICA decomposition (bottom).

For the analysis of subject 1 we chose three intervals time during eyes closed condition, because in this condition the amplitude of EEG signal in alpha range is high. The intervals were: 1) 120-125s, 2) 184-196s, 3) 256-271s. After the application of wavelet transform in these ranges, we found that components that

exceeded mean value ± standard deviation were # 4, 5, 13 and 27 for interval 1), # 4, 13, 27, 28 for interval 2) and # 4, 8, 17, 27, 30 for interval 3) (Fig. 6.5). The components shared among intervals were # 4 and 27 and they were chosen for the analysis. The channel O2, related to alpha rhythm and with a high correlation coefficient (r=0.89), was selected for the construction of EEG regressor (Fig. 6.6). Alpha rhythm was chosen since it was most intensely modulated by the task. As expected, alpha rhythm was suppressed during eyes open and reappeared during eyes closed; in reverse to the experimental paradigm where the active condition is express by opening eyes.

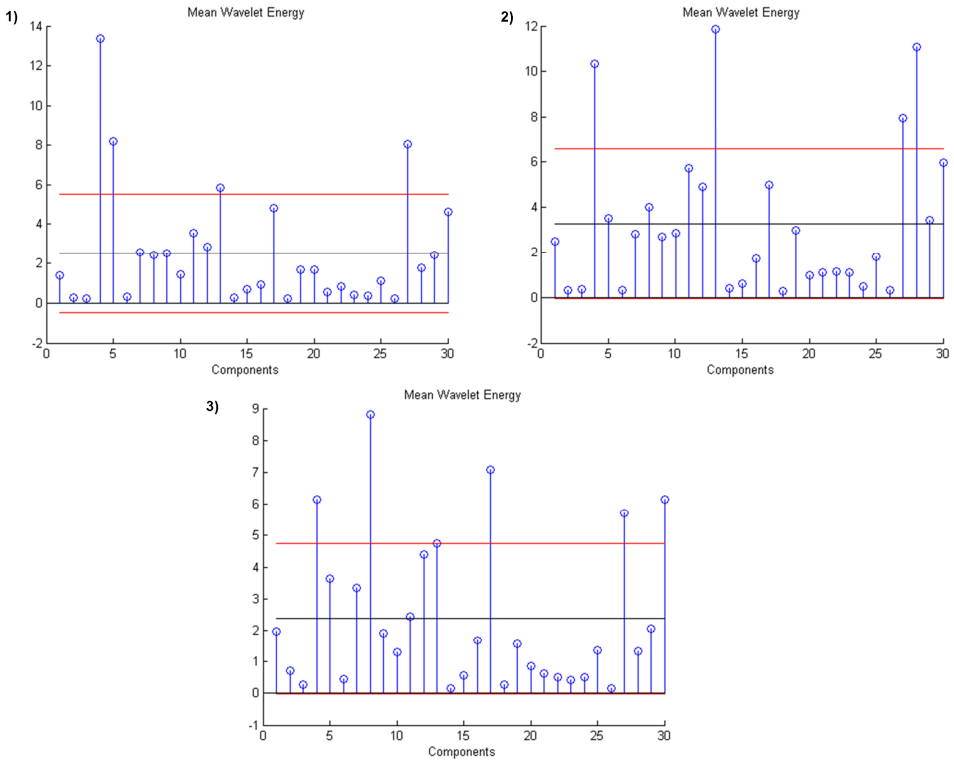

Figure 6.5. Subject #1: Mean Wavelet Energy in time for each component (blue). Mean value (black) ± standard deviation (red).

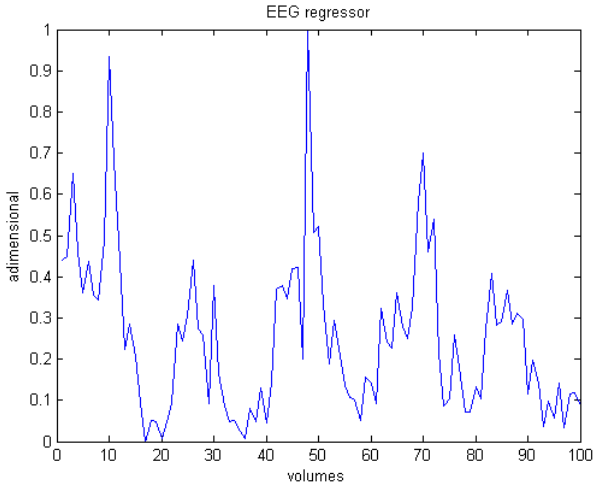

Figure 6.6. Subject #1: EEG regressor model for channel O2.

Using this model we obtained a significant activation extending from a frontocentral cluster bilaterally to the back of the head, probably the result of the associated eye and lid movements (Fig. 6.7). A significant deactivation is seen in Fig. 6.8.

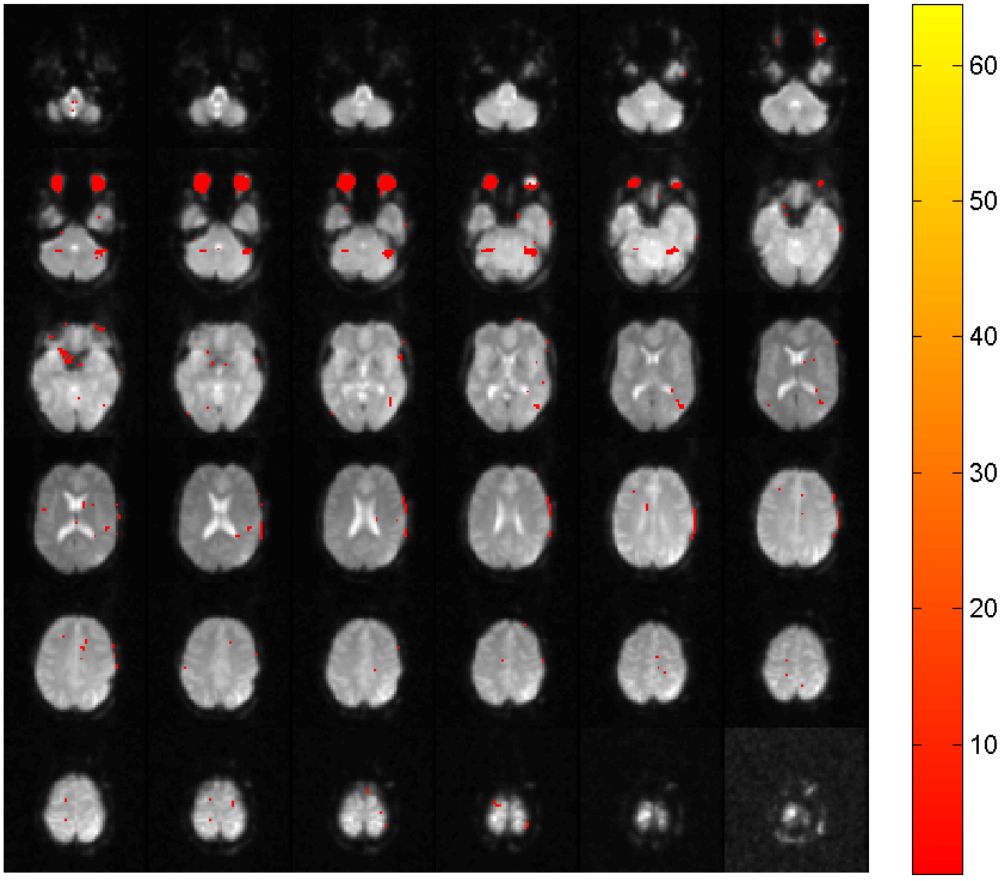

Figure 6.7. fMRI activation maps (positive t-value) for subject #1.

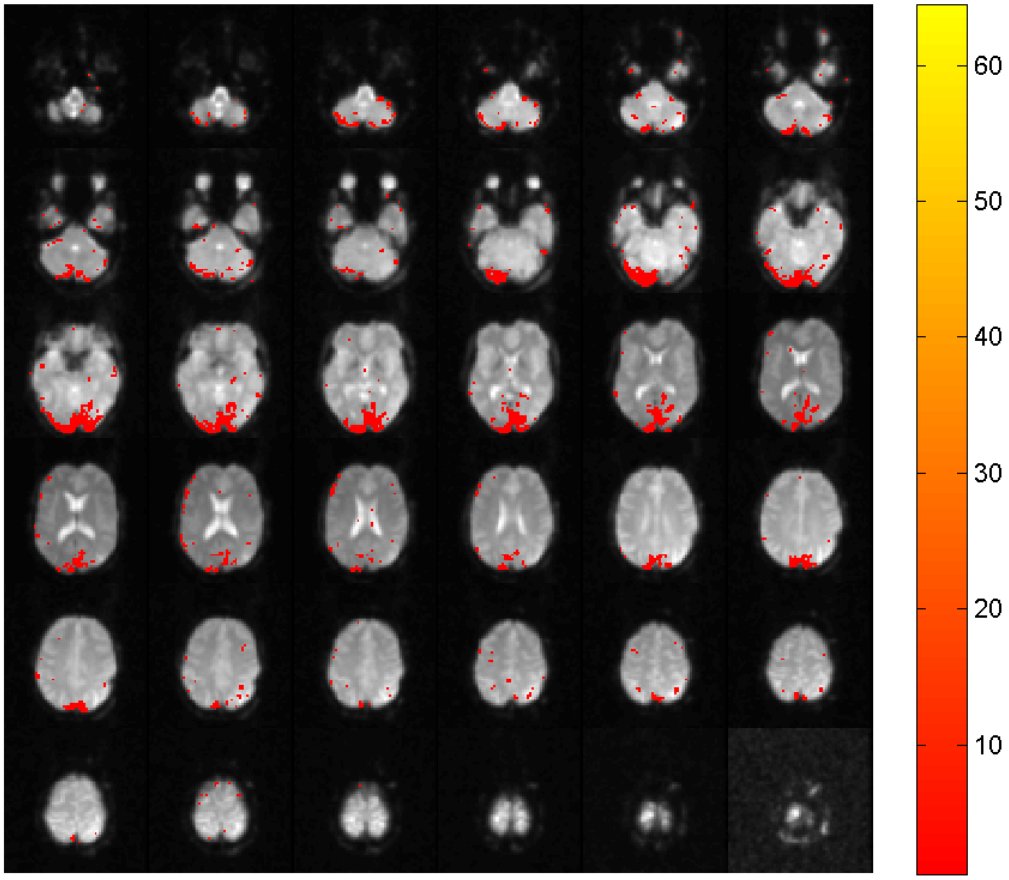

Figure 6.8. fMRI deactivation maps (negative t-value) for subject #1.

The area deactivated during increased alpha includes the calcarine and fusiform gyri as well as medial parietal cortex (Broodmann area 7). These results are the same obtained using a GLM analysis with a block model (Fig. 6.9), the conventional analysis described in paragraph 3.2. Alpha is positive correlated with protocol in frontocentral area, but it is negative correlated in occipital cortex.

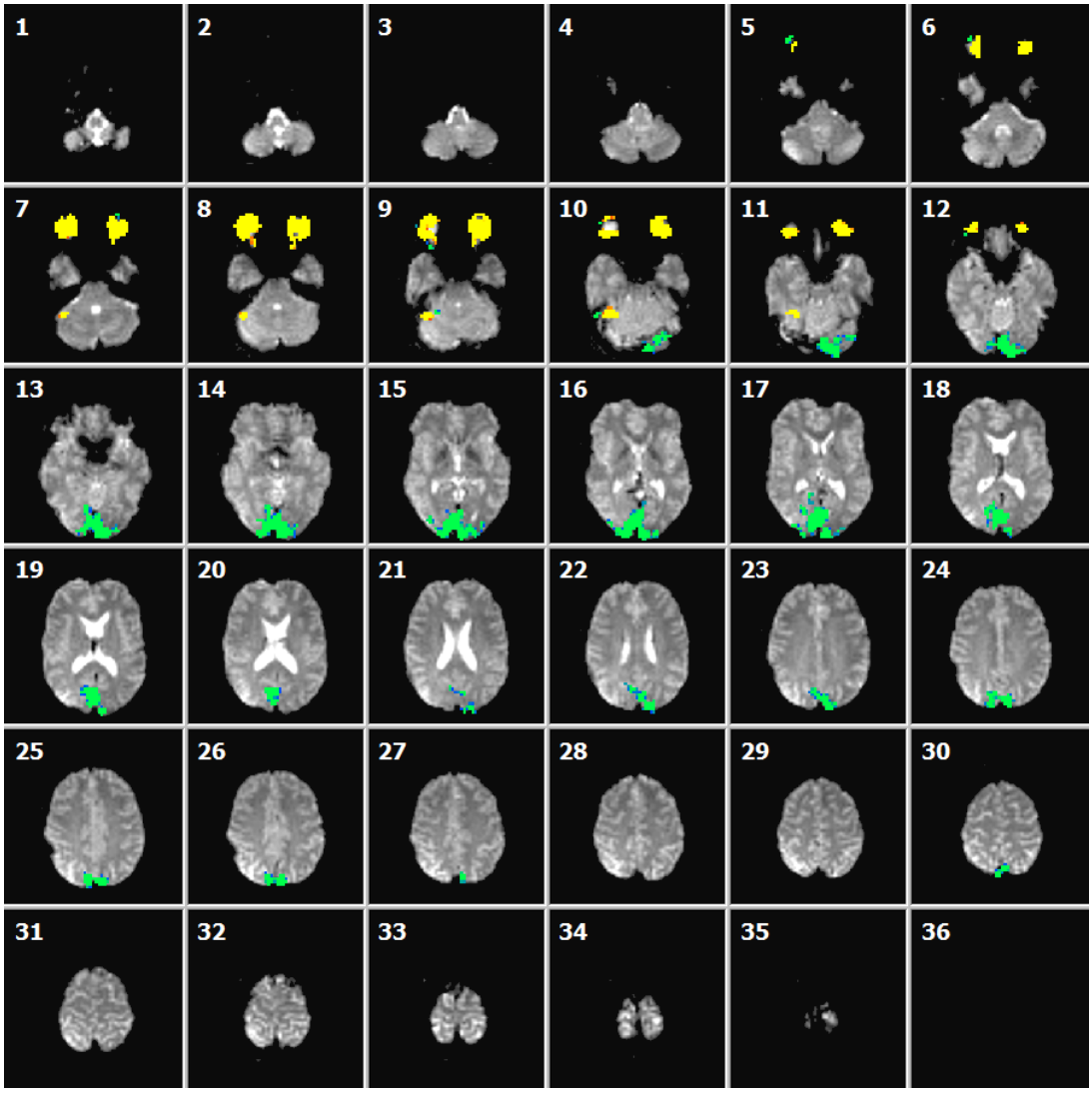

Figure 6.9. Subject #1: Brain Voyager analysis using a block model. fMRI activation (yellow) and deactivation (green) maps.

Subject #2: For subject #2 the intervals chosen were: 1) 23-33s, 2) 88-98s, 3) 235-245s. After ICA decomposition (Fig. 6.10) and the application of wavelet transform, components that exceeded mean value ± standard deviation were # 5, 6, 7, 13 for interval 1), # 7, 13 for interval 2) and # 7, 13 for interval 3) (Fig. 6.11). Components selected were # 7 and 13 and the EEG regressor was obtained from channel PO4 (r=0.83) (Fig. 6.12). Regions of activation were the same as that of subject #1 (Fig. 6.13 and Fig. 6.14).

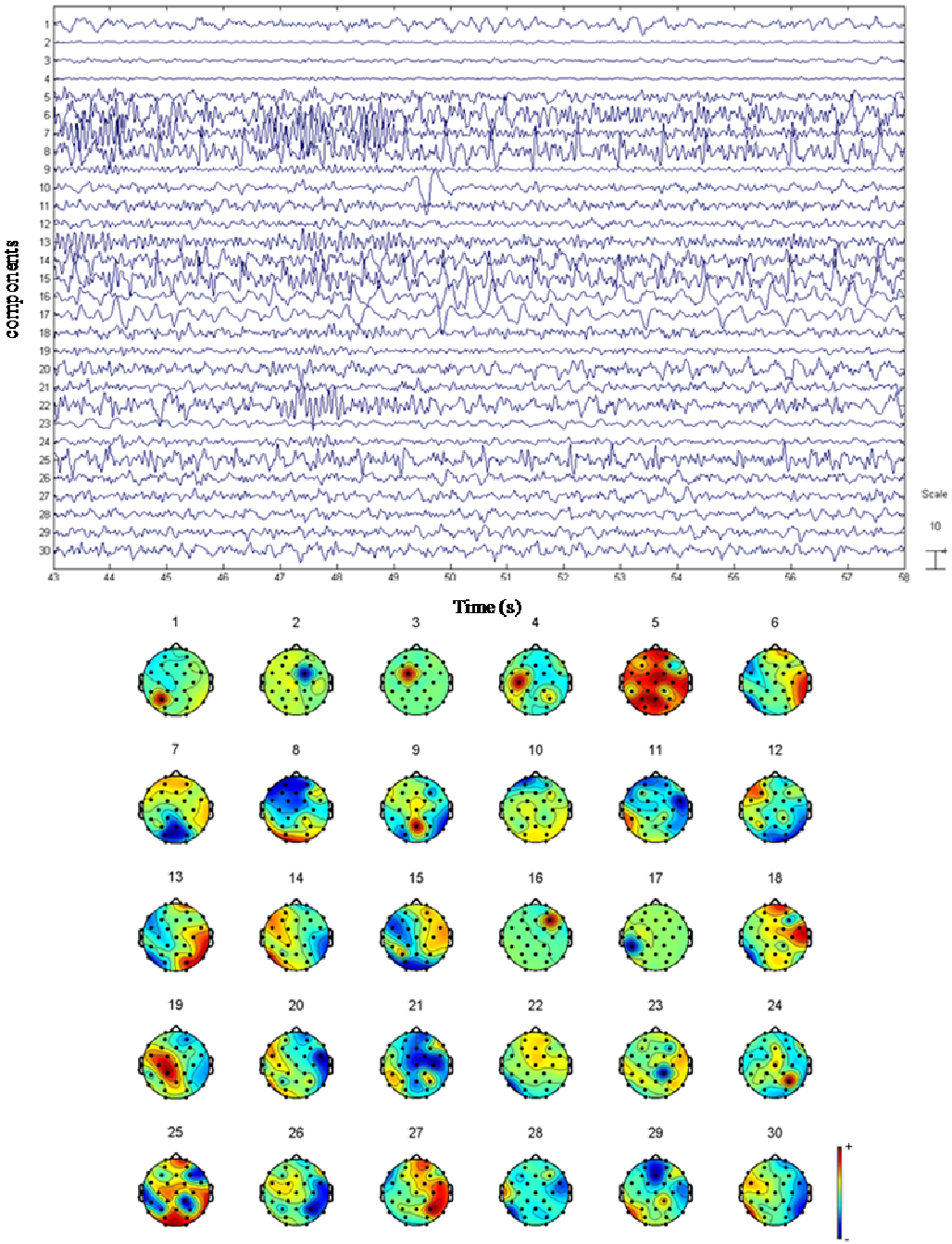

Figure 6.10. Subject #2: EEG components after ICA decomposition (top). EEG component scalp maps (W^{-1}) obtained from ICA decomposition (bottom).

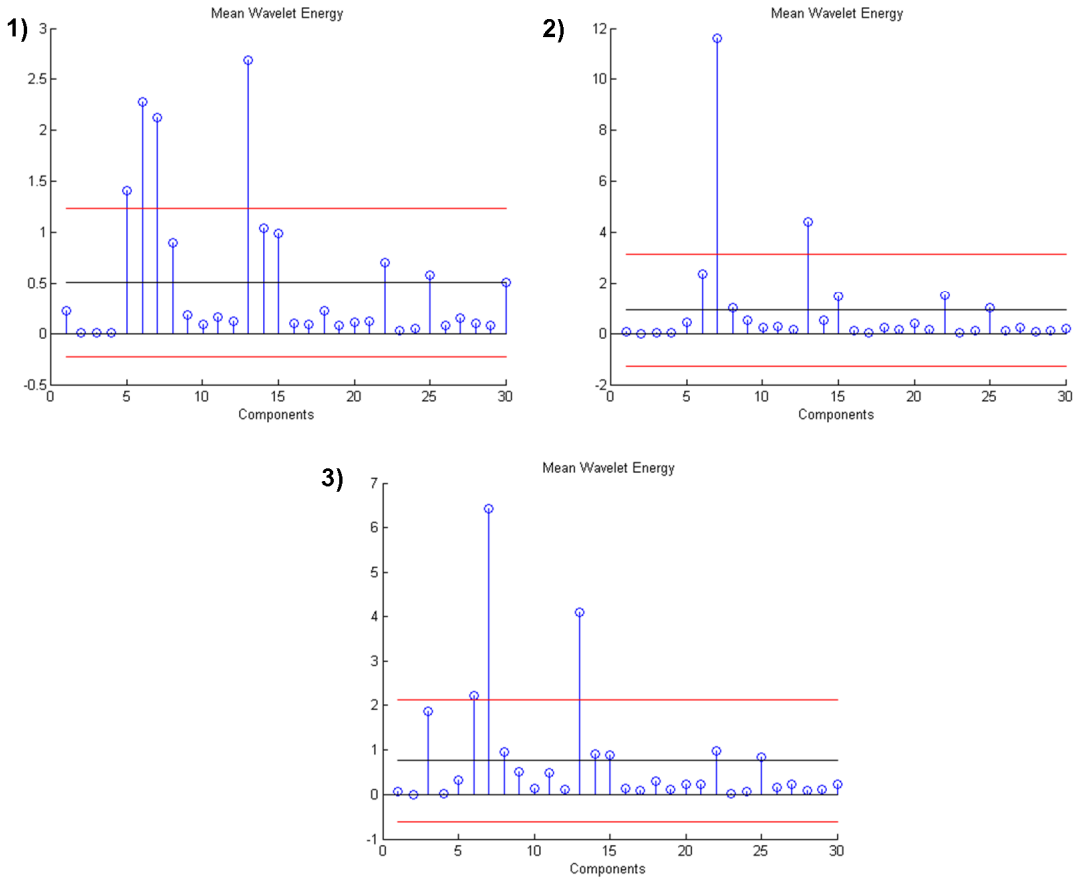

Figure 6.11. Subject #2: Mean Wavelet Energy in time for each component (blue). Mean value (black) ± standard deviation (red).

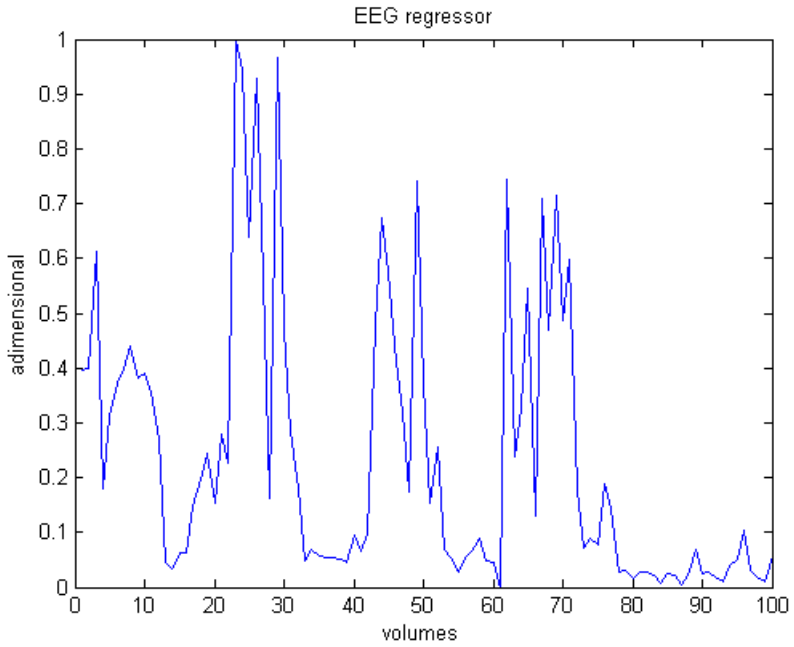

Figure 6.12. Subject #2: EEG regressor model for channel PO4.

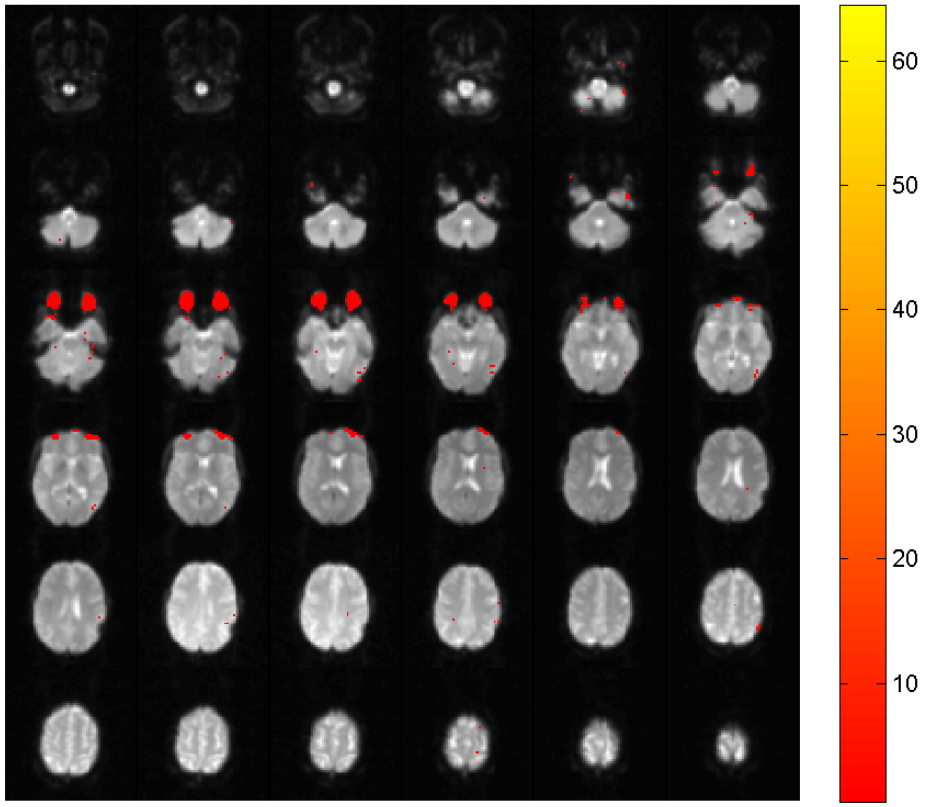

Figure 6.13. fMRI activation maps (positive t-value) for subject #2.

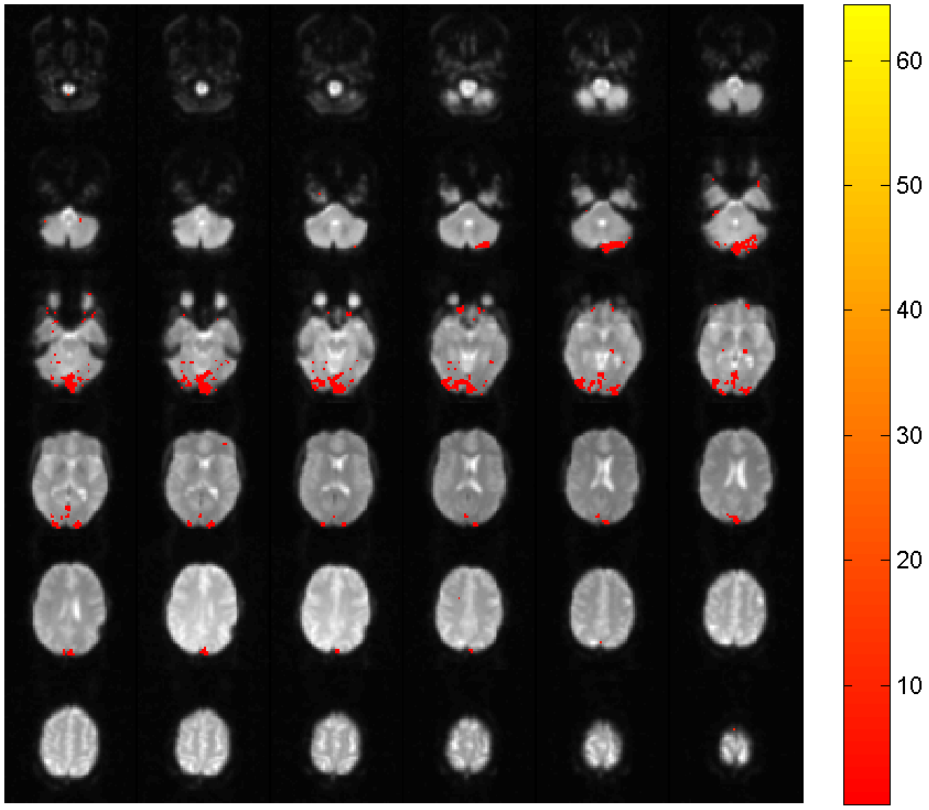

Figure 6.14. fMRI deactivation maps (negative t-value) for subject #2.

Patients

The results were obtained for each patient individually, because its variability.

No clinical or EEG manifestations of ictal events developed during scanning session. None of the patients reported discomfort or other adverse reactions related to the EEG recording procedure. In all patients, except for patient #5, EEG-fMRI analysis showed a significant activation. IEDs recorded inside the scanner had a localization, amplitude and morphology similar to those in previous routine EEG recordings.

Patient #1:

The routine EEG showed an high amplitude rhythmic activity at 4-5 Hz over the right central temporal electrodes. This activity occasionally showed spike morphology developing a spike and slow wave complex. During the recording this activity has a rapid diffusion over the contralateral central and temporal electrodes with long sequence of spikes and slow waves complexes (Fig. 6.15). In this patient we had recorded a focal seizure with head version over the right, tonic posturing of left arm and leg and short lasting loss of consciousness.

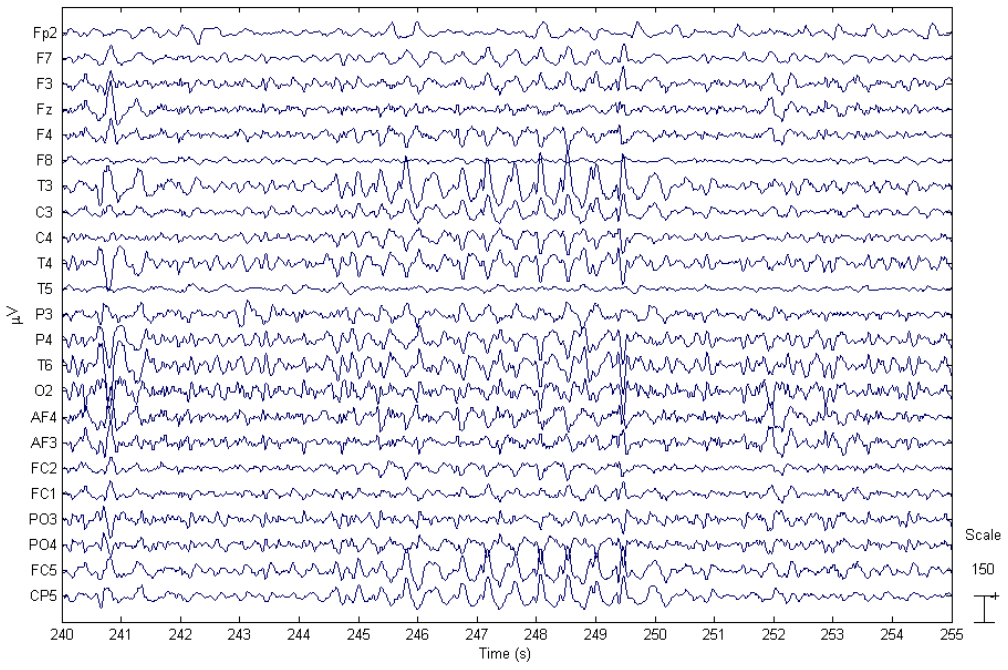

Figure 6.15. Patient #1: EEG signal after pre-processing.

ICA decomposition point out the preponderance of component #11 (Fig. 6.16). Components with higher wavelet energy are two and they changes in time. We obtained component # 11 in the range 212-220s and in 242-250s , and component # 14 in the range 287-313s and 428-457s (Fig. 6.17).

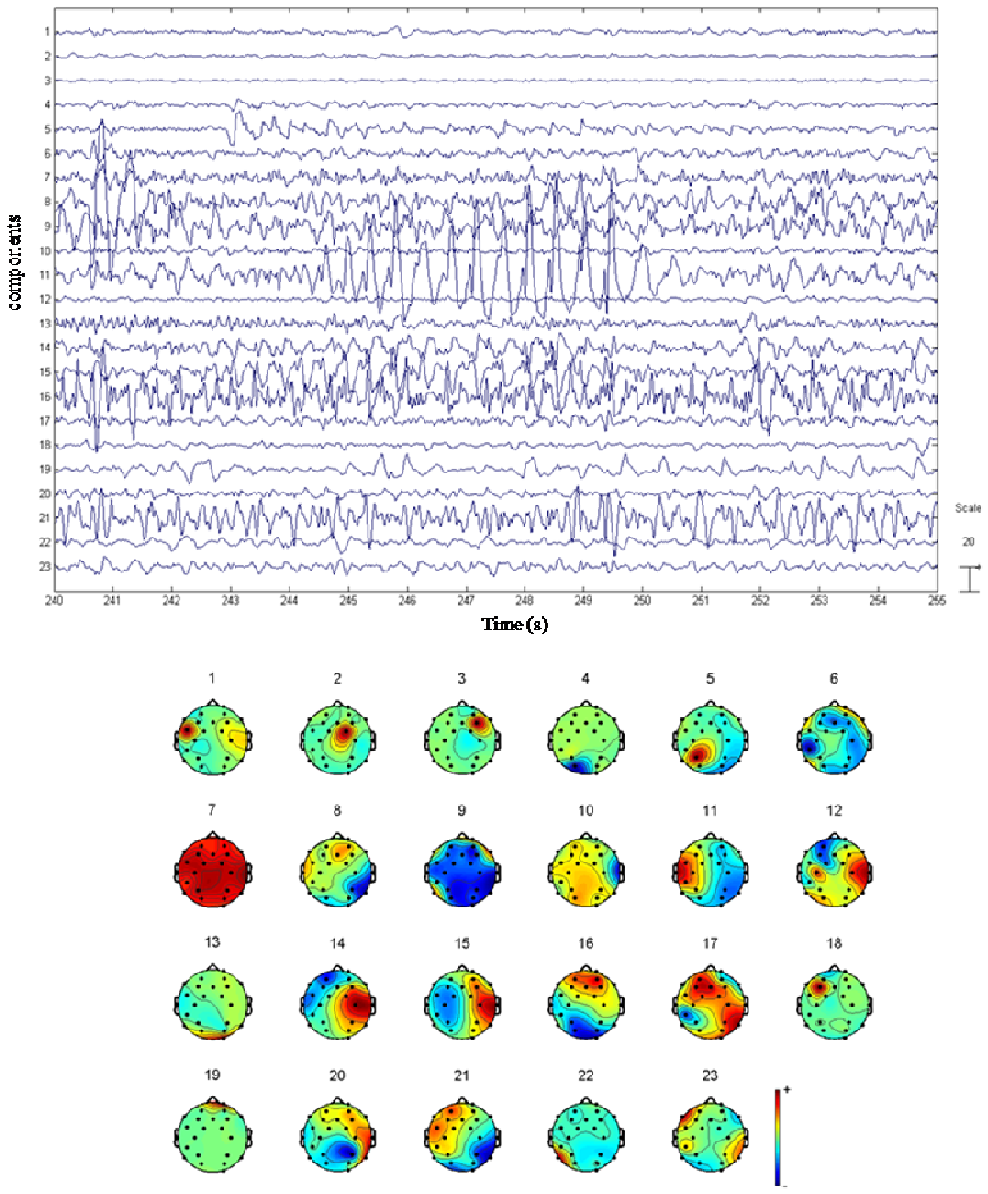

Figure 6.16. Patient #1: Components obtained by ICA decomposition of EEG signal shown in Fig. 6.15. Component # 11 has 'spike-wave' waveform appearing the same as channel T3, component # 14 as channels AF3, AF4 shown in Fig. 6.15 (top). EEG component scalp maps (W^{-1}) obtained from ICA decomposition (bottom).

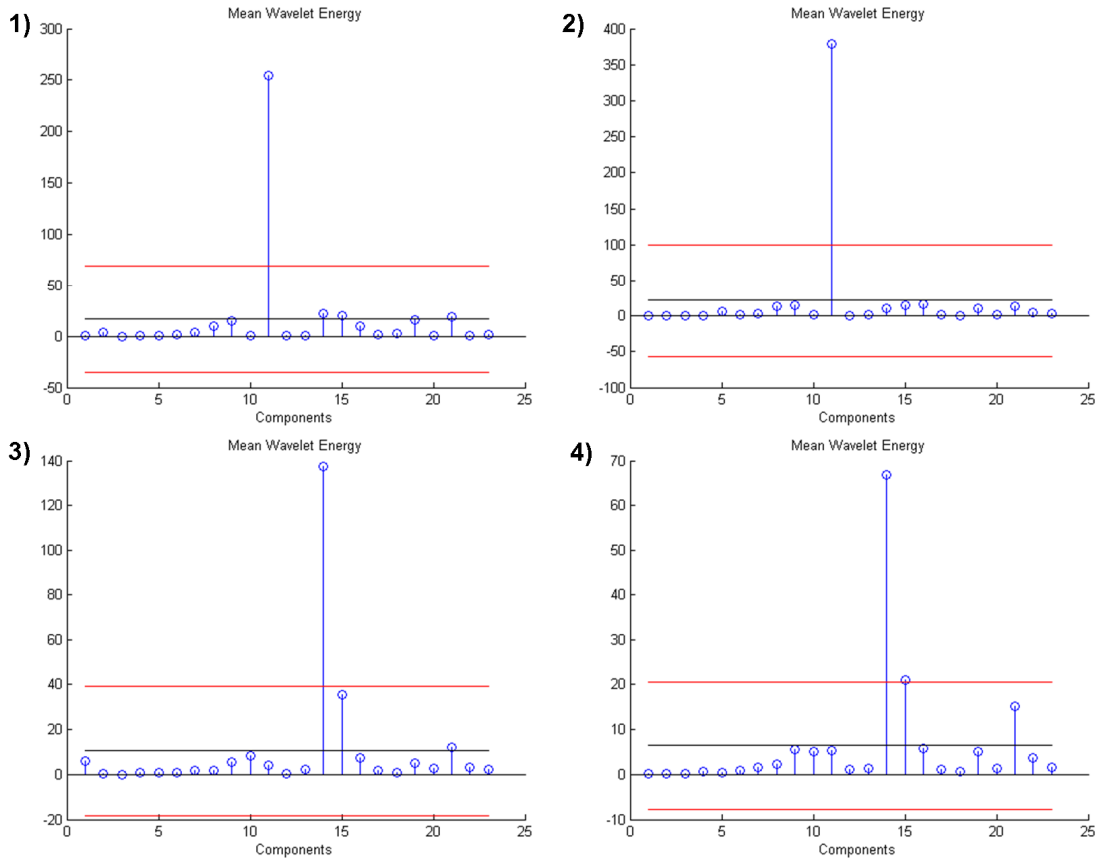

Figure 6.17. Patient #1: Mean Wavelet Energy in time for each component (blue). Mean value (black) ± standard deviation (red). Intervals range: 1) 212-220s, 2) 242-250s, 3) 287-313s, 4) 428-457s.

The first is responsible for the channel T3, while the second one for the channels AF3 and AF4. The two EEG regressor, derived from the two components, produce the same fMRI activation maps. We chose to report only results obtained using component # 11 in the analysis. Comparing the original EEG (Fig. 6.15) to the EEG derived from the component (Fig. 6.18) we chose the channel T3, with correlation coefficient r=0.97, for the construction of the EEG regressor (Fig. 6.19).

fMRI maps shows several activations: in perilesional regions with a diffusion over the parieto-temporal regions controlateral to the lesion. There are also some activations in left frontal areas, in left medial and parietal regions (Fig. 6.20)

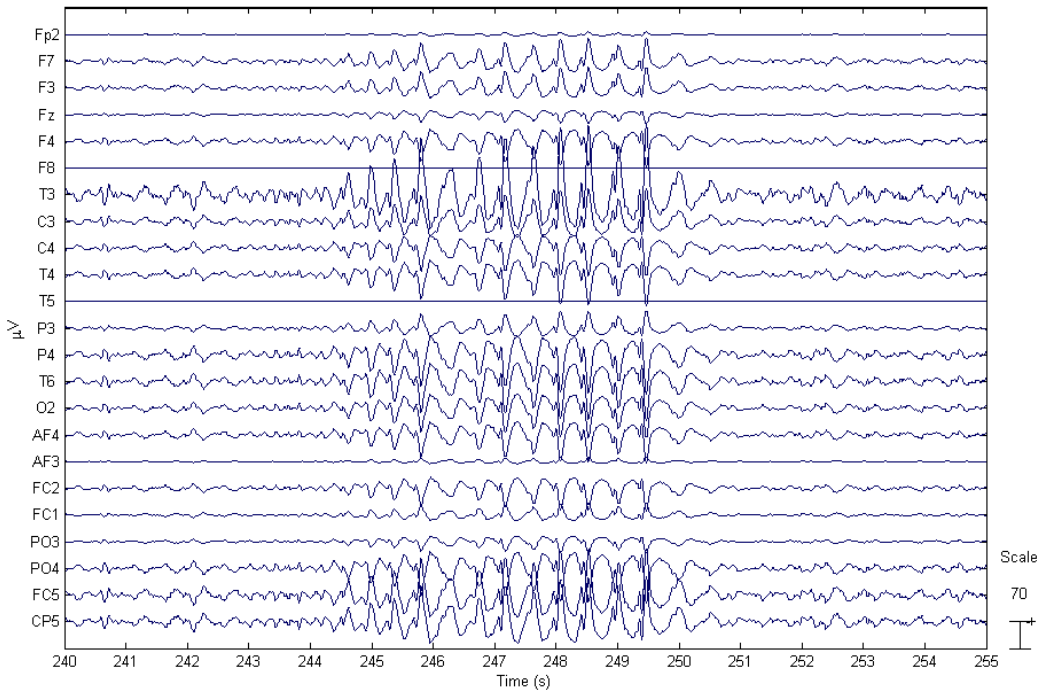

Figure 6.18. Patient #1: EEG derived from the component #11.

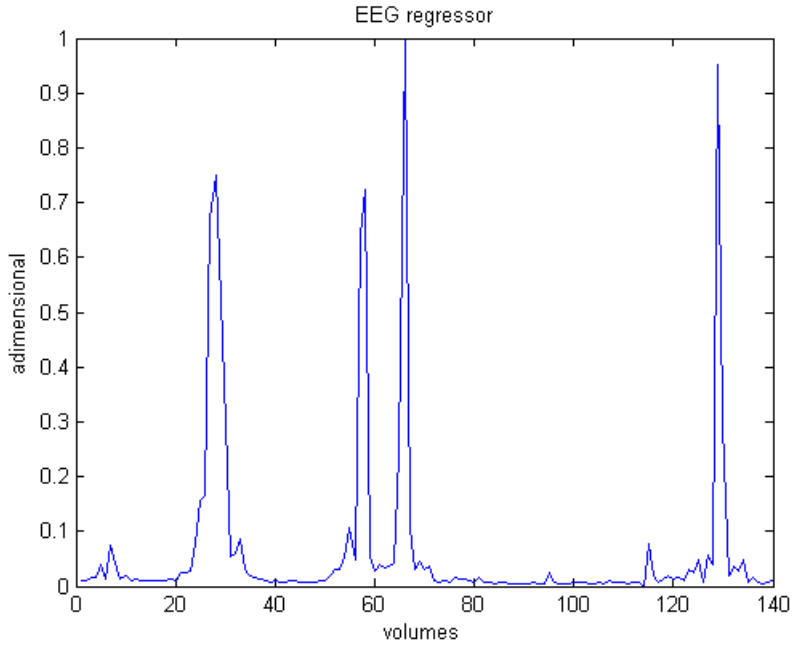

Figure 6.19. Patient #1: EEG regressor model for channel T3.

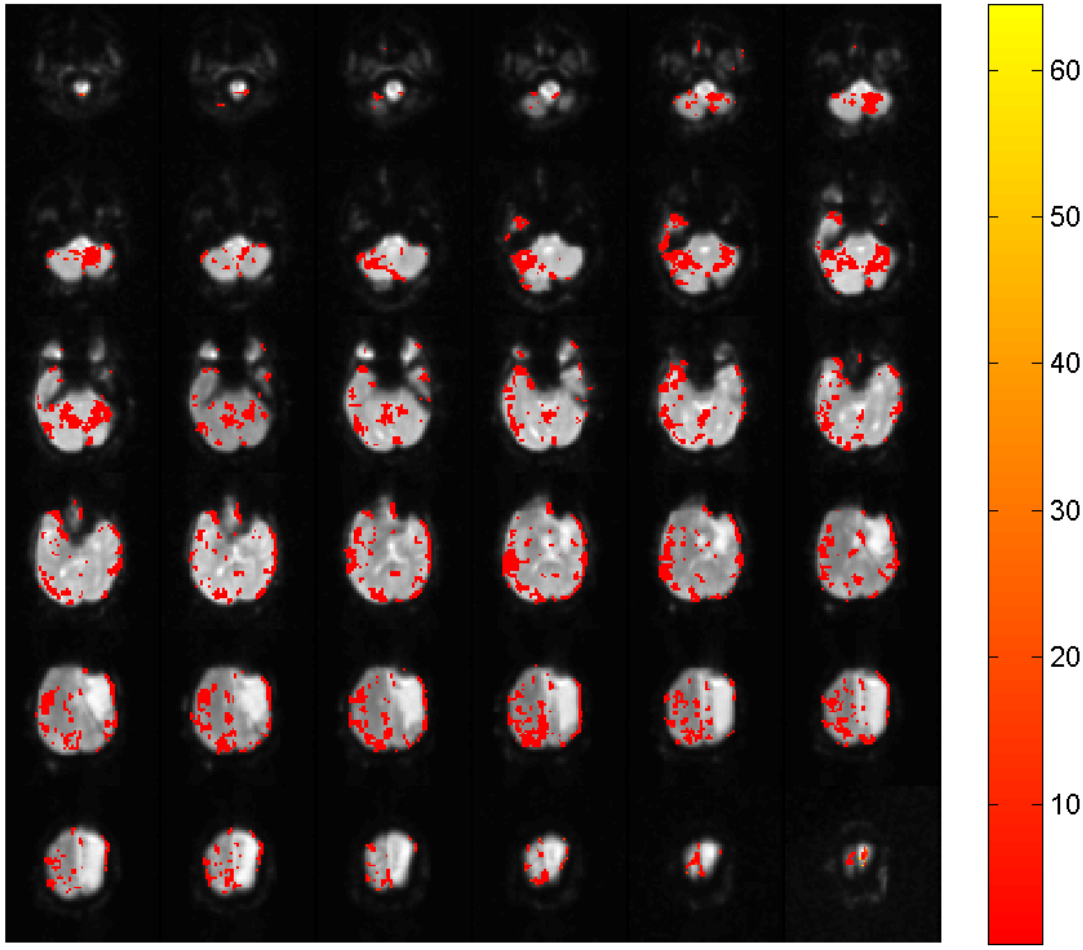

Figure 6.20. fMRI activation maps for patient #1.

Patient #2:

EEG showed rhythmic activity of slow waves (delta range) with spiked morphology short lasting over the all electrodes with a greater amplitude over the left frontal and temporal electrodes (Fig. 6.21). Channels F8, FC2, Cp1, Cp2, PO3, Cz and C4 were excluded from analysis because the EEG signal was bad.

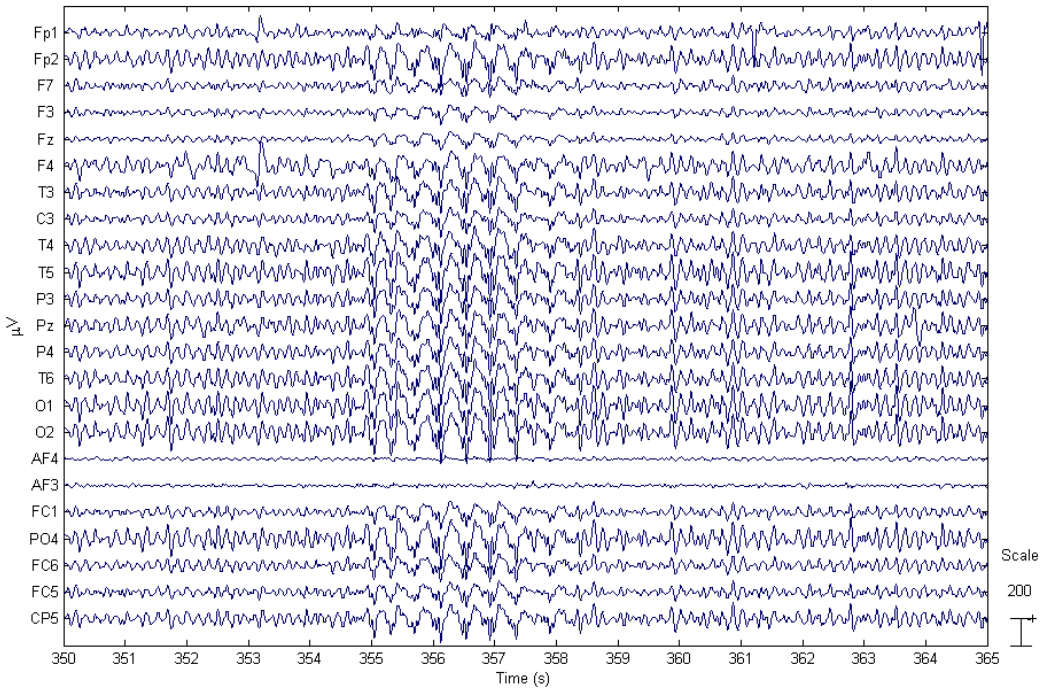

Figure 6.21. Patient #2: EEG signal after pre-processing.

After ICA decomposition analysis we obtained 23 components (Fig. 6.22). Component # 13 is a good representation of the IED activity; it shows a slow activity in delta range and its time course is similar to that of original EEG.

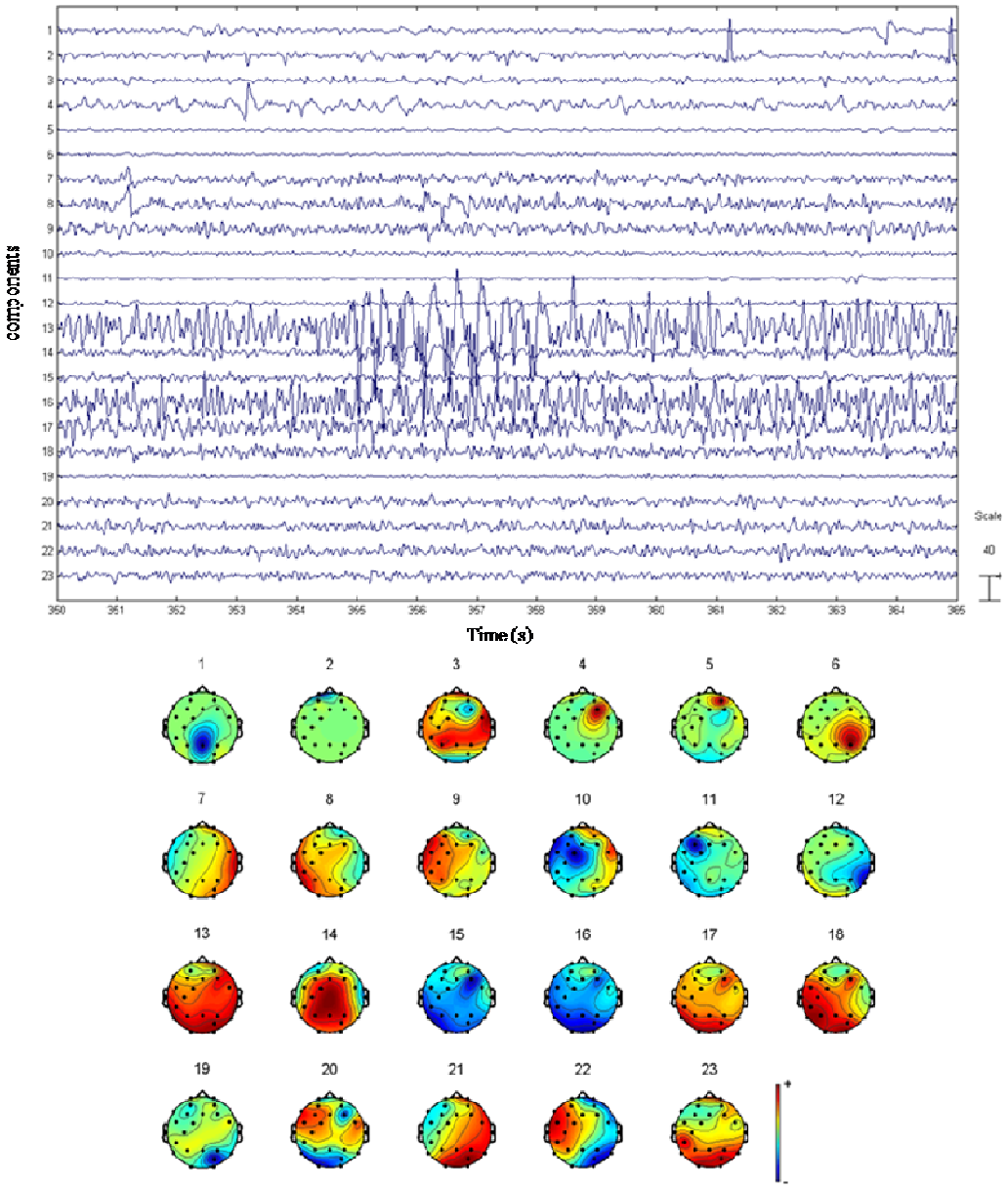

Figure 6.22. Patient #2: Components obtained by ICA decomposition of EEG signal shown in Fig. 6.21. Component # 13 has 'spike-wave' waveform appearing the same as the original EEG shown in Fig. 6.21 (top). EEG component scalp maps (W^{-1}) obtained from ICA decomposition (bottom).

This observation is supported by the results of wavelet transform applied in the two time ranges: 269-277s and 354-358s (Fig. 6.23), where the slow waves activity is clearly visible: component # 13 is responsible for the epileptiform activity.

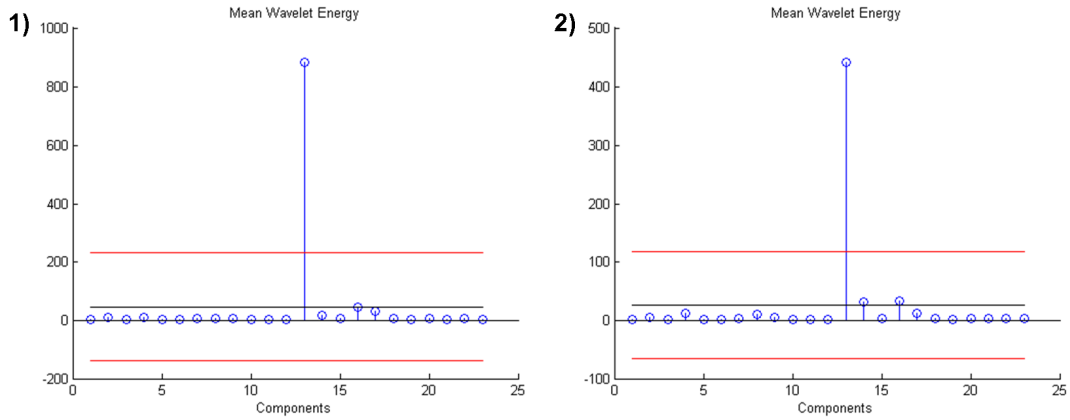

Figure 6.23. Patient #2: Mean Wavelet Energy in time for each component (blue). Mean value (black) ± standard deviation (red). Intervals range: 1) 269-277s, 2) 354-358s.

After the reconstruction of EEG signal from component # 13 (Fig. 6.24), the channel T3, with a high correlation coefficient (r=0.93), was selected for the construction of EEG regressor (Fig. 6.25). It reflects the time intervals chosen previously from the neurophysiologist.

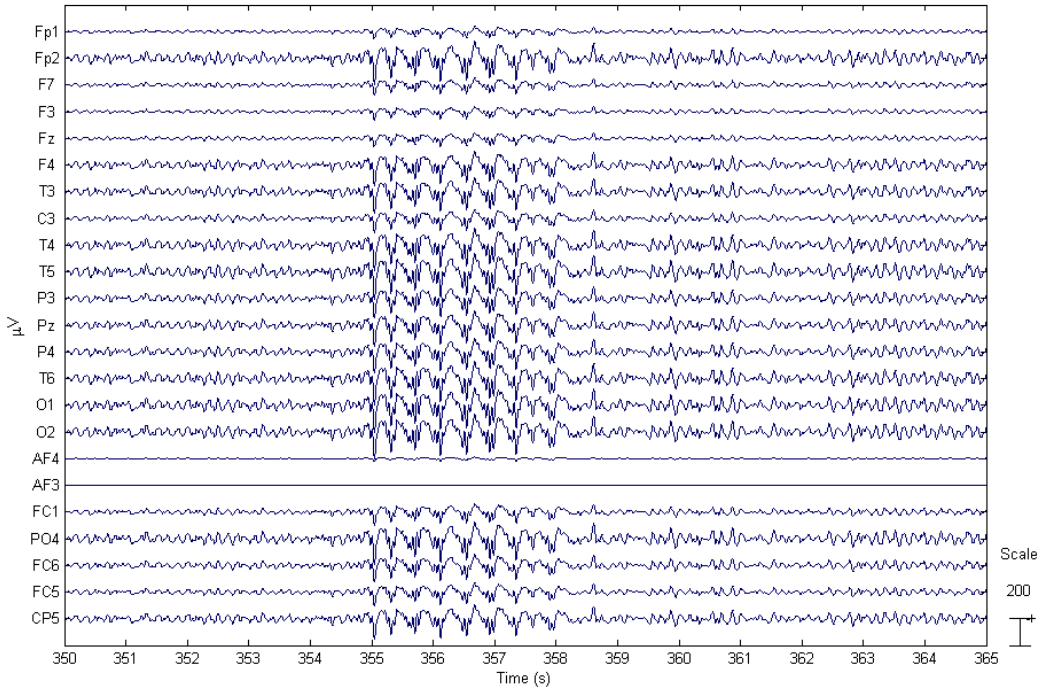

Figure 6.24. EEG derived from the component #13.

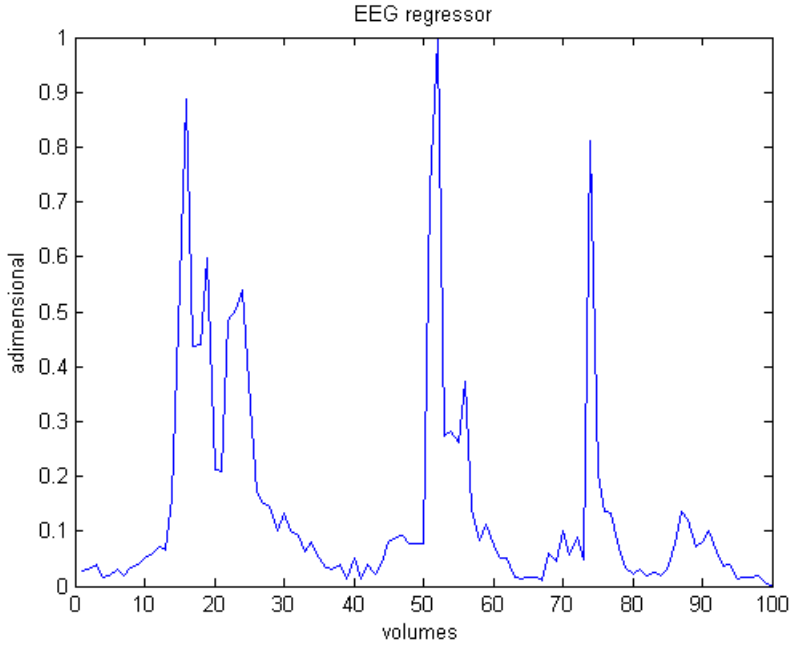

Figure 6.25. Patient #2: EEG regressor model for channel T3.

EEG-fMRI integration shows an important activation over SMA according to the clinical evaluation: speech arrest as manifestation of seizures. There is also a significant activation extending from a frontocentral cluster bilaterally to the back of the head, probably the result of the associated eye and lid movements (Fig. 6.26).

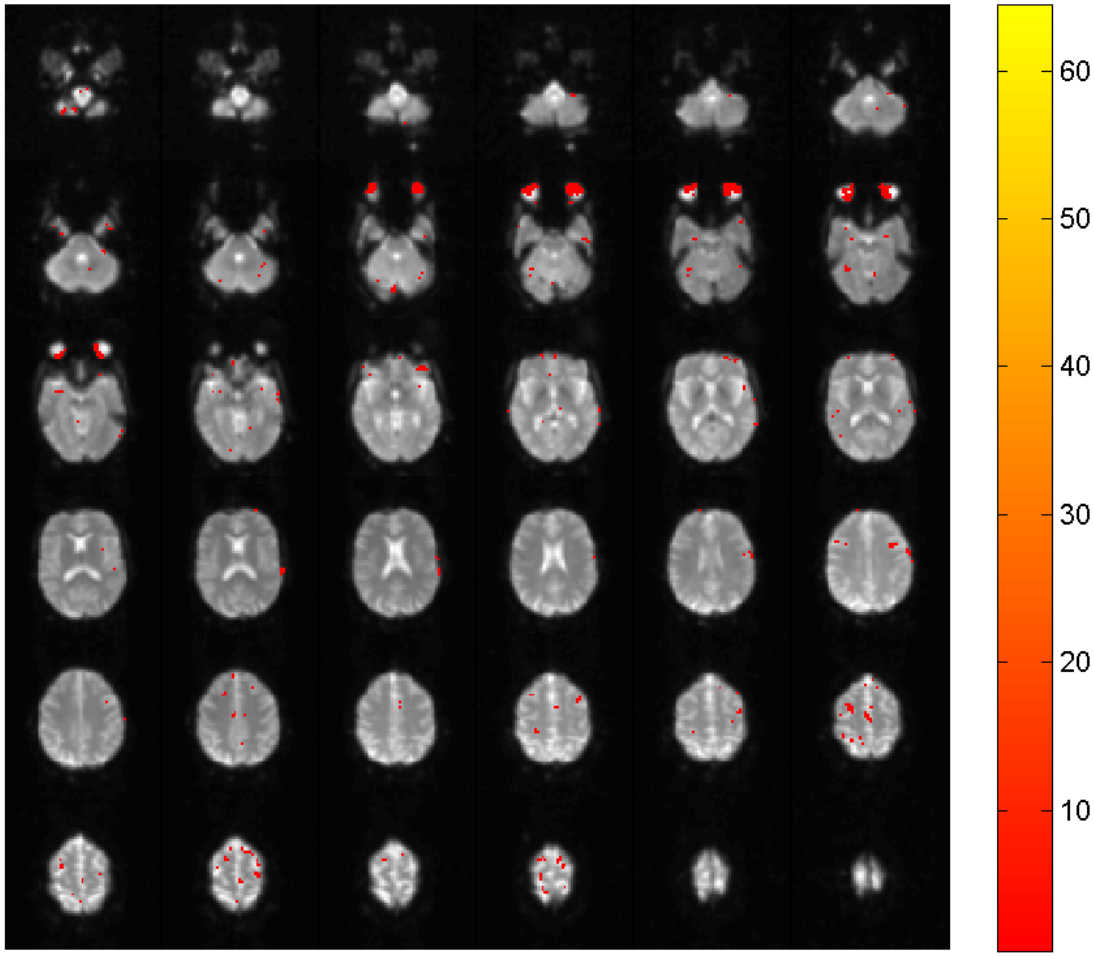

Figure 6.26. fMRI activation maps for patient #2.

Patient #3:

EEG shows spikes and waves over the right central temporal regions (Fig. 6.27); more evident during drowsiness and sleep. Theta activity over the right frontal temporal regions was also present. Electrodes Fp1, F7, F8, Cp1, Cp2, PO3, PO4, FC5, CP5 and CP6 were excluded from the analysis because the signal acquired was bad. ICA decomposition highlight the components # 3, 4, 7, 9 and 11 (Fig. 6.28).

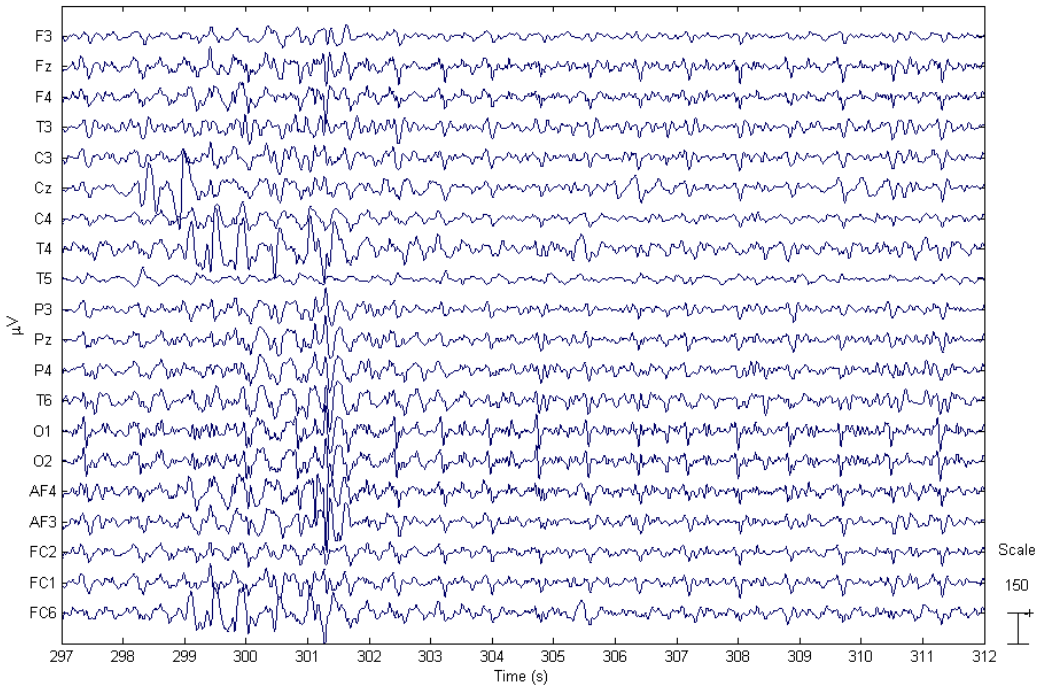

Figure 6.27. Patient #3: EEG signal after pre-processing.

Unlike the others, component # 11 is the same over the duration of the signal and its time-frequency representation reflects its periodicity relative to the repetition time proper to the gradient artifact; for this reason it was excluded from the analysis. After application of the selection criterion, based on wavelet transform, in the two temporal ranges 184-187s and 299-302s, components # 3, 4, 7 and 9 were chosen for the analysis (Fig. 6.29). As shown in Fig. 6.30, T4 was the channel which better describe the IED activity and with the higher correlation coefficient (r=0.89), therefore it was used as a regressor (Fig. 6.31). fMRI maps show a significant activation ($p<0.05$) over the right temporal region according to the spatial distribution of her IED activity (Fig. 6.32).

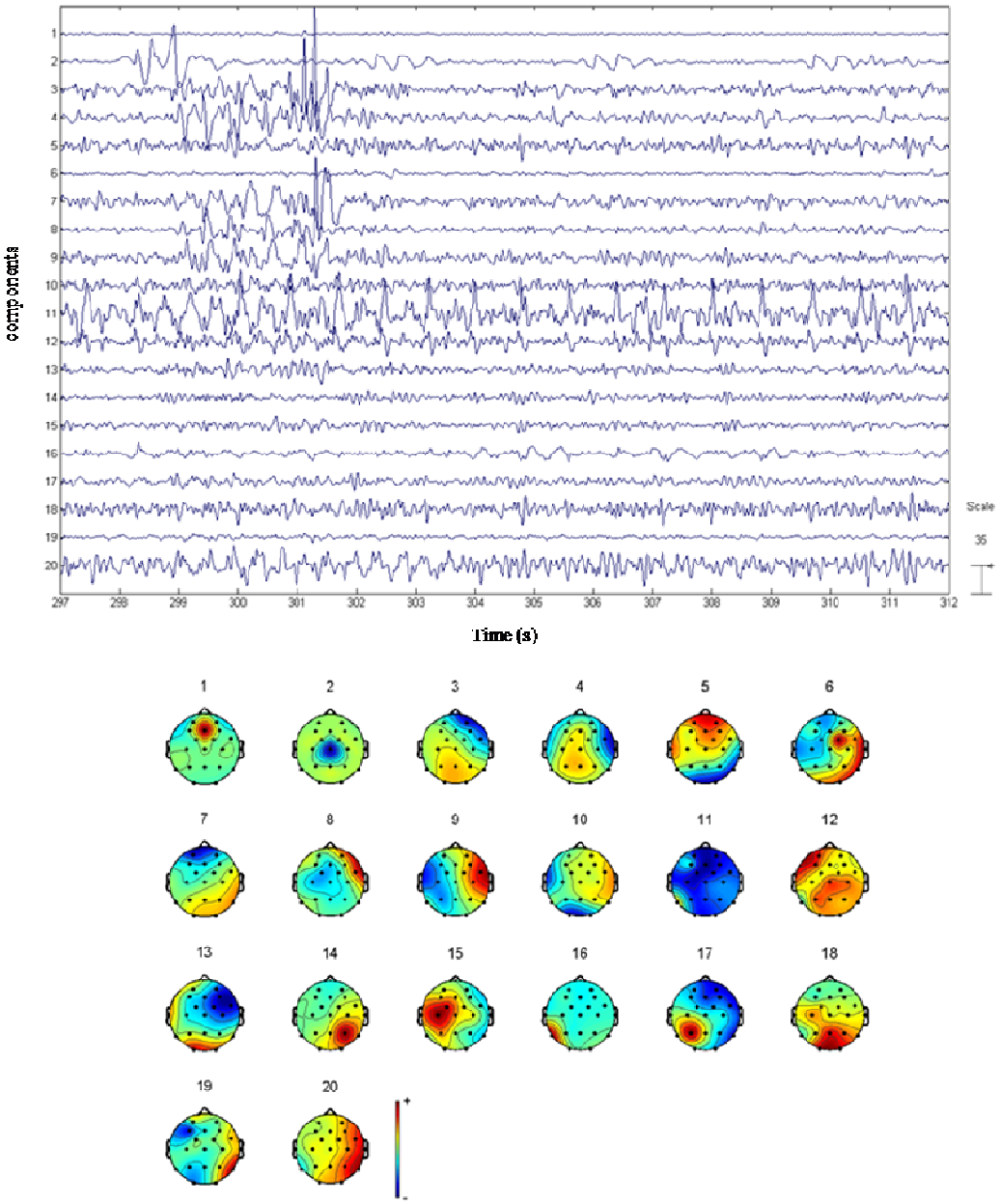

Figure 6.28. Patient #3: Component obtained by ICA decomposition of EEG signal shown in Fig. 6.27. Component # 3, 4, 7, 9 have 'spike-wave' waveform appearing the same as channel T4 shown in Fig. 6.27 (top). EEG component scalp maps (W^{-1}) obtained from ICA decomposition (bottom).

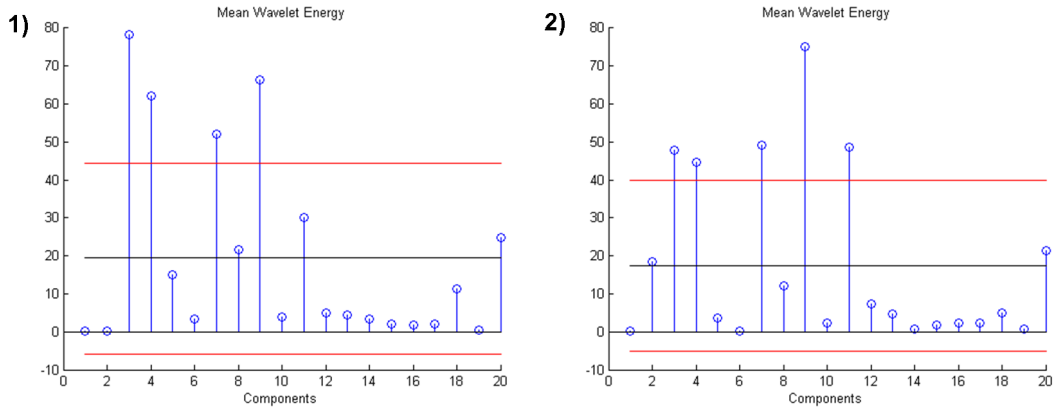

Figure 6.29. Patient #3: Mean Wavelet Energy in time for each component (blue). Mean value (black) ± standard deviation (red). Intervals range: 1) 184-187s, 2) 299-302s.

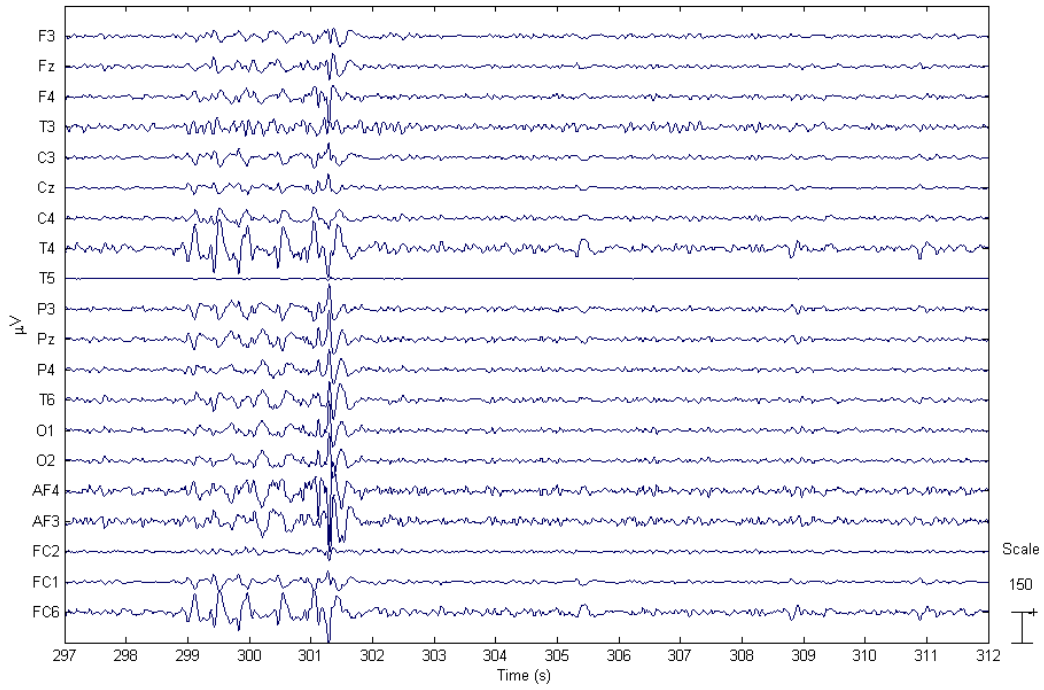

Figure 6.30. Patient #3: EEG derived from components # 3, 4, 7 and 9.

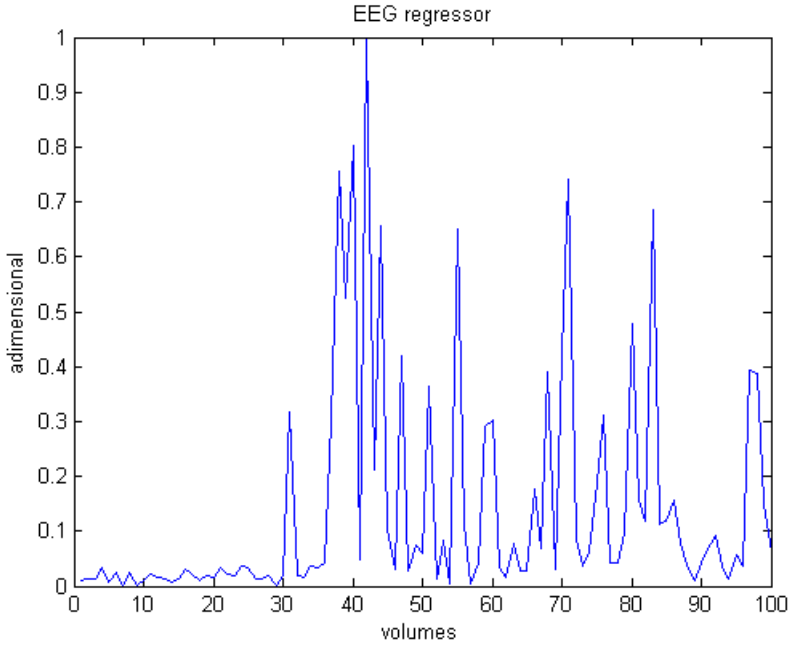

Figure 6.31. Patient #3: EEG regressor model for channel T4.

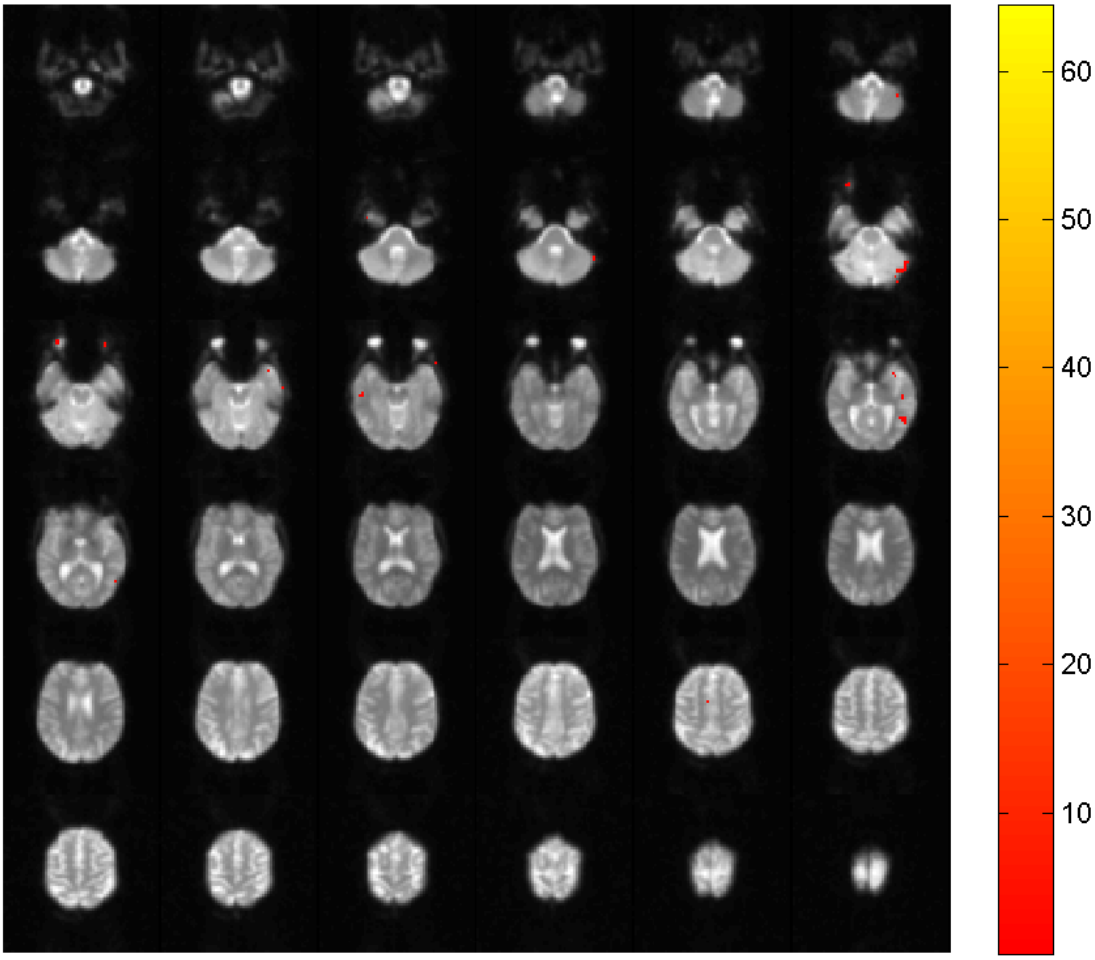

Figure 6.32. fMRI activation maps for patient #3.

Patient #4:

The EEG activity showed sequence of spikes and wave complexes over the left fronto-central regions (F3, FC1) lasting more then 10s. This activity occasionally showed an high amplitude over the fronto-polar electrodes with a phase reversal over the frontal and central electrodes. It is possible observe the presence of slow activity over the central electrodes (Fz, Cz) synchronous with the lateralized activity (Fig. 6.33).

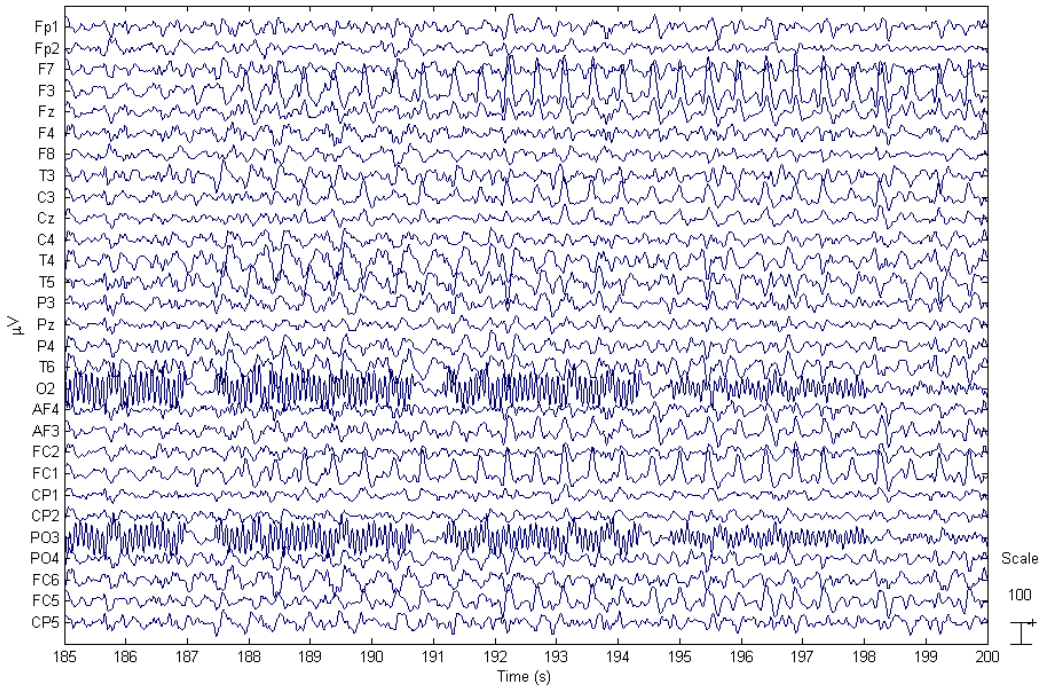

Figure 6.33. Patient #4: EEG signal after pre-processing.

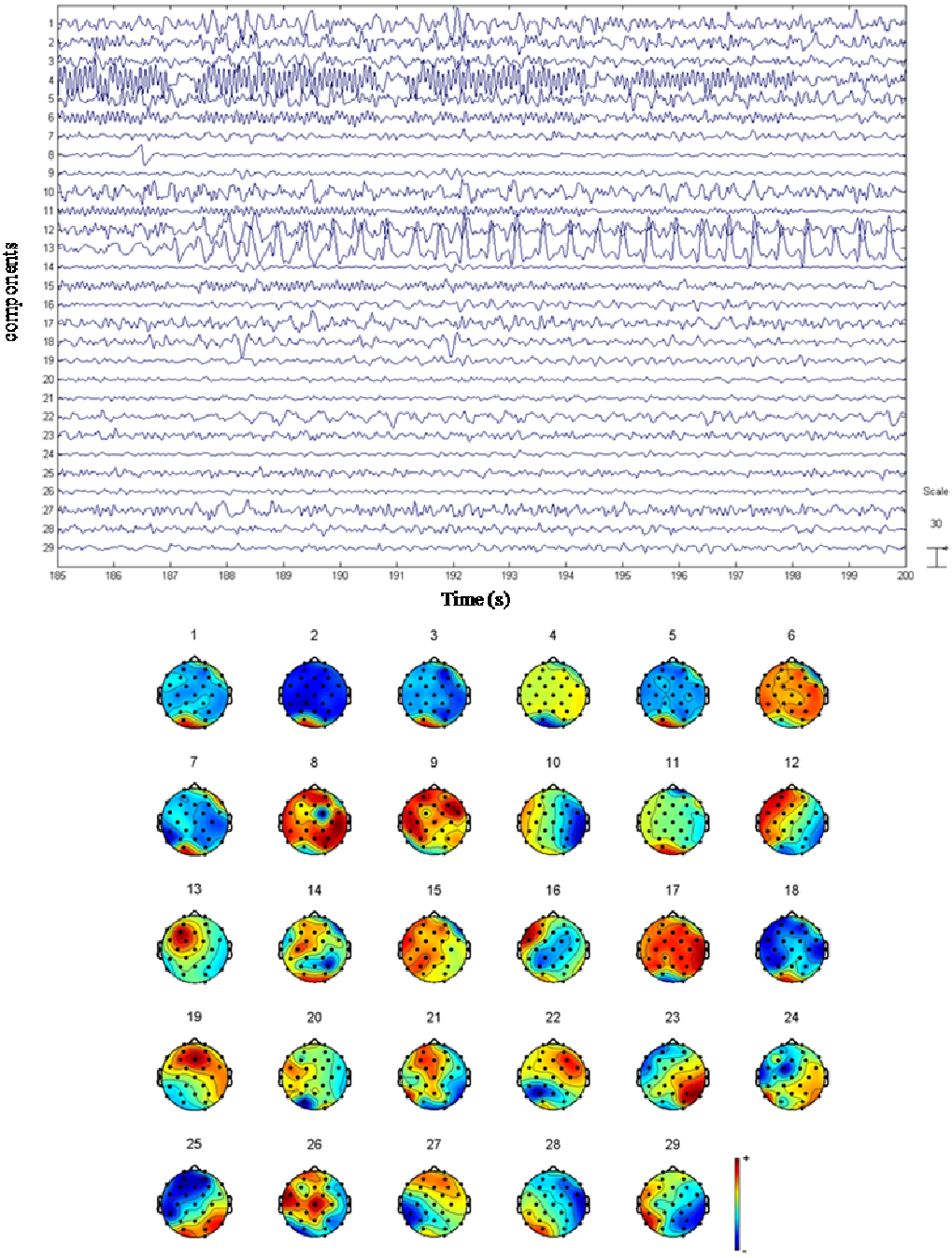

Figure 6.34. Patient #4: Components obtained by ICA decomposition of EEG signal shown in Fig. 6.33. Component # 13 has 'spike-wave' waveform appearing the same as channel F3 shown in Fig. 6.33 (top). EEG component scalp maps (W^{-1}) obtained from ICA decomposition (bottom).

After ICA decomposition analysis we obtained 29 components (Fig. 6.34). After a visual inspection, component # 13 seems to be a good representation of the IED activity; its time course is similar to that of F3 channel. Conclusions obtained through visual inspection are supported by the results of wavelet transform (Fig. 6.35) which show the preponderance of component # 13. The channel F3, related to

patient's IED activity (Fig. 6.36) and with a high correlation coefficient (r=0.95), was selected for the construction of EEG regressor (Fig. 6.37).

EEG-fMRI integration shows several activations; in left centro-temporal area (perilesional regions), related to the cerebral damage (break bone in left temporal region) and another activation anterior to ventricular dilatation. There are also a somatosensory motor (SM) area and a right centro-temporal area activations triggered by EEG signal while the patient was not doing any movements (Fig. 6.38).

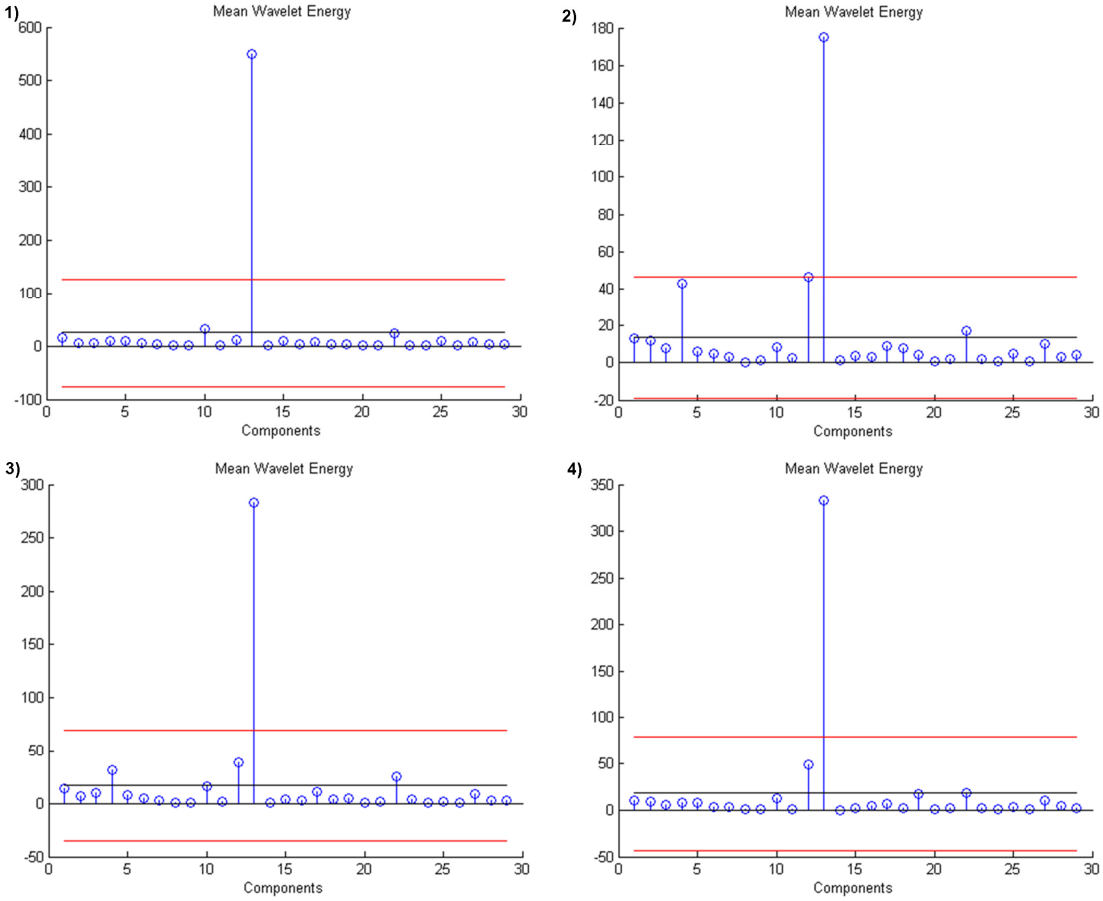

Figure 6.35. Patient #4: Mean Wavelet Energy in time for each component (blue). Mean value (black) ± standard deviation (red). Intervals range: 1) 84-88s, 2) 148-160s, 3) 187-201s, 4) 257-272s.

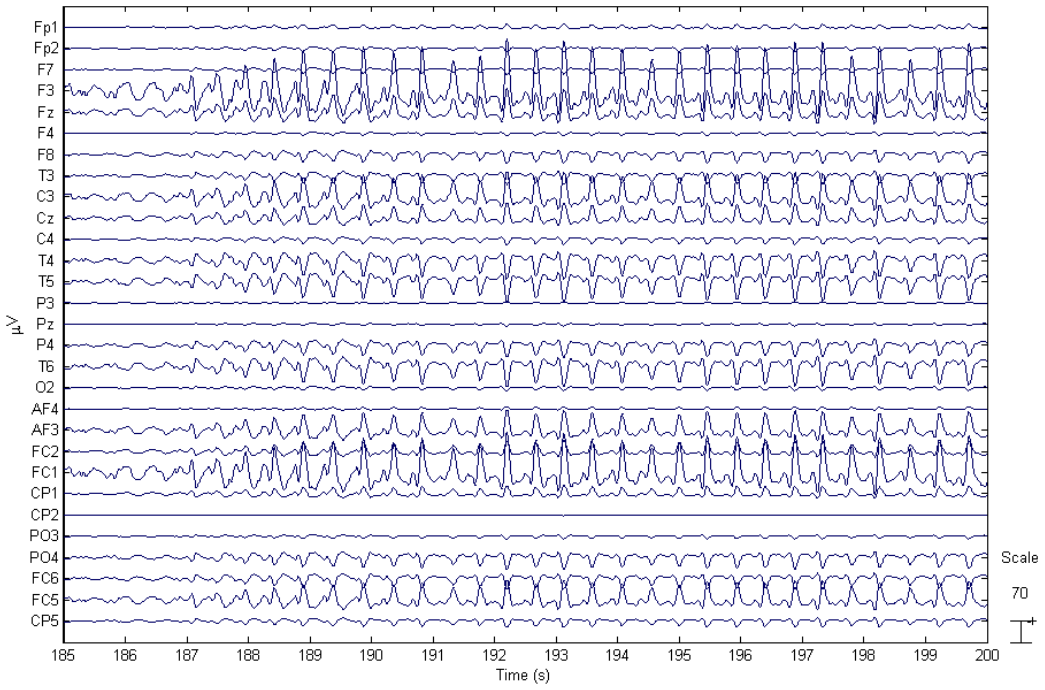

Figure 6.36. Patient #4: EEG derived from component # 13.

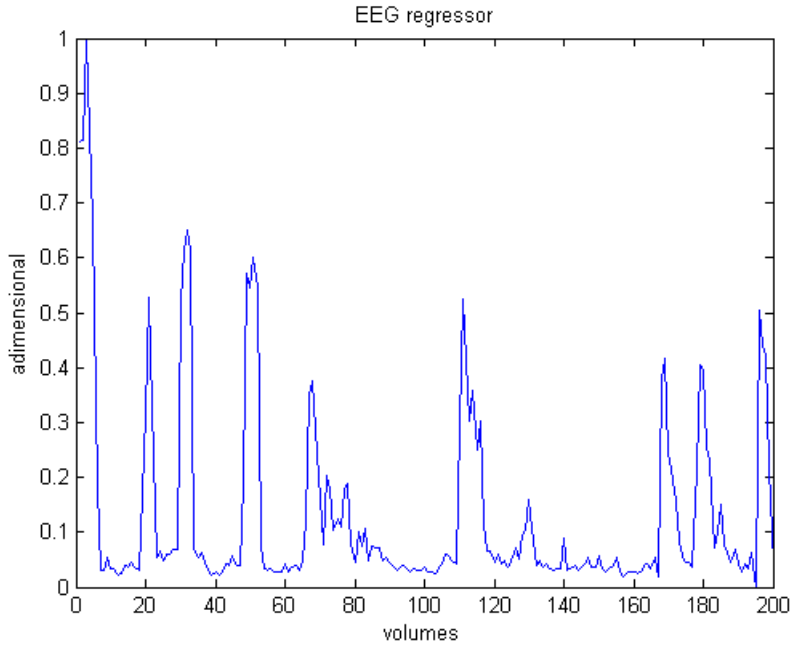

Figure 6.37. Patient #4: EEG regressor model for channel F3.

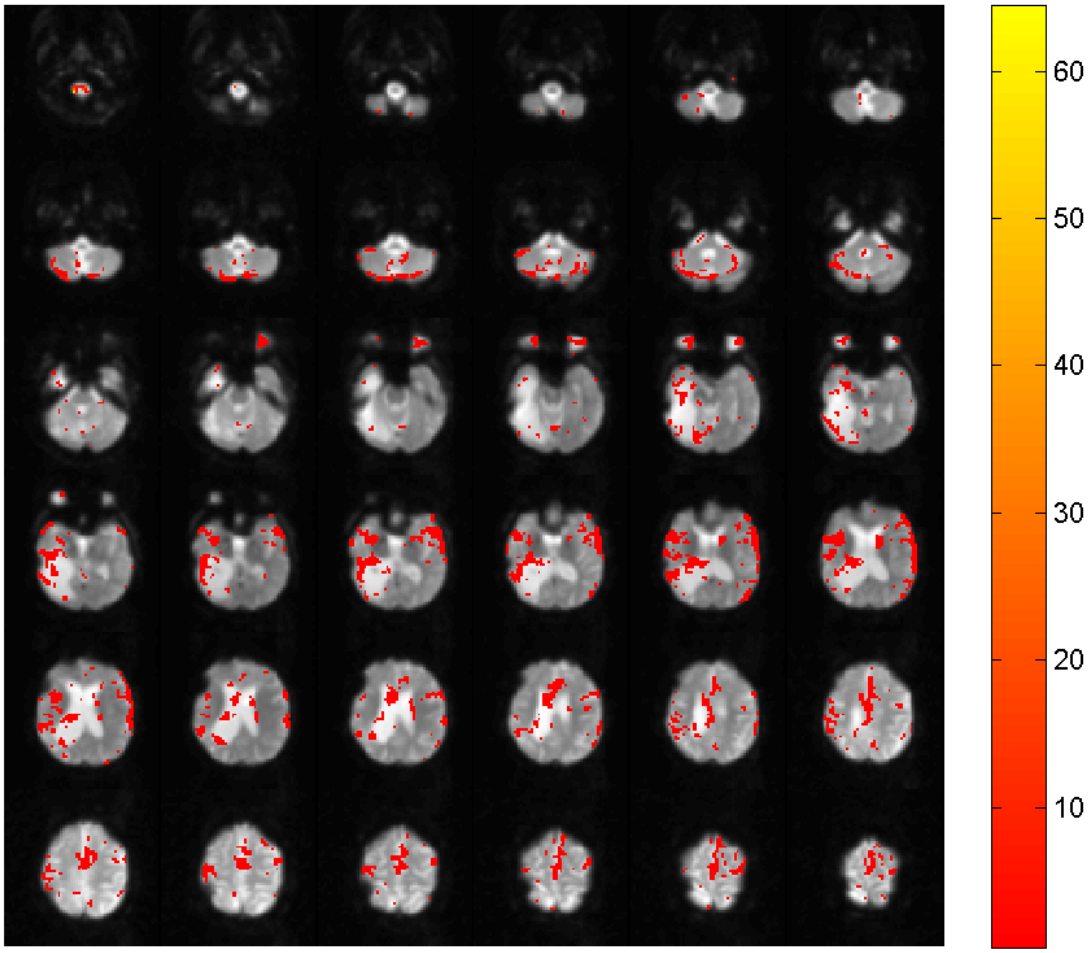

Figure 6.38. fMRI activation maps for patient #4.

Patient #5:

EEG showed slow waves activity in left temporal regions, according to the head trauma, with contralateral diffusion (Fig. 6.39).

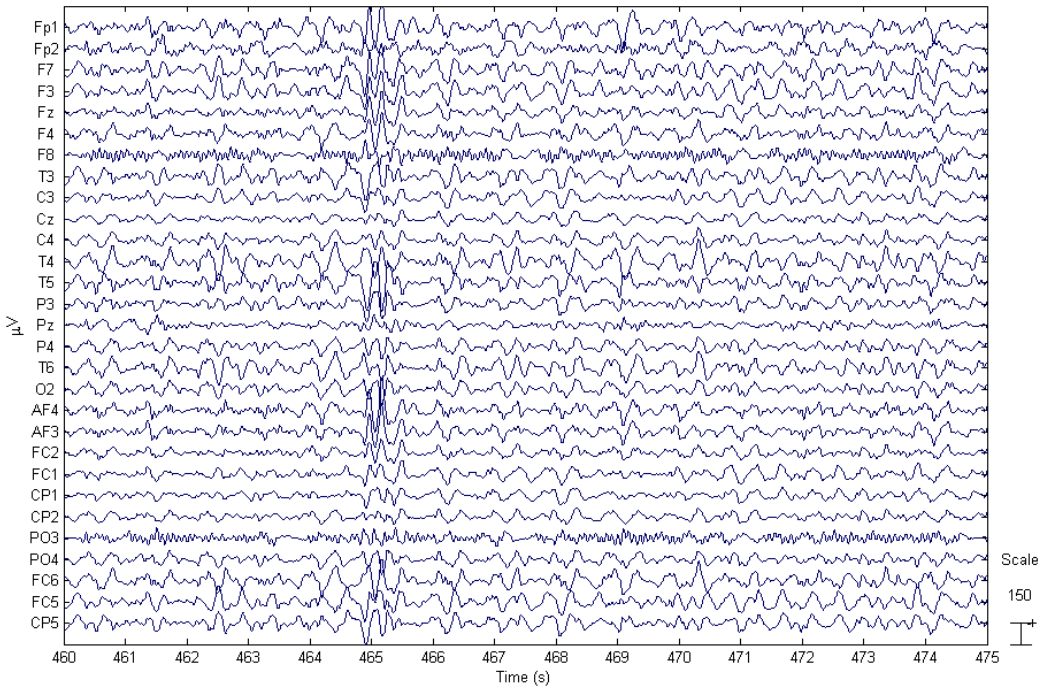

Figure 6.39. Patient #5: EEG signal after pre-processing.

ICA decomposition point out the preponderance of component #14 and 20 (Fig. 6.40). It is interesting to note that component # 29 represents a gradient artifact residual on the EEG signal. Components with higher wavelet energy in the two time ranges (168-178s and 457-474s) are # 14 and 20 (Fig. 6.41). The EEG derived from these components shows that the IED activity is predominant on F3 channel (Fig. 6.42) according to the original EEG. The correlation coefficient of channel F3 is similar to that of channels C3, FC1 and CP1 in the range of 0.70-0.75, for the further analysis channel F3 was selected for the construction of the EEG regressor because the clinical history of the patient (Fig. 6.43).

The fMRI activation maps (Fig. 6.44) didn't show a significant activation, probably due to the short duration of sequences characterized by IED activity.

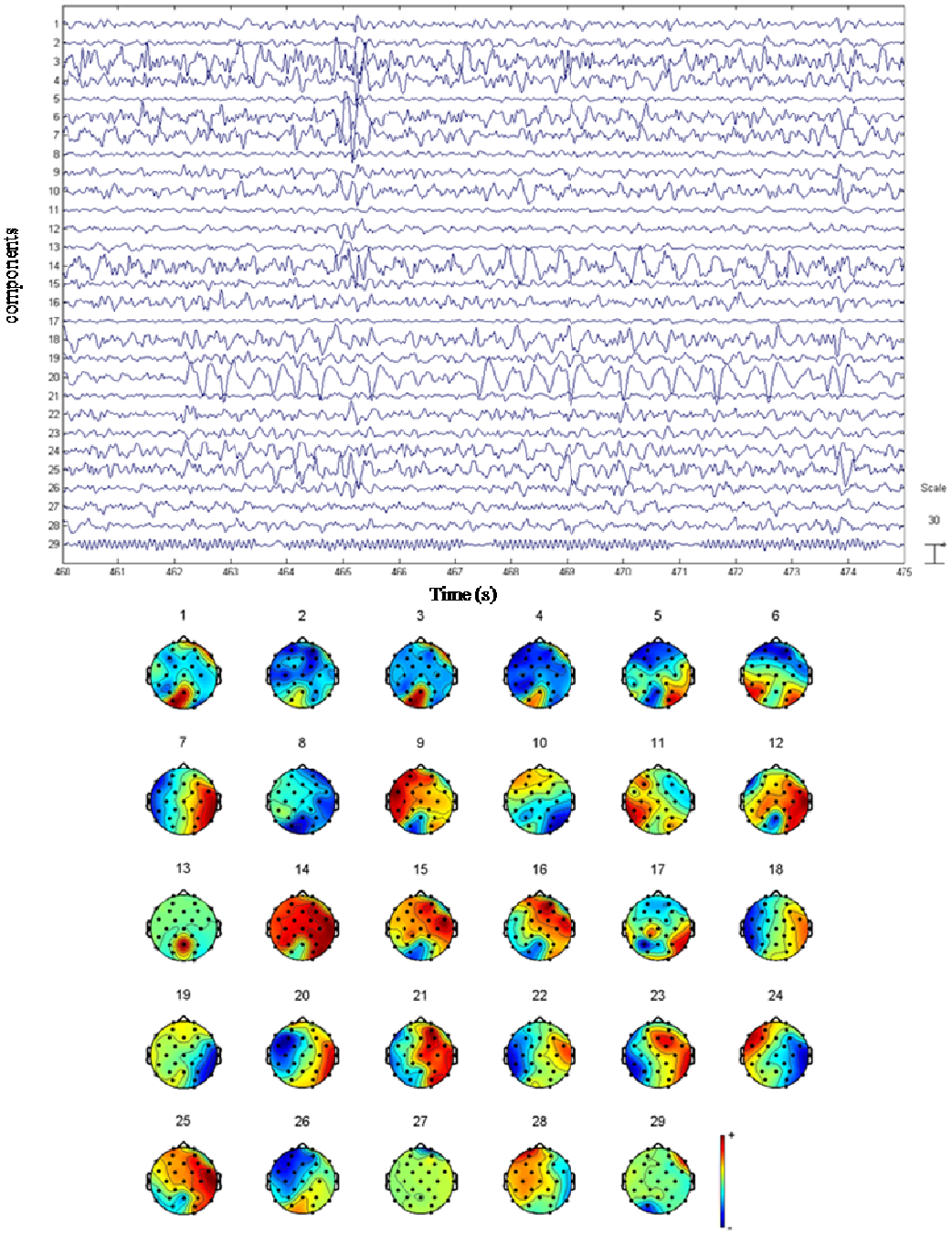

Figure 6.40. Patient #5: Components obtained by ICA decomposition of EEG signal shown in Fig. 6.39 (top). EEG component scalp maps (W^{-1}) obtained from ICA decomposition (bottom).

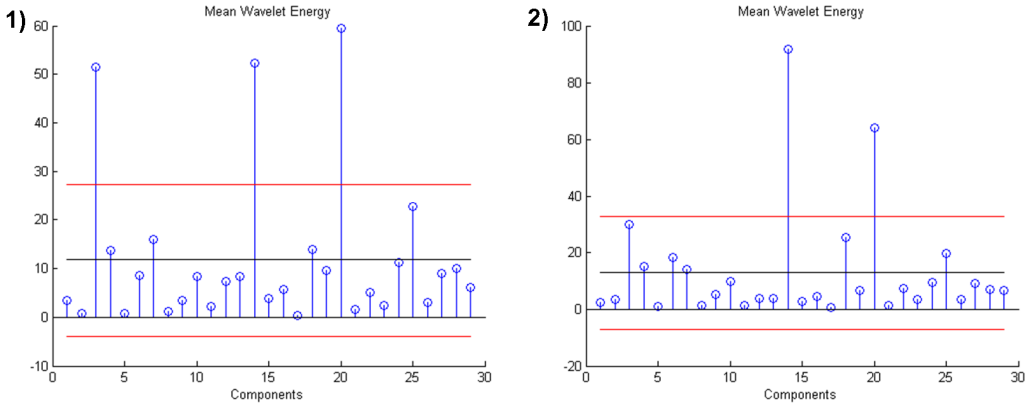

Figure 6.41. Patient #5: Mean Wavelet Energy in time for each component (blue). Mean value (black) ± standard deviation (red). Intervals range: 1) 168-178s, 2) 457-474s.

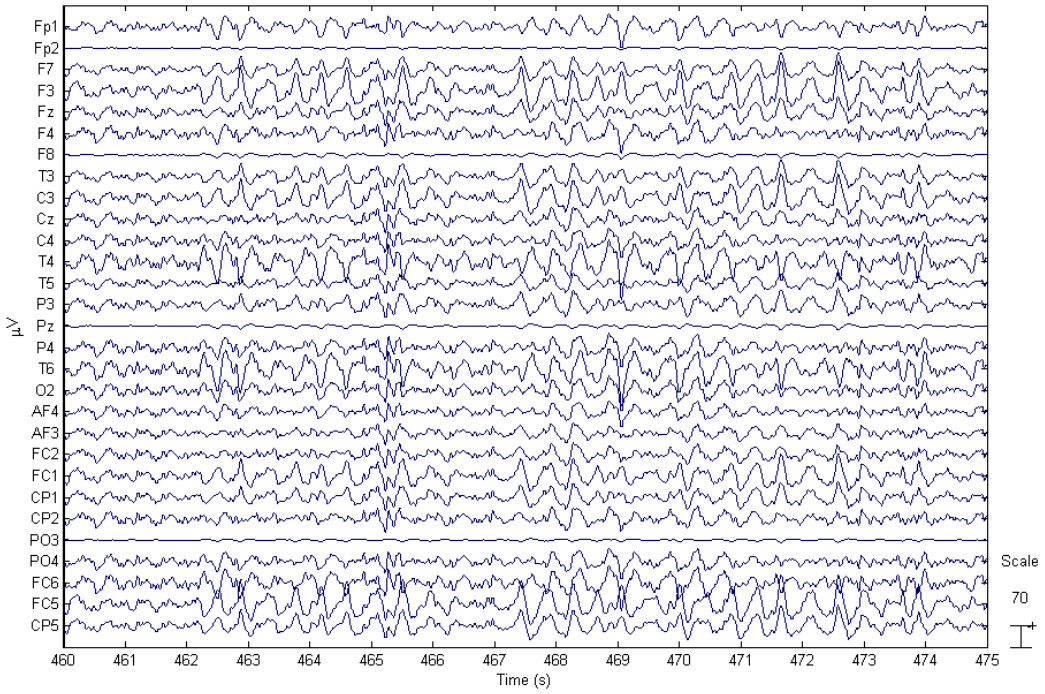

Figure 6.42. Patient #5: EEG derived from components # 14 and 20.

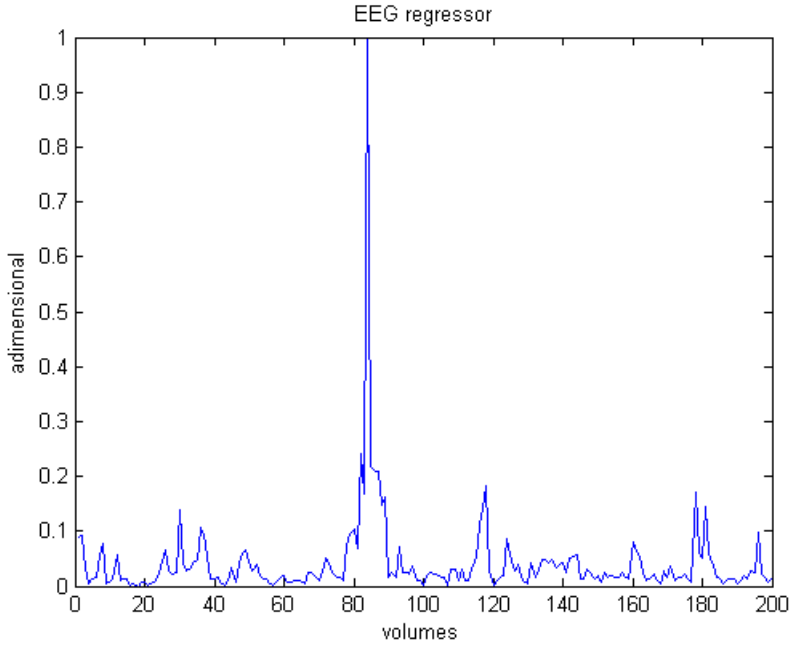

Figure 6.43. Patient #5: EEG regressor model for channel F3.

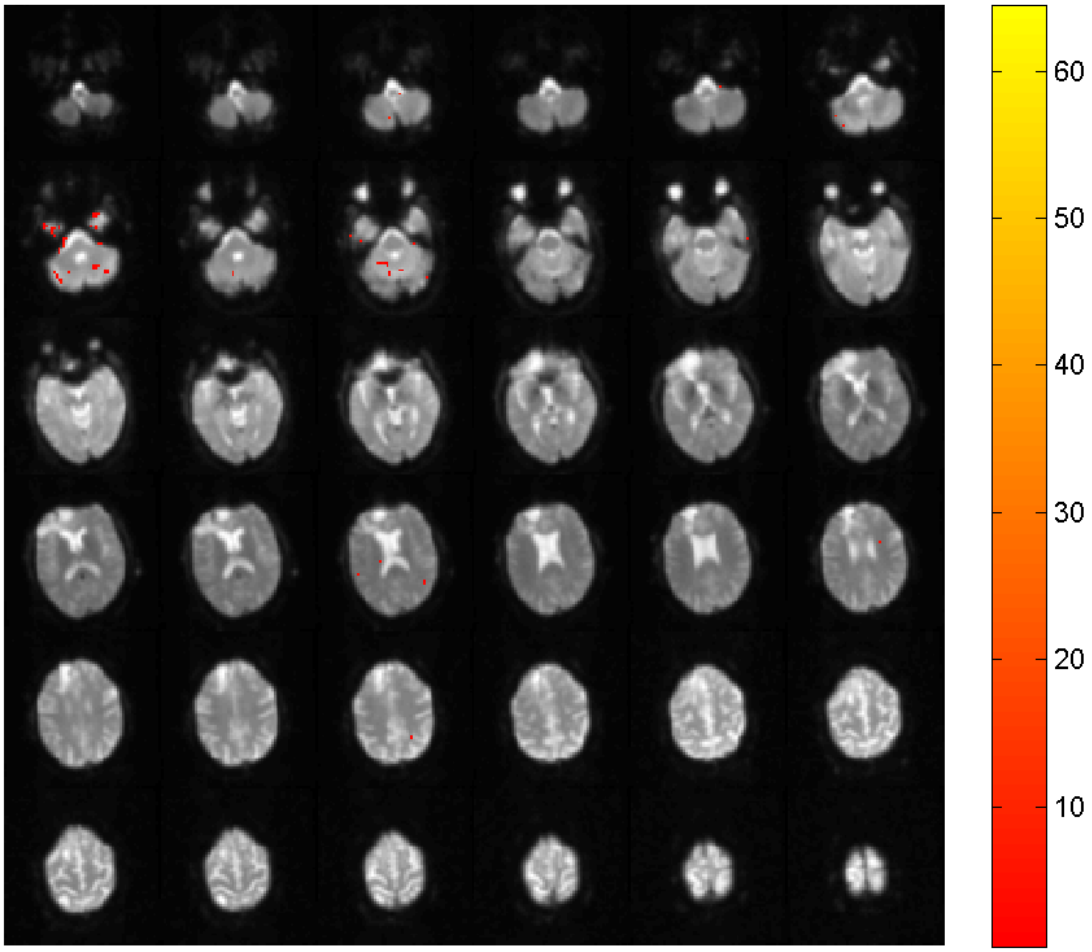

Figure 6.44. fMRI activation maps for patient #5.

DISCUSSION

The aim of the research project here described is the development of an innovative procedure for integrating neurophysiological and functional neuroimaging data. The EEG-fMRI integration project had as principal aim the development of a method allowing the use of the General Linear Modeling approach to detect activation areas even when there is not a task performance. In fact, the basic principle for the analysis of fMRI data is to identify the voxels at which the BOLD signal is significantly correlated with a postulated time course. Therefore the selection of the experimental paradigm as difference between task and rest conditions is of great importance; in fact, the information related to the experimental events (stimuli) and to the rest condition are to be used as input in GLM analysis. Regressors of interest are typically obtained by convolving impulses or boxcar functions, which are representations of the events or conditions of interest, with a model of the BOLD response (HRF). In detail, in the study of spontaneous EEG activity without a task condition we can use the EEG signal to derive the input for GLM. We present an easy-to-use and automatic approach for combined EEG-fMRI analysis able to improve the identification of the IEDs, based on ICA.

In literature, several methods for the analysis of simultaneous acquired EEG-fMRI data are proposed. Since the first applications of EEG-fMRI were in patients with epilepsy, the first attempts at data integration were in the study of subclinical epileptic discharges (Salek-Haddadi et al., 2003; Gotman et al., 2004, 2006). The aim of this strategy is to find regions of BOLD change linked to the discharges. In the conventional approach each event is marked by visual inspection of the EEG data recorded in the scanner, then a series of identical impulses functions (delta functions) are created and convolved with a canonical HRF, obtaining the regressor for a GLM. The methods presented in Formaggio et al., 2008 and Manganotti et al., 2008 are two attempts of EEG and fMRI integration. However in the first study signals were recorded simultaneous but their correlation analysis was as whether they were recorded in separate sessions, while in the second one we used a conventional approach based on the creation of the regressor as a set of stick functions

representing the timing of IED activity. Hence the necessity to developed a new method of integration.

The new method aimed to improve upon existing methods since the epileptiform activity, recorded from a scalp EEG, is used to modulate changes in BOLD signal. ICA decomposition is used to identify signals representing activity of interest but one of the major difficulties is their identification. We proposed an automatic selection based on wavelet analysis, because typically IEDs activity is higher in amplitude than background activity and its power increases. The reconstructed EEG signal is obtained with the only contribution of the selected components, method used in many studies to remove artifact from EEG traces. Like in the resting state studies, where alpha rhythm or its spectrum is used as a regressor in GLM analysis, the power time series of EEG signal is used as GLM input. Using conventional approach each event is treated as equal, although epileptic spikes may vary in amplitude, duration and also in appearance. They ignore the fact that IED activity is continuous and contains also fluctuating subthreshold epileptic activity, not clearly seen on surface EEG recordings. In contrast, such meaningful information is contained in the ICA factors employed in our method.

The results of the ICA based method of decomposition of EEG signal for fMRI processing, presented here, exhibit an increased sensitivity for the detection of brain regions associated with IED activity compare to the results of a conventional data processing approach. Several factors contribute to the increased sensitivity of the ICA method described in this thesis, particularly the reduced subjectivity in classification of the IEDs, which makes it more objective and less prone to human error. Apart from these algorithmic solution, the use of consensus peaks of multiple experienced EEG reviewers when scoring the EEG recorded during fMRI scanning is strongly recommend.

Analysis of in silico data validates the method, since demonstrates the reliability of reconstructed IED regressor. All five patients with partial epilepsy we enrolled in this study had frequent interictal focal slow wave activity on routine EEG. In all continuous EEG-fMRI recording sessions, after fMRI artifact removal, we obtained a good quality EEG that allowed us to detect spontaneous IEDs and analyze the related BOLD activation. In their focal distribution, these BOLD activations resembled the focal IEDs seen on routine scalp EEG and EEG recorded during EEG-fMRI sessions; and they are in agreement with the clinical history of the patients.

The main clinical finding in EEG-fMRI studies of patients with partial epilepsy is that focal interictal slow-wave activity was invariably associated with increased focal BOLD responses in a spatially related brain area. Our study extends current knowledge on epileptic foci localization and confirms previous reports suggesting that BOLD activation associated with modelled slow activity might have a role in localizing the epileptogenic region even in the absence of clear interictal spikes. Its application in presurgical evaluation is not yet warranted, as more needs to be learned about the meaning of the various response. It could be considered, however, in the context of indicating potential regions for further investigation, such as focused anatomical MRI analysis or possibly electrode implantation.

We plan to increase the number of patients and test this method on EEG with various patterns other than the epileptiform discharges, for example in resting state analysis where, like in the context of epilepsy, the activation task used to drive GLM analysis is missing. For this reason EEG signal is necessary to evaluate hemodynamic changes in fMRI and its analysis is fundamental to derive information on the electrical activity.

Even if it is believed that the HRF to epileptic spikes does not vary significantly from that to external stimuli, HRF could shows different peak times or even non canonical shape in the epileptogenic zone. This observation may be advanced as a working hypothesis for further investigating the choice of HRF in patients with epilepsy; future developments possibly involve a study of BOLD signal in this category of patients, and its relation with the electrical activity. In this way the sensitivity of EEG-fMRI studies in epilepsy could be improved with the use of different HRFs.

Since data quality is a crucial issue in multimodal functional imaging and data integration, an accurate pre-processing is necessary for both EEG and fMRI data. While for fMRI data the pre-processing is generally standard independently from the analysis technique (GLM, ICA etc.), the pre-processing of the EEG recorded during fMRI acquisition requires a complex and not one-way procedure to remove the atifacts. In literature different methods have been developed to remove gradient and pulse artifacts, based on both hardware and software solutions. The gradient EEG artifact removal method implemented in our EEG system acquisition did not give completely satisfactory results; therefore, we have developed a parallel activity to test available pre-processing method and develop new methods if necessary. We

developed a novel method, based on the average-subtraction approach, to remove gradient artifact, able to preserve EEG integrity and adapt to any dataset avoiding MRI trigger, using complexity-free mathematical procedures. After a realignment process of EEG data depending on slice repetition time, the algorithm performs an iterative subtraction of the estimated slice artifact, according to the following steps: artifact waveform analysis, computation of signal average waveform affected by gradient artifact, artifact estimate by weighted least squares minimization, subtraction of estimated artifact. Since the project regarding the gradient filter started together with the novel EEG-fMRI integration method and the analysis on patients with partial epilepsy are still in progress and to avoid the introduction of a further variable in the validation of the method we decided to use the algorithms implemented in the SystemPlus software (Micromed, Treviso, Italy). In the future we will test the integration method to data filtered with the new algorithm in order to conclude this project.

APPENDIX

A.1 Independent Component Analysis (ICA) in EEG analysis

Indipendent Component analysis (ICA) is a new technique to separate statistically independent components from a mixture of data. The central limit theorem ensures that a linear mixture of any source signals tends to be Gaussian; source signals tend to be statistically independent from each other. These considerations suggest that, if a signal mixture can be decomposed into a set of statistically independent, non-Gaussian signals, these signals are likely to be the source signals of that signal mixture.

ICA may cancel only the source we want, without modifying the rest of the brain signal (Vigario, 1997; Jung et al., 1998, 2000). The relationship between M linear mix signals $x(t) = [x_1(t)...x_M(t)]^T$ (with $x \in \Re^{M\times 1}$) and N independent components $s(t) = [s_1(t)...s_N(t)]^T$ (with $s \in \Re^{N\times 1}$) can be written as:

$$x = As \tag{1}$$

where **x** is the data, **s** the original sources (the components) and **A** the mixing matrix (with $A \in \Re^{M\times N}$). Typically M≥N, so that **A** is usually of full rank. The starting point for ICA is the assumption that the components are statistically independent and must have nongaussian distributions. The matrix **A** may be estimated using several algorithms. Typical algorithms for ICA use centering, whitening (usually with the eigenvalue decomposition) and dimensionality reduction as preprocessing steps in order to simplify and reduce the complexity of the problem for the actual iterative algorithm. Whitening and dimension reduction can be achieved with principal component analysis (PCA) or singular value decomposition (SVD). Whitening ensures that all dimensions are treated equally *a priori* before the algorithm is run. The inverse matrix of **A**, $W = A^{-1}$, is computed and the independent components are obtained by:

$$y = Wx, \tag{2}$$

where $y(t) = [y_1(t)...y_N(t)]^T$ (with $y \in \Re^{N\times 1}$) is a good approximation of sources **s** and $W \in \Re^{N\times M}$ is the unmixing matrix.

After an adequate selection of the components of interesting, they can be back projected to obtain a corrected EEG signal. A method to remove the unwanted components is the following (Mantini et al., 2007) applied for gradient artifact removal: Z is a diagonal matrix, each element z_{ii} is set equal to 1 if the i-th component is to delete, while it is set equal to 0 otherwise. The new vector x_p (the new clean EEG signal) could be then obtained by:

$$x_p = x - W^{-1}Zy \tag{3}$$

In this way, the unwanted components are subtracted from the EEG recordings, and the reconstruction of the EEG signal is completed, maintaining its correct spatial distribution.

A.1.1 FastICA algorithm

FastICA is an efficient and popular algorithm for independent component analysis invented by Aapo Hyvärinen at Helsinki University of Technology (Hyvärinen et al., 1999). The FastICA package is a free Matlab program that implements an algorithm based on a fixed-point iteration scheme maximizing non-Gaussianity as a measure of statistical independence. It can be also derived as an approximative Newton iteration.

This algorithm maximizes the non-Gaussianity using the Negentropy method.

Entropy is defined by:

$$H(y) = -\int f_Y(y)\log(f_Y(y))dy\,, \tag{4}$$

where $y = [y_1...y_N]^T$ is a random vector and f(y) its probability density function.

A result of Information Theory is that of all random variables of equal variance the normal one has the largest entropy. Thus normals are the 'least structured' of all random variables, and entropy is generally small for spikey or clearly clustered variables.

Then Negentropy is defined by:

$$J(y) = H(y_{gauss}) - H(y)\,, \tag{5}$$

where y_{gauss} is a multivariate normal with the same covariance matrix as y. Hence we have that $J(y) \geq 0$ and $J(y) = 0 \Leftrightarrow y$ is normal.

J may be approximated by:

$$J(y) \approx k[E(G(y)) - E(G(\nu))]^2, \tag{6}$$

where $k \geq 0, \nu$ ~N(0,1), E(·) denotes the expected value and G is a non-quadratic function.

Before getting stuck into the algorithm the data should be pre-processed. Firstly centre each variable, so $E(X) = 0$ and 'whiten' so $E(XX^T) = I$. To achieve this take $X' = PD^{-1/2}P^T X$ where $E(XX^T) = PDP^T$ and $P^T P = I$ and D is diagonal. As a result, after this transformation, the A we seek is orthogonal: $I = E(XX^T) = E(ASS^T A^T) = AA^T$, by assumption on S.

One version of the algorithm, known as deflation, seek successive vectors w to solve: $\max J(w^T x)$ such that $Var(w^T x) = 1$, ie $\|w\| = 1$ (for centred whitened data), and such that w is orthogonal to all previously determined directions.

Aliter we may seek the required number of directions all at once, in this case decorrelating $w_1^T x, ..., w_N^T x$ after each iteration so that they converge to different maxima.

In either case the algorithm follows an approximate Newton Iteration until a certain tolerance is met. The deflationary scheme achieves orthogonality using a simple Gram-Schmidt scheme, and the other method utilises the eigenvalue decomposition of a symmetric matrix.

A.2 General Linear Model (GLM) in fMRI analysis

An fMRI experiment requires an adequate setup, with a proper alternation of stimuli and resting conditions and a sufficient number of repetitions, so that the difference in signal between two or more conditions correlates in a selective way with the function of interest and so that a sufficient statistical power is obtained. Many techniques have been proposed for statistically analysing fMRI data, and a variety of these are in general use. The aim of such analysis is to produce an image identifying the regions which show significant signal change in response to the task.

Such an image is called a statistical parametric map. The most used and robust approach is the General Linear Model (GLM). To measure the magnitude of the signal intensity change due to activation, fMRI time courses at each voxel are modelled as a linear combination of explanatory variables and a residual error term. Then, a statistical parametric map is produced, reflecting the significance of the given explanatory variable in the data.

The theoretical basis of GLM in fMRI analysis can be found in (Friston et al., 1995). For each voxel the observed response vector ($Y \in \Re^{N\times 1}$ with N equal to the number of the acquired volumes) is expressed in terms of a linear combination of explanatory variables, contained in the known matrix ($X \in \Re^{N\times M}$ with M equal to the number of the unknown regression coefficients), commonly called design matrix, via the unknown parameter vector ($\beta \in \Re^{M\times 1}$), plus an error term ($\varepsilon \in \Re^{N\times 1}$):

$$Y = X \cdot \beta + \varepsilon \tag{7}$$

If the errors $\varepsilon_i \quad i = 1,...,N$ are independent and identically distributed normal random variables with zero mean and variance σ^2 and the product matrix $X^T \cdot X$ is invertible, the parameter estimates $\hat{\beta}_i \quad i = 1,...,M$ can be obtained by linear least squares:

$$\hat{\beta} = \left(X^T \cdot X\right)^{-1} \cdot X^T \cdot Y \tag{8}$$

The error variance can be estimated a posteriori from:

$$\hat{\sigma}^2 = \frac{RSS(\hat{\beta})}{N-M} = \frac{(Y - X \cdot \hat{\beta})^T (Y - X \cdot \hat{\beta})}{N-M} \tag{9}$$

where RSS is the residual sum of squares, and the precision of the estimates in term of variance-covariance matrix, $\hat{\Sigma}_{\hat{\beta}}$, from:

$$\hat{\Sigma}_{\hat{\beta}} = \hat{\sigma}^2 \cdot \left(X^T \cdot X\right)^{-1} \tag{10}$$

In real data the errors consisting of no neural noise due to respiration and blood flow pulsation through the cardiac cycle, so if the errors ε_i are not independent but correlated, as is usually assumed in fMRI data, both sides of Eq. 7 are multiplied by a proper matrix $W \in \Re^{N\times N}$:

$$W \cdot Y = W \cdot X \cdot \beta + W \cdot \varepsilon \tag{11}$$

so as the additive error vector $W \cdot \varepsilon$ consists of independent and identically distributed normal random variables with zero mean and equal variance,

$\varepsilon \sim N(0,\sigma^2 I)$. Assuming a first-order autoregressive model for the error, the matrix **W** is thus a temporal whitening filter, which can be generated as in (Friston et al., 2002) or (Jezzard et al., 2001). To construct the W, we consider a generic voxel i:

$$\mathrm{y_i} = \mathrm{X} \cdot \beta_\mathrm{i} + \varepsilon_\mathrm{i} \tag{12}$$

where the error: $\varepsilon_\mathrm{i} \sim \mathrm{N}(0,\sigma^2\mathrm{V})$. After the estimation of V, the model was pre-multiplied for the matrix $\mathrm{W} = \mathrm{V}^{-1/2}$:

$$W \cdot y_i = W \cdot X \cdot \beta_i + W \cdot \varepsilon_i = W \cdot X \cdot \beta_i + \tilde{\varepsilon}_i \tag{13}$$

where $\tilde{\varepsilon}_i \sim N(0,\sigma^2 I)$. In particular, we suppose that the variability in time of error $\varepsilon(\mathrm{t})$ is described by a first order autoregressive model AR(1) in which we suppose that the error from the previous scan is combined with white noise to produce the current scan:

$$\varepsilon(\mathrm{t}) = \rho \cdot \varepsilon(\mathrm{t}-1) + \xi_{\mathrm{t1}} \tag{14}$$

where $|\rho| < 1$ and $\xi_{t1} = N(0,\sigma_1^{\,2})$ is a gaussian white noise with mean 0 and variance $\sigma_1^{\,2}$.

We identified the AR(1) model, estimating the parameters: the coefficient of model ρ and the variance of white noise $\sigma_1^{\,2}$. We used the Yule-Walker equation, that describes the autocorrelation of out process of the AR model, to construct matrix V. If a first order autoregressive model is used, the Yule Walker equation system yields a single equation:

$$R(0)\rho = R(1) \tag{15}$$

where R is a known autocorrelation function and according to variance expression we obtain:

$$\sigma_1^{\,2} = R(0) - \rho R(1) \tag{16}$$

Where V is compound by coefficients of the Yule-Walker equation and is a Toeplitz matrix, a symmetric matrix whose diagonal or sub diagonal elements are equal. V is an nxn matrix:

$$V = \begin{pmatrix} 1 & \rho & \rho^2 & \dots & \rho^{n-1} \\ \rho & 1 & \rho & \dots & \rho^{n-2} \\ \rho^2 & \rho & \ddots & \dots & \rho^{n-3} \\ \vdots & \vdots & \vdots & 1 & \vdots \\ \rho^{n-1} & \rho^{n-2} & \rho^{n-3} & \dots & 1 \end{pmatrix} \text{ (Jezzard et al., 2001)} \tag{17}$$

Our code envisaged a fixed order (one) of the autoregressive model. We estimated the variance of white noise and the coefficient ρ, which we assumed constant for all voxels and calculated as the mean of all changing values for every slice and every voxel. Although considerable evidence shows that ρ is not constant (Purdon et al., 2001), the robustness conferred by temporal smoothing appeared to alleviate this problem. First we estimated $\varepsilon(t)$ with the W identity matrix, we then applied the AR(1) model to the error. In this way we constructed W for the next estimate. After estimating of V, in SOHIA we used a Cholesky factorization, inverting the transpose of the factor:

$$\mathrm{V} = (\mathrm{H})^{\mathrm{T}} \cdot \mathrm{H}, \quad W = \left((H)^T\right)^{-1}, \quad WVW^T = I \tag{18}$$

where I is the nxn identity matrix.

We constructed W in this way:

$$W = \begin{pmatrix} 1 & 0 & 0 & \dots & 0 \\ -\rho R & R & 0 & \dots & 0 \\ 0 & -\rho R & R & \dots & 0 \\ \vdots & \vdots & \vdots & \ddots & \vdots \\ 0 & \dots & 0 & -\rho R & R \end{pmatrix}, \tag{19}$$

where $R = \frac{1}{\sqrt{1-\rho^2}}$ (Jezzard et al., 2001)

Introduction of **W** allows one to estimate β_i $\mathrm{i} = 1,...,\mathrm{M}$, σ^2 and Σ_β by linear least squares, as:

$$\hat{\beta} = \left(X^T \cdot W \cdot X\right)^{-1} \cdot X^T \cdot W \cdot Y \tag{20}$$

$$\hat{\sigma}^2 = \frac{WRSS(\hat{\beta})}{N-M} = \frac{(Y - X \cdot \hat{\beta})^T \cdot W^T \cdot W \cdot (Y - X \cdot \hat{\beta})}{N-M} \tag{21}$$

Finally,

$$\hat{\Sigma}_{\hat{\beta}} = \hat{\sigma}^{-2} \cdot \left(X^T \cdot W^T \cdot W \cdot X\right)^{-1} \tag{22}$$

where WRSS is the weighted residual sum of squares.

The design matrix X contains values at acquisition time, of the continuous explanatory variables x(t) equal to the convolution of the stimulus function, u(t), with the impulse response, HRF(t), representing the hemodynamic response function:

$$x(t) = u(t) \otimes HRF(t) = \int_0^{\infty} HRF(\tau) \cdot u(t-\tau) d\tau \quad (23)$$

where $\otimes$ denotes the convolution operation. The stimulus function u(t) is known since it depends on the experimental set-up.

A.3 Wavelet Time Frequency Representation

Continuous Morlet Wavelet Transform (CWT) is an implementation of the wavelet transform. Unlike Fourier transform, CMT constructs a time-frequency representation of a signal that offers a time and frequency localization. The Morlet ψ(t) is a function of time t consisting of a complex exponential modulated by a Gaussian envelope. It has a Gaussian distribution in both time and frequency domains. This 'mother' wavelet was then used to build a set of daughter wavelets by translating ψ(t) in time, and by dilating or contracting ψ(t). This operation, served to adjust the mean frequency and also the spread of the daughter wavelet.

The wavelet transform is the inner-product of the wavelet function with the signal s(t). Each wavelet has a Gaussian distribution in the time (SD: σ_t) and frequency domains (SD: σ_f) around the centre frequency f_0 (Tallon-Baudry et al. 1997):

$$w(t, f_o) = (\sigma_t \sqrt{\pi})^{-\frac{1}{2}} \exp\left(\frac{-t^2}{2\sigma_t^2}\right) \exp(2i\pi f_0 t) \quad (24)$$

with

$$\sigma_f = \frac{1}{2\pi\sigma_t} \quad (25)$$

This function depends on a parameter, the number of oscillations (f_0 / σ_f), which has to be chosen by the user in order to best investigate power changes as the optimal compromise in time-frequency. To compute the time varying power in a frequency band the recorded signal s(t) is then convolved with the corresponding set of functions generated by the mother wavelet. The convolution can be computed by using FFT. Normally, the output is a real function except when the mother wavelet is complex. The power spectrum calculated from the result of convolution can be represented by (Tallon-Baudry et al. 1997):

$$E(t, f_0) = \left| w(t, f_0) \otimes s(t) \right|^2 \tag{26}$$

The result of a wavelet transform can be graphically represented by a scalogram. In this plot each power spectrum value is plotted as a filled rectangle whose color corresponds to the magnitude of the power. The location and size of the rectangle are related to the time interval and the frequency range for this value.

REFERENCES

Aghakhani Y, Bagshaw AP, Benar CG, Hawco C, Andermann F, Dubeau F, Gotman J. fMRI activation during spike wave discharges in idiopathic generalized epilepsy. Brain 2004; 127:1127-44.

Aghakhani Y, Kinay D, Gotman J, Soualmi L, Andermann F, Olivier A, Dubeau F. The role of periventricular nodular heterotopia in epileptogenesis. Brain 2005; 128:641-51.

Allen PJ, Polizzi G, Krakow K, Fish DR, Lemieux L. Identification of EEG events in the MR scanner: the problem of pulse artifact and a method for its subtraction. NeuroImage 1998; 8 (3): 229-239.

Allen PJ, Joseph O, Turner R. A Method for Removing Imaging Artifact from Continuous EEG Recorded during Functional MRI. Neuroimage 2000; 12: 230-239.

Al Asmi A, Bénar CG, Gross DW, Agha Khani Y, Andermann F, Pike B, Dubeau F, Gotman J. fMRI activation in continuous and spike-triggered EEG-fMRI studies of epileptic spikes. Epilepsia 2003; 44 (10): 1328-1339.

Archer JS, Briellmann RS, Syngeniotis A, Abbott DF, Jackson GD. Spike-triggered fMRI in reading epilepsy. Neurology 2003; 60: 415–-421.

Ardekani BA, Kershaw J, Kashikura K, Kanno I. Activation detection in functional MRI using subspace modeling and maximum likelihood estimation. IEEE Transaction on Medical Imaging 1999; 18(2): 101-114.

Babiloni F, Babiloni C, Carducci F, Fattorini L, Anello C, Onorati P, Urbano A. High resolution EEG: a new model-dependent spatial deblurring method using a

realistically shaped MR-constructed subject's head model. Electroencephalogr. Clin. Neurophysiol. 1997; 102(2): 69-80.

Babiloni F, Babiloni C, Carducci F, Angelone L, Del Gratta C, Romani GL, Rossini PM, Cincotti F. Linear inverse estimation of cortical sources by using high resolution EEG and fMRI priors. IJBEM 2001; *3*, p 1.

Babiloni F, Babiloni C, Carducci F, Romani GL, Rossini PM, Angelone LM, Cincotti F. Multimodal integration of high-resolution EEG and functional magnetic resonance imaging data: a simulation study. Neuroimage. 2003; 19(1): 1-15.

Baillet S, Leahy RM, Singh M, Shattuck DW, Mosher JC. Supplementary motor area activation preceding voluntary finger movements as evidenced by magnetoencephalography and fMRI. IJBEM 2001; 3, p 1.

Bagshaw AP, Aghakhani Y, Benar CG, Kobayashi E, Hawco C, Dubeau F, Pike G.B, Gotman J. EEG-fMRI of focal epileptic spikes: analysis with multiple haemodynamic functions and comparison with gadoliniumenhanced MR angiograms. Hum Brain Mapp 2004; 22:179-92.

Bagshaw AP, Kobayashi E, Dubeau F, Pike GB, Gotman J. Correspondence between EEG-fMRI and EEG dipole localisation of interictal discharges in focal epilepsy. Neuroimage 2006; 30:417-25.

Bandettini PA, Wong EC, Hinks RS, Tikofsky RS, Hyde JS. Time course EPI of human brain function during task activation. Magn Reson Med; 1992, 25(2): 390-397.

Bell AJ and Sejnowski T J. An information-maximization approach to blind separation and blind deconvolution. Neural Computation 1995; 7(6): 1129-59.

Benar CG, Gross DW, Wang Y, Petre V, Pike B, Dubeau F, Gotman J. The BOLD responses to interictal epileptiform discharges. Neuroimage 2002; 17:1182-92.

Benar CG, Grova C, Kobayashi E, Bagshaw AP, Aghakhani Y, Dubeau F, Gotman J. EEG-fMRI of epileptic spikes: concordance with EEG source localization and intracranial EEG. Neuroimage 2006; 30:1161-70.

Benbadis SR, GersonWA, Harvey JH, Luders HO. Photosensitive lobe epilepsy. Neurology 1996; 46:1540-2.

Berger H. Uber das elektrenkephalogram des menschen. Archiv für Psychiatrie und Nervenkrankheiten 1929; 87: 527-570.

Boor S, Vucurevic G, Pfleiderer C, Stoeter P, Kutschke G, Boor R. EEG-related functional MRI in benign childhood epilepsy with centrotemporal spikes. Epilepsia 2003; 44:688-92.

Boynton GM, Engel SA, Glover GH, Heeger DJ. Linear systems analysis of functional magnetic resonance imaging in human V1. J Neurosci 1996; 16: 4207-4241.

Cardoso JF and Souloumiac A. Blind beamforming for non Gaussian signals. IEEE Proceedings-F 1993; 140: 362-370.

Caton R. The electric currents of the brain. Br Med J 1875; 2:278.

Cohen MS. Parametric analysis of fMRI data using linear systems methods. Neuroimage 1997; 6: 93-103.

Cope M, Delpy DT, Reynolds EO, Wray S, Wyatt J, van der Zee P. Methods of quantitating cerebral near infrared spectroscopy data. Adv Exp Med Biol 1988; 222: 183-189.

Dale A, Liu A, Fischl B, Buckner R, Belliveau JW, Lewine J, Halgren E. Dynamic statistical parametric mapping: combining fMRI and MEG for high-resolution imaging of cortical activity. Neuron 2000; 26: 55-67.

De Munck JC, Gonçalves SI, Huijboom L, Kuijer JP, Pouwels PJ, Heethaar RM, Lopes da Silva FH. The hemodynamic response of the alpha rhythm: an EEG/fMRI study. Neuroimage. 2007; 35(3): 1142-51.

De Tiege X, Laufs H, Boyd SG, Harkness W, Allen PJ, Clark CA, Connelly A, Cross JH. EEG-fMRI in children with pharmacoresistant focal epilepsy. Epilepsia 2007; 48: 385-389.

Delorme A, Makeig S. EEGLAB: an open source toolbox for analysis of single-trial EEG dynamics including independent component analysis. J Neurosci Methods 2004;134:9–21.

Delpy DT, Cope MC, Cady EB, Wyatt JS, Hamilton PA, Hope PL, Wray S, Reynolds EO. Cerebral monitoring in newborn infants by magnetic resonance and near infrared spectroscopy. Scand J Clin Lab Invest Suppl 1987; 188: 9-17.

Ebersole JS, Wade PB. Spike voltage topography identifies two types of frontotemporal epileptic foci. Neurology 1991; 41:1425–33.

Eichele T, Calhoun VD, Debener S. Mining EEG-fMRI using independent component analysis. Int J Psychophysiol. 2009; 73(1): 53-61.

Feige B, Scheffler K, Esposito F, Di Salle F, Henning J, Seifritz E. Cortical and subcortical correlates of electroencephalographic alpha rhythm modulation. J Neurophysiol 2005; 93: 2864-2872.

Formaggio E, Storti S.F, Avesani M, Cerini R, Milanese F, Gasparini A, Acler M, Pozzi Mucelli R, Fiaschi A, Manganotti P. EEG and fMRI coregistration to investigate the cortical oscillatory activities during finger movement. Brain Topography 2008; 21(2): 100-111.

Friston KJ, Holmes AP, Worsley KJ, Poline JP, Frith CD, Frackowiak RSJ. Statistical parametric maps in functional imaging: A general linear approach. Hum Brain Mapp. 1995; 2(4): 189-210.

Friston KJ, Fletcher P, Josephs O, Holmes A, Rugg MD, Turner R. Event-related fMRI: characterizing differential responses. Neuroimage 1998; 7(1): 30-40.

Friston KJ, Glaser DE, Henson RN, Kiebel S, Phillips C, Ashburner J. Classical and Bayesian inference in neuroimaging: applications. Neuroimage 2002; 16(2): 484-512.

Gevins A. Dynamic functional topography of cognitive task. Brain Topogr. 1989; 2: 37-56.

Gevins A, Brickett P, Reutter B, Desmond J. Seeing through the skull: advanced EEGs use MRIs to accurately measure cortical activity from the scalp. Brain Topogr. 1991; 4: 125-131.

Gevins A, Le J, Leong H, McEvoy LK, Smith M.E. Deblurring. J. Clin. Neurophysiol. 1999; 16 (3): 204-213.

Gibbs FA, Lennox WG, Gibbs EL. Cerebral blood flow preceding and accompanying epileptic seizures in man. Arch Neurol Psychiatry. 1934; (32): 257-72.

Glover GH. Deconvolution of impulse response in event-related BOLD fMRI. NeuroImage 1999; 9: 416-429.

Goldman RI, Stern JM, Engel J, Cohen MS. Acquiring simultaneous EEG and functional MRI. Clin. Neurophysiol. 2000; 111: 1974-1980.

Goldman RI, Stern JM, Engel J and Cohen M. Simultaneous EEG and fMRI of the alpha rhythm, NeuroReport. 2002, 13(18): 2487-2492.

Gonçalves SI, De Munck JC, Pouwels PJW, Schoonhoven R, Kuijer JPA, Maurits NM, Hoogduin JM, Van Someren EJW, Heethaar RM, Lopes da Silva FH. Correlating the alpha rhythm to BOLD using simultaneous EEG/fMRI: inter-subject variability, NeuroImage 2006; 30(1): 203-213.

Gonçalves SI, Pouwels PJ, Kuijer JP, Heethaar RM, de Munck JC. Artifact removal in co-registered EEG/fMRI by selective average subtraction. Clin Neurophysiol 2007; 118: 2437-2450.

Gossl C, Auer DP, Fahrmeir L. Bayesian spatiotemporal inference in functional magnetic resonance imaging. Biometrics 2001a; 57(2): 554-562.

Gossl C, Fahrmeir L, Auer DP. Bayesian modeling of the hemodynamic response function in BOLD fMRI. NeuroImage 2001b; 14: 140-148.

Gotman J, Benar CG, Dubeau F. Combining EEG and FMRI in epilepsy: methodological challenges and clinical results. J Clin Neurophysiol 2004; 21: 229-40.

Gotman J, Grova C, Bagshaw A, Kobayashi E, AghakhaniY, Dubeau F. Generalized epileptic discharges show thalamocortical activation and suspension of the default state of the brain. PNAS 2005; 142: 15236-40.

Gotman J, Kobayashi E, Bagshaw AP, Bénar CG, Dubeau F. Combining EEG and fMRI: a multimodal tool for epilepsy research. J Magn Reson Imaging 2006; 23(6): 906-20. Review.

Goutte C, Nielsen FA, Hansen LK. Modeling the haemodynamic response in fMRI using smooth FIR filters. IEEE Transactions on Medical Imaging 2000; 19(12): 1188-1201.

Grinvald A, Lieke E, Frostig RD, Gilbert CD, Wiesel TN. Functional architecture of cortex revealed by optical imaging of intrinsic signals. Nature 1986; 324 (6095): 361-364.

Hamandi K, Salek-Haddadi A, Fish DR, Lemieux L. EEG/functional MRI in epilepsy: The Queen Square Experience. J Clin Neurophysiol. 2004; 21(4): 241-8. Review.

Henning S, Merboldt KD, Frahm J. Task and EEG-correlated analyses of BOLD MRI responses to eyes opening and closing. Brain Res 2006; 1073-1074: 359-64

Hyvärinen A. Fast and Robust Fixed-Point Algorithms for Independent Component Analysis. IEEE Transactions on Neural Networks 1999; 10(3): 626-634.

He B, Lian J. Spatio-temporal functional neuroimaging of brain electric activity. Crit. Rev. Biomed. Eng. 2002; 30: 283-306.

He B, Zhang Z, Lian J, Sasaki H, Wu S, Towle VL. Boundary element method based cortical potential imaging of somatosensory evoked potentials using subjects' magnetic resonance images. NeuroImage 2002; 16: 564-576.

Hesse CW, James CJ. A time-frequency approach to blind source separation using statistically optimal wavelet packets applied to ictal EEG. In: Proceedings of 2nd IEE Medical Signal and Information Processing Conferencr 2004; pp. 137:144.

Hoffmann A Jäger L, Werhahn KJ, Jaschke M, Noachtar S, Reiser M. Electroencephalography during functional echo-planar imaging: detection of epileptic spikes using post-processing methods. Magn Res Med 2000; 44:791-8.

Hyvärinen A, Karhumen J, Oja E. Independent Component Analysis. New York: Wiley, 2001.

Iriarte J, Urrestarazu E, Valencia M, Alegre M, Malanda A, Viteri C, Artieda J. Independent component analysis as a tool to eliminate artifacts in EEG: a quantitative study. J Clin Neurophysiol 2003; 20(4): 249-57.

Ives JR, Warach S, Schmitt F, Edelman RR, Schomer DL. Monitoring the patient's EEG during echo planar MRI. Electroenceph clin Neurophysiol 1993; 87: 417-420.

Ives JR. Apparatus and method for recording an electroencephalogram during magnetic resonance imaging. USA. August 29, 1995. Patent No: 5445162.

Jäger L, Werhahn KJ, Hoffmann A, Berthold S, Scholz V, Weber J, Noachtar S, Reiser M. Focal epileptiform activity in the brain: detection with spike-related functional MR imaging-preliminary results. Radiology 2002; 223: 860-869.

Jezzard P, Matthews PM, Smith SM. Functional MRI an introduction to methods. Great Britain, Oxford University Press, 2001, chapter 10, pp. 255-256.

Jobsis FF. Noninvasive, infrared monitoring of cerebral and myocardial oxygen sufficiency and circulatory parameters. Science 1977; 198 (4323): 1264-1267.

Jung TP, Humphies C, Lee TW, Makeig S, McKeownl MJ, Iragui V, Sejinowski TJ. Extended ICA removes artifacts from electroencephalographic recordings. Adv Neural Inform Process Syst. 1998; 10: 894-900.

Jung TP, Makeig S, Humphries C, Lee TW, Mckeown MJ, Iragui V, Sejnowski TJ. Removing electroencephalographic artifacts by blind source separation. Psychophysiol 2000; 37: 163-178.

Kobayashi K, James CJ, Nakahori T, Akiyama T, Gotman J. Isolation of epileptiform discharges from unaveraged EEG by independent component analysis. Clin Neurophysiol 1999; 110: 1755-1763.

Kobayashi E, Bagshaw AP, Jansen A, Andermann F, Andermann E, Gotman J, Dubeau F. Intrinsic epileptogenicity in polymicrogyric cortex suggested by EEG-fMRI BOLD responses. Neurology 2005; 64: 1263-6.

Kobayashi E, Bagshaw AP, Grova C, Gotman J, Dubeau F. Grey matter heterotopia: what EEG-fMRI can tell us about epileptogenicity of neuronal migration disorders. Brain 2006a; 129: 366-74.

Kobayashi E, Hawco CS, Grova C, Dubeau F, Gotman J. Widespread and intense BOLD changes during brief focal electrographic seizures. Neurology 2006b; 66: 1049-55.

Kobayashi E, Bagshaw AP, Grova C, Dubeau F, Gotman J. Negative BOLD responses to epileptic spikes. Hum Brain Mapp 2006c; 27: 488-97.

Kobayashi E, Bagshaw AP, Benar CG, Aghakhani Y, Andermann F, Dubeau F, Gotman J. Temporal and extratemporal BOLD responses to temporal lobe interictal spikes. Epilepsia 2006d; 47: 343-54.

Krakow K, Woermann FG, Symms MR, Allen PJ, Lemieux L, Barker GJ, Duncan JS, Fish DR. EEG-triggered functional MRI of interictal epileptiform activity in patients with partial seizures. Brain 1999; 122: 1679-1688.

Krakow K, Lemieux L, Messina D, Scott CA, Symms MR, Duncan JS, Fish DR. Spatio-temporal imaging of focal interictal epileptiform activity using EEG-triggered functional MRI. Epileptic Disord. 2001; 3(2): 67-74.

Kruggel F and von Cramon DY. Modeling the hemodynamic response in single-trial functional MRI experiments, Magn. Reson. Med. 1999a; 42(4): 787-797.

Kruggel F, von Cramon DY, Descombes X. Comparison of filtering methods for fMRI datasets. Neuroimage 1999b; 10(5): 530-543.

Kwong KK Belliveau JW, Chesler DA, Goldberg IE, Weisskoff RM. Dynamic magnetic resonance imaging of human brain activity during primary sensory stimulation. Proc Nat Acad Sci USA 1992; 89: 5675-5679.

Lange N and Zeger SL. Non-linear fourier time series analysis for human brain mapping by functional magnetic resonance imaging (with discussion). Applied Statistics, Journal of the Royal Statistical Society, Series C 1997; 46(1): 1-29.

Laufs H, Krakow K, Sterzer P, Eger E, Beyerle A, Salek-Haddadi A, Kleinschmidt A, Electroencephalographic signatures of attentional and cognitive default modes in spontaneous brain fluctuations at rest, Proc. Natl. Acad. Sci. 2003a; 100(19): 11053-11058.

Laufs H, Kleinschmidt A, Beyerle A, Eger E, Salek-Haddadi A, Preibisch C, Krakow K. EEG-correlated fMRI of human alpha activity, NeuroImage 2003b; 19: 1463-1476.

Laufs H, Lengler U, Hamandi K, Kleinschmidt A, Krakow K. Linking generalized spike-and-wave discharges and resting state brain activity by using EEG-fMRI in a patient with absence seizures. Epilepsia 2006; 47: 444-8.

Laufs H and Duncan JS. Electroencephalography/functional MRI in human epilepsy: what it currently can and cannot do. Curr Opin Neurol. 2007; 20(4): 417-23. Review.

Lazeyras F, Zimine I, Blanke O, Perrig SH, Seek M. Functional MRI with simultaneous EEG recording: feasibility and application to motor and visual activation. J Magn Reson Imaging 2001; 13:943-8.

Lemieux L, Allen PJ, Franconi F, Symms MR, Fish DR. Recording of EEG during fMRI experiments: patient safety. Magnetic Resonance in Medicine 1997; 38 (6): 943-952.

Lemieux L, Salek-Haddadi A, Josephs O, Allen P, Toms N, Scott C, Krakow K., Turner R., Fish D.R. Event-related fMRI with simultaneous and continuous EEG: description of the method and initial case report. Neuroimage 2001; 1: 780-7.

Lemieux L. Electroencephalography-correlated functionalMR imaging studies of epileptic activity. Neuroimaging Clin N Am 2004; 14:487-506.

Liu AK, Belliveau JW, Dale AM. Spatiotemporal imaging of human brain activity using functional MRI constrained magnetoencephalography data: Monte Carlo simulations. Proc. Natl. Acad. Sci. 1998; 95(15): 8945–8950.

Logan BR, Rowe DB. An evaluation of thresholding techniques in fMRI analysis. Neuroimage 2004; 22 (1): 95-108.

Logothetis NK, Pauls J, Augath M, Trinath T, Oeltermann A. Neurophysiological investigation of the basis of the fMRI signal. Nature 2001; 412 (6843): 150-157.

Lovblad KO, Thomas R, Jakob PM, Scammell T, Bassetti C, Griswold M, Ives J, Matheson J, Edelman RR, Warach S. Silent functional magnetic resonance imaging demonstrates focal activation in rapid eye movement sleep. Neurology 1999; 53: 2193-2195.

Lu Y, Grova C, Kobayashy E, Dubeau F, Gotman J. Using voxel-specific hemodynamic response function in EEG-fMRI data analysis: An estimation and detection model. Neuroimage 2007; 34: 196-203.

Magistretti PJ, Pellerin L, Rothman DL Shulman RG. Energy on demand. Science 1999; 283 (5401): 496-497.

Manganotti P, Formaggio E, Gasparini A, Cerini R, Bongiovanni L.G, Storti S.F, Pozzi Mucelli R, Fiaschi A, Avesani M. Continuous EEG-fMRI study in patients with partial epilepsy and focal interictal slow-wave discharges on EEG. Magnetic Resonance Imaging 2008; 26(8): 1089-100.

Mantini D, Perrucci M.G, Cugini S, Ferretti A, Romani G.L, Del Gratta C. Complete artefact removal for EEG recorded during continuous fMRI using independent component analysis. Neuroimage 2007; 34: 598-607.

Marques JP, Rebola J, Figueiredo P, Pinto A, Sales F, Castelo-Branco M. ICA decomposition of EEG signal for fMRI processing in epilepsy. Hum Brain Mapp. 2009; 30(9): 2986-96.

Michel CM, de Peralta RG, Lantz G, Andino SG, Spinelli L, Blanke O, Landis T., Seeck M. Spatiotemporal EEG analysis and distributed source estimation in presurgical epilepsy evaluation. J Clin Neurophysiol 1999; 16: 239-66.

Moosmann M, Ritter P, Krastel I, Brink A, Thees S, Blankenburg F, Taskin B, Obrig H, Villringer A. Correlates of alpha rhythm in functional magnetic resonance imaging and near infrared spectroscopy, NeuroImage 2003; 20: 145-158.

Muri RM, Felblinger J, Rosler KM, Jung B, Hesse CW, Boesch C. Recording of electrical brain activity in a magnetic resonance environment: distorting effects of the static magnetic field. Magnetic Resonance in Medicine 1998; 39: 18-22.

Niazy RK, Beckmann CF, Iannetti GD, Brady JM, Smith SM. Removal of FMRI environment artifacts from EEG data using optimal basis sets. Neuroimage 2005; 28(3): 720-37.

Nunez, P.L. and Katznelson, R.D. Electric Fields of the Brain: The Neurophysics of EEG, Oxford University Press, New York, 1981.

Nunez PL. Neocortical Dynamics and Human EEG Rhythms. Oxford Univ. Press, New York, 1995.

Ogawa S, Tank D.W, Menon RS, Ellermann G.M, Kim SG. Intrinsic signal changes accompanying sensory stimulation: functional brain mapping with magnetic resonance imaging. Proc Nat Acad Sci USA 1992; 89: 5951-5955.

Ossadtchi A, Baillet S, Mosher J, Thyerlei D, Sutherling W, Leahy R. Automated interictal spike detection and source localization in magnetoencephalography using independent components analysis and spatio-temporal clustering. Clin Neurophysiol 2004; 115: 508-522.

Parkers LM, Bastiaansen CM, Norris DG. Combining EEG and fMRI to investigate the post movement beta rebound. Neuroimage 2006; 29: 685-696

Patel MR, Blum A, Pearlman JD, Yousuf N, Ives JR, Saeteng S, Schomer DL, Edelman RR. Echo-planar functional MR imaging of epilepsy with concurrent EEG monitoring. Am J Neuroradiol 1999; 20: 1916-1919.

Puce A, Allison T, Spencer SS, Spencer DD, McCarthy G. Comparison of cortical activation evoked by faces measured by intracranial field potentials and functional MRI: two case studies. Hum. Brain Mapp. 1997; 5 (4): 298-305.

Pfurtscheller G, Aranibar A. Evaluation of event-related desynchronization (ERD) preceding and following voluntary self-paced movement. Electroencephalogr Clin Neurophysiol 1979; 46: 138-46.

Pfurtscheller G, Neuper C. Event-related synchronization of mu rhythm in the EEG over the cortical hand area in man. Neurosci Lett 1994; 174: 93-6.

Purdon PL, Solo V, Weisskoff RM, Brown E. Locally regularized spatiotemporal modeling comparison for functional MRI. Neuroimage 2001; 14 (4): 912-923.

Rajapakse JC, Kruggel F, Maisog JM, von Cramon DY. Modeling hemodynamic response for analysis of functional MRI time-series. Hum Brain Mapp., 1998; 6(4): 283-300.

Salek-Haddadi A, Lemieux L, Merschhemke M, Friston K, Duncan JS, Fish DR. Functional magnetic resonance imaging of human absence seizures. Ann Neurol 2003; 53:663-7.

Salek-Haddadi A, Diehl B, Hamandi K, Merschhemke M, Liston A, Friston K, Duncan J.S, Fish D.R., Lemieux L. Hemodynamic correlates of epileptiform discharges: an EEG-fMRI study of 63 patients with focal epilepsy. Brain Res 2006; 1088: 148-66.

Scherg M and Cramon DV. Two bilateral sources of the late AEP as identified by a spatio-temporal dipole model. Electroencephalogr. Clin. Neurophysiol. 1985; 62: 32-44.

Seeck M, Lazeyras F, Michel CM, Blanke O, Gericke CA, Ives J, Delavelle J, Golay X, Haenggeli CA, de Tribolet N, Landis T. Non-invasive epileptic focus localization using EEG-triggered functional MRI and electromagnetic tomography. Electroenceph clin Neurophysiol 1998; 106: 508-512.

Singh M, Patel P, Al-Dayeh L. fMRI of brain activity during alpha rhythm. Int. Soc. Mag. Res. Med. 1998; 3, p. 1493.

Stern JM. Simultaneous electroencephalography and functional magnetic resonance imaging applied to epilepsy. Epilepsy Behav 2006; 8: 683-692.

Symms MR, Allen PJ, Woermann FG, Polizzi G, Krakow K, Barker GJ, Fish DR, Duncan JS. Reproducible localization of interictal epileptiform discharges using EEG-triggered fMRI. Phys Med Biol 1999; 44: N161-N168.

Tallon-Baudry C, Bertrand O, Delpuech C, Pernier J. Oscillatory gammaband (30–70 Hz) activity induced by a visual search task in humans. J Neurosci 1997; 17(2): 722-34.

Warach S, Ives JR, Schlaug G, Patel MR, Darby DG, Thangaraj V, Bdelman RR, Schomer DL. EEG-triggered echo-planar functional MRI in epilepsy. Neurology 1996; 47: 89-93.

Worsely K, Friston K. Analysis of time-series revisited—again. Neuroimage 1995; 2: 173-181.

Worsely K, Liao C, Aston J, Petre V, Duncan G, Morales F, Evans A. A general statistical analysis for fMRI data. Neuroimage 2002; 15: 1-15.

van Duinen H, Zijdewind I, Hoogduin H, Maurits N. Surface EMG measurements during fMRI at 3T: accurate EMG recordings after artifact correction. NeuroImage 2005; 27(1): 240-246

Vigario RN. Extraction of ocular artefacts from EEG using independent component analysis. Electroencephalogr Clin Neurophisiol. 1997; 103: 395-404.

Villringer A, Chance B. Non-invasive optical spectroscopy and imaging of human brain function. Trends Neurosci 1997; 20(10): 435-442.

Yu AH, Li KC, Piao CF, Li HL. Application of functional MRI in epilepsy. Chin Med J (Engl) 2005; 118: 1022-1027.